63-2-4

HUGHES

RESEARCH LABORATORIES

RESEARCH ON COHERENT GENERATION OF OPTICAL RADIATION

Prepared under Contract AF 33(616)-8233 by
G. F. Smith

Task No. 523701
Project No. 5237

ASD-TDR-62-938

NOTICES

When Government drawings, specifications, or other data are used for any purpose other than in connection with a definitely related Government procurement operation, the United States Government thereby incurs no responsibility nor any obligation whatsoever; and the fact that the Government may have formulated, furnished, or in any way supplied the said drawings, specifications, or other data, is not to be regarded by implication or otherwise as in any manner licensing the holder or any other person or corporation, or conveying any rights or permission to manufacture, use, or sell any patented invention that may in any way be related thereto.

Qualified requesters may obtain copies of this report from the Armed Services Technical Information Agency, (ASTIA), Arlington Hall Station, Arlington 12, Virginia.

Copies of this report should not be returned to the Aeronautical Systems Division unless return is required by security considerations, contractual obligations, or notice on a specific document.

58

ASD-TDR-62-938

RESEARCH ON COHERENT GENERATION OF OPTICAL RADIATION

TECHNICAL DOCUMENTARY REPORT NO. ASD-TDR-62-938
October 1962

Navigation and Guidance Laboratory
Aeronautical Systems Division
Air Force Systems Command
United States Air Force
Wright-Patterson Air Force Base, Ohio

Task No. 523701
Project No. 5237

Prepared under Contract AF 33(616)-8233 by
G. F. Smith
Hughes Research Laboratories
A Division of Hughes Aircraft Company
Malibu, California

FOREWORD

This report was prepared by the Hughes Research Laboratories, Malibu, California, on Air Force Contract AF 33(616)-8233, "Research on Coherent Generation of Optical Radiation." The basic and applied research reported in this document was administered under the direction of the Electronic Technology Laboratory of the Aeronautical Systems Division. Mr. E.B. Champagne was Project Engineer for the Laboratory.

The studies presented began on 1 May 1961 and were concluded on 31 August 1962. The work was conducted in the Quantum Physics Department of the Hughes Research Laboratories under the direction of Dr. G.F. Smith.

Although this composite study represents a group effort, the chief contributors and their general fields of endeavor were: Dr.G.F. Smith, program administration and technical direction; Dr. G. Birnbaum, Dr. R.W. Hellwarth, and Dr. W. Wagner, theoretical investigations; Dr. C.K. Asawa, Dr. F.J. McClung, Jr., Dr. V. Evtuhov, Mr. D.A. Buddenhagen, Mr. I.J. D'Haenens, and Mr. J.K. Neeland, experimental investigations; Mr. N. Stevens, spark discharge investigation; and Dr. A. Gentile and Mr. M. Robinson, laser materials investigation and preparation. Mr. D'Haenens also provided special assistance with the writing and editing of this report.

This report is the final report and it concludes the work on Contract AF 33(616)-8233.

ABSTRACT

The production of extremely high peak power pulses was demonstrated during the term of the contract. In experiments with a refined "pulsed reflector laser" (PRL), single pulses of 14 MW peak power and 35 nsec duration (0.2-J energy and 10^{-3} rad beam angle) have been generated. Recent experiments with the Kerr-cell PRL yielded anomalous results: In addition to the 6943 Å ruby pulse, the Kerr-cell PRL emits a number of satellite lines at 7660 Å, 8530 Å, and 9640 Å which are spectrally narrow and well collimated. These lines were found to be associated with the nitrobenzene. A study of the temperature-dependent stimulated emission spectra of ruby has resulted in the identification of the Fabry-Perot axial mode resonances of wave number $\bar{\nu} = p/2\ell\sqrt{\epsilon}$. In addition to the axial modes, which determine the gross frequency characteristics of the laser, discrete transverse modes, which determine the transverse field configurations and precise frequency, have been observed. These observations have been made by studying the near field radiation patterns near threshold pumping. The frequency characteristics of these modes have been studied both spectroscopically and by observing the microwave beats between adjacent axial modes. Excellent agreement was obtained between theoretical calculations and the results of a comprehensive experimental study of the dependence of oscillation threshold on ruby length, concentration, and temperature; cavity length and reflectivity, and pumping rate. Attempts to obtain cw laser action in ruby at room temperature were unsuccessful. The pumping efficiency of microsecond-duration, high-intensity spark discharges was investigated. Peak temperatures of 30,000°K for periods of 2 μsec were generated in several pumping configurations, but oscillation in ruby was not achieved. By use of substitutional feeds (i.e., powdered ruby or other desired end product) in the Verneuil (flame fusion) process, crystals have been grown which are free of undissolved particles of guest ion oxide.

TABLE OF CONTENTS

I. INTRODUCTION AND SUMMARY 1

II. PULSED REFLECTOR MODE FOR GENERATION OF HIGH PEAK POWER 5

A. Principle of Operation 5

B. Experimental Procedure 12

C. Experimental Results 13

D. Problem Areas 24

III. GENERAL INVESTIGATION OF THE RUBY LASER 27

A. Spectral Analysis and Modes of a Ruby Laser . . . 27

B. Oscillation Threshold Considerations 42

C. CW Ruby Laser Study 55

D. Optimization of Energy Output in the Pulsed Ruby Laser 57

IV. PUMPING CONFIGURATIONS AND FLASH LAMPS FOR OPTICAL EXCITATION 71

A. Pumping Configurations 71

B. Flash Lamp Evaluation 79

C. High Intensity Spark Discharges 81

V. CONSTRUCTION OF A PULSED REFLECTOR LASER FOR THE AIR FORCE 97

VI. LASER MATERIALS RESEARCH 101

A. Inorganic Crystals 101

B. Colloids 102

C. Glasses 103

D. Organic Materials 104

VII. CONCLUSIONS 107

VIII. RECOMMENDATIONS 109

APPENDIX 113

ABSTRACTS 115

REFERENCES 131

LIST OF ILLUSTRATIONS

Fig. 1. Typical time sequence of effective reflectivity, population excess n, and output beam power for a giant pulse with fast switching 8

Fig. 2. Pulse power output versus time; moderate power but fast switching (Kerr cell without polarizer). 11

Fig. 3. Schematic of apparatus for extreme switching of regeneration 11

Fig. 4. Power output versus time for a typically fast (about 5 nsec) switching condition with apparatus shown in Fig. 3 16

Fig. 5. Power output versus time for intermediate (0.11 μsec) switching time 16

Fig. 6. Power output versus time for slow (0.5 μsec) switching time 16

Fig. 7. PRL spectra for various switching times 19

Fig. 8. Streak photographs of the PRL taken through the Fabry-Perot interferometer 20

Fig. 9. Normal laser action without streaking and streaked PRL output as seen through a 0.8-mm-separation Fabry-Perot interferometer 20

Fig. 10. The spectra of the PRL showing the satellite lines in nitrobenzene 22

Fig. 11. The spectra of the PRL with a KDP modulator replacing the nitrobenzene Kerr cell 22

Fig. 12. Far field beam patterns of fast switching with beam attenuated 23

Fig. 13. Output of a ruby laser at low temperature 29

Fig. 14. Fabry-Perot analysis of the laser output at room temperature 29

Fig. 15. Fabry-Perot analysis of the laser output at room temperature 29

Fig. 16. Fabry-Perot analysis of the laser output at room temperature 29

Fig. 17. Ruby line shape at 300°K and longitudinal cavity mode structure 31

Fig. 18. Spectral shift and width of R_1 fluorescence versus temperature 32

Fig. 19. Energy-level diagram for ruby showing the ground-state splitting 32

Fig. 20. Fabry-Perot spectrograms for a 2.13-cm-long ruby at different temperatures 34

Fig. 21. Ruby line shape and cavity modes at 78°K 35

Fig. 22. Photographs of the end of a 3-mm by 2.54-cm ruby showing some of the typical transverse mode patterns 38

Fig. 23. Separation s between the two maxima of a two-lobe pattern as a function of distance p from the ruby face 39

Fig. 24. Computed intermediate-field intensity distribution for a two-lobe pattern at 50 cm from ruby face. 41

Fig. 25. Emission pattern showing greater far field divergence angle (approximately 3.4 mrad) between the principal maxima than that resulting from the two-lobe pattern. . . 41

Fig. 26. Output characteristics near threshold. 43

Fig. 27. Output characteristics approximately 10% above threshold 43

Fig. 28. Output characteristics approximately 10% above threshold 44

Fig. 29. Hypothetical mode spectrum of a ruby laser showing two kinds of mode hopping 44

Fig. 30. Computed oscillation threshold as a function of Cr^{3+} ion concentration for various ruby rod diameters and gain parameters 48

Fig. 31. Experimentally measured oscillation threshold as a function of concentration with reflectivity as the parameter 49

Fig. 32. Experimentally measured oscillation threshold as a function of concentration with temperature as the parameter 49

Fig. 33. Threshold inside crystal as a function of gain and concentration 53

Fig. 34. Threshold conditions for various rubies as functions of pumping pulse length 54

Fig. 35. BTL ruby sapphire trumpet configuration for 78°K cw ruby laser 58

Fig. 36. Power output as a function of fractional inversion f. . . . 62

Fig. 37. Laser beam energy versus percent transmission with temperature as parameter (°C) 64

Fig. 38. 22,000-J laser power supply. 65

Fig. 39. 22,000-J laser power supply with operator switching storage condensers 65

Fig. 40. 8000-J pulse-shaped laser power supply 66

Fig. 41. Power output versus time for 9.5-in.-long ruby driven with shaped supply 66

Fig. 42. Room-temperature high-energy laser assembly with power supply control panel 67

Fig. 43. Laser assembly in Fig. 42 with outer housing removed 68

Fig. 44. Power output versus time for laser assembly in Figs. 42 and 43 68

Fig. 45. Low temperature laser disassembled to show component parts 70

Fig. 46. A reflector in the form of an elliptical cylinder employing an artificial source 72

Fig. 47. Focusing properties of an elliptical cavity. 76

Fig. 48. Ellipsoidal reflector employing an artificial source. . . . 77

Fig. 49. (a) Pumping efficiency comparison of xenon-krypton in a Hughes coaxial flash lamp. (b) Pumping efficiency of xenon-krypton versus pressure in a Hughes coaxial lamp. (c) Pumping efficiency comparison of xenon-krypton-argon-helium in helical lamp (gases at optimum pressure, ~ 150 mm Hg) 80

Fig. 50. EGG FX-1 flash lamp with 2-in. arc spectral distribution 82

Fig. 51. Schematic of short-duration optical pump (discharge circuit shown in heavy black). 84

Fig. 52. Black-body radiance and ruby absorption bands 85

Fig. 53. Coaxial 0.4-μF source with pressurized Fiberglas housing 88

Fig. 54. Elliptical pressurized cavity. 89

Fig. 55. Ruby fluorescence versus energy with source configuration and gas type as parameters 91

Fig. 56. Ruby fluorescence as a function of gas type and configuration. 92

Fig. 57. Energy-level diagram of ruby 94

Fig. 58. Complete PRL assembly. 98

Fig. 59. PRL – optical apparatus 99

Fig. 60. PRL – power supply apparatus. 99

Fig. 61. Excitation and emission spectrum of europium-tris-dibenzoylmethide 105

Fig. 62. Excitation of fluorescence spectrum of Eu(BAA) 105

I. INTRODUCTION AND SUMMARY

The purpose of this program was to conduct intensive and comprehensive research on the generation of high-power, coherent, and highly collimated radiation at optical frequencies by solid-state devices. Although emphasis was placed on the attainment of extremely high peak power, the program was necessarily directed toward fundamental investigations rather than toward the development of specific devices. It included a concurrent effort on the investigation of pulsed ruby lasers, optical resonators, efficient excitation sources and new laser configurations, materials preparation and study (spectroscopy), and basic laser physics.

The production of extremely high peak power pulses was demonstrated during the term of the contract. This original demonstration resulted from the embodiment of Dr. R. W. Hellwarth's proposal of a "pulsed reflector laser" (PRL) at the 2nd international Quantum Electronics Conference (Ref. 1). In experiments with a refined PRL, single pulses of 14 MW peak power and 35 nsec duration (0.2-J energy and 10^{-3} rad beam angle) have been generated. The refinements in the PRL were the result of step-by-step identification of problem areas and their elimination by replacement with more suitable circuit elements; the present PRL can be operated indefinitely without degradation of performance. A PRL of this type has been constructed for delivery to the contracting agency. Pulsed reflector lasers have been constructed both with a liquid-nitrobenzene Kerr cell and with a solid-state KDP Pockells cell as the switching element. Faster switching times (and correspondingly shorter and more intense laser pulses) have been achieved with the Kerr cell. Spectroscopy of the PRL with the Pockells and Kerr cells, respectively, has been performed with most interesting results. The time-integrated spectrum of the Kerr-cell PRL is the order of 2 Å, while that of the Pockells-cell PRL is 0.5 Å. Time resolution spectroscopy was also performed on the Kerr-cell PRL. In recent experiments with the Kerr-cell PRL, some anomalous results were obtained Briefly, in addition to the 6943-Å ruby pulse, the Kerr-cell PRL also emits a number of satellite lines at 7660 Å, 8530 Å, and 9640 Å which are spectrally narrow and well collimated. These lines were found to be associated with the nitrobenzene. A complete explanation of this effect is currently the object of an intensive investigation being carried out with Hughes-sponsored funds.

The above mentioned anomalous behavior tends to limit the power output at 6943 Å and poses a severe limitation for systems applications. An analysis of propagation through an optically dense

Manuscript released by author November 1962 as an ASD Technical Documentary Report.

amplifying medium indicates the desirability of using a power amplifier to increase the power output of the PRL. In addition, such a system would also shorten the pulse length.

A major part of this research program was devoted to extending the state of the art in ruby lasers – both in advancing our understanding of the physics involved and in optimizing the performance of the laser. Excellent agreement was obtained between theoretical calculations and the results of a comprehensive experimental study of the interaction of the various parameters which determine oscillation threshold (i.e., ruby length, concentration, and temperature; cavity length and reflectivity; and pumping rate), thus indicating that this phase of laser physics is well understood. These results were extended to the beam energy variation and gave good qualitative agreement with experiment; this facilitates the optimization of a given laser configuration (i.e., flash lamp and ruby).

A study of the spectral characteristics of the ruby laser has resulted in an understanding of the interaction of the ruby (characterized by the absorption intensity and line width) and the optical Fabry-Perot resonator. The Fabry-Perot resonator has modes at wave numbers $\overline{\nu} = \frac{p}{2l\sqrt{\epsilon}}$, with separation between adjacent axial modes of $\overline{\Delta\nu} = \frac{1}{2l\sqrt{\epsilon}}$. A thorough investigation of the spectral characteristics of the ruby laser verified the existence of these modes. At threshold the system oscillates in one or more of these modes. The spectroscopy of ruby indicates that the R_1 transition is actually an unresolved doublet, the separation between center frequencies of the doublet being 0.38 cm^{-1} (zero-field splitting of the $^4A_2$ ground state). The number of modes excited most likely depends on the number contained in the frequency separation corresponding to this splitting and on residual inhomogeneous line broadening due to crystalline imperfections. The temperature variation of the line width in ruby is such that at 300°K the spectral character of the stimulated emission is determined by the length of the ruby. At low temperatures, where the R_1 doublet is well resolved, the system can oscillate in modes at the center of the transitions and also in axial modes within the transition line width.

At high power levels, in addition to more longitudinal modes being excited, the spectral character of the output becomes continuous (over a spectral band) rather than discrete. It is believed that this is caused by the inhomogeneous broadening in ruby which, in effect, limits the rate at which energy can diffuse within the excited level, resulting in the excitation of mode packets (large number of closely spaced off-axis transverse modes). This interpretation explains the divergence of the beam angle at high output levels. Beam divergence can be minimized by making the frequency separation between modes as small as practical, i.e., increasing the length of the Fabry-Perot resonator.

In addition to the axial modes, which determine the gross frequency characteristics of the laser, discrete transverse modes, which determine the transverse field configurations and precise frequency, have been observed. These observations have been made by studying the near field radiation patterns near threshold pumping. The frequency characteristics of these modes have been studied both spectroscopically and by observing the microwave beats between adjacent axial modes. These observations were made with a phototube which incorporates a built-in section of traveling-wave amplification and operates similarly to a tube recently used by Siegman (Ref. 2). Such a phototube can serve as a spectrometer of extremely high resolution and is a useful tool for examining the spectral properties of lasers and, in particular, for the study of single mode operation.

Experiments with high energy ruby laser systems have resulted in the generation of 16-J pulses at room temperature. Extrapolation of this series of experiments to reduced temperatures and higher flash lamp loadings indicates that energy outputs in excess of 100 J will be achieved.

In another phase of the program, theoretical studies have been made of several pumping configurations and of pumping pulse length. These investigations have led to an elliptical configuration that gives a room-temperature oscillation threshold of ~50J for a ruby laser, which is believed to be the minimum thus far achieved. Attempts to obtain cw laser action in ruby at room temperature were unsuccessful.

Flash lamp filling gas and pressure were investigated, and it was found that xenon at ~1/5 atmosphere of pressure is optimum for pumping ruby; this, coincidentally, is approximately the pressure to which commercially available xenon lamps are filled. Spectral distribution measurements of a xenon flash lamp were completed and pumping efficiency related to various experiments.

The pumping efficiency of microsecond-duration high-intensity spark discharges was investigated. Peak pump temperatures of 30,000°K for periods of 2 μsec were generated in several pumping configurations. However, oscillation in ruby was not achieved, conceivably because of population of the conduction band due to the intense ultraviolet generated in the high temperature discharge, the resulting free carrier absorption inhibiting pumping efficiency and increasing losses at the laser transition.

In the materials research program, significant progress has been made in the art of crystal growth. By use of substitutional feeds (i.e., powdered ruby or other desired end product) with the Verneuil (flame fusion) process, crystals have been grown which are free of undissolved particles of guest ion oxide. Experiments with mixed Cr^{3+} doped spinels, i.e., $MgAl_2O_4$ and $ZnAl_2O_4$, showed displacement of the Cr^{3+} emission from 6970 Å in the magnesium spinel to 7020 Å in the zinc spinel. If laser action can be obtained in such a mixed crystal system, it may be possible to systematically vary the emission wavelength.

II. PULSED REFLECTOR MODE FOR GENERATION OF HIGH PEAK POWER

The purpose of this phase of the program was to demonstrate a means of producing pulses of optical radiation at extremely high power levels. The original demonstration of a PRL (Ref. 3), proposed by R. W. Hellworth (Ref. 1), was reported in Interim Scientific Report No. 1. This section of the Final Report will outline the principles of the technique and summarize the earlier experimental results given in ISR's No. 1, 2, 3, and 4. New information disclosed relates to the temporal, spectral, and spatial character of the Kerr-cell PRL.

A. PRINCIPLE OF OPERATION

When a laser (or maser) oscillator is operating normally, the gain of the material at the laser frequency nearly balances the losses of the cavity in which regeneration takes place. The gain per cm α of the material is a function of frequency and population inversion $n \equiv n_2 - n_1$, where n_2 is the population of (i.e., number of laser atoms in) the upper laser level(s) and n_1 that of the lower level(s). We assume that the laser transition is homogeneously broadened so that the gain (loss) $\alpha(\nu)$ per unit length near the laser frequency always has the same shape and depends on the inversion n according to

$$\alpha(\nu) = \alpha_o(\nu)\, n/N \quad . \tag{1}$$

The normal absorption per cm $\alpha_o(\nu)$ for the line in question is that measured by ordinary spectroscopic techniques at some condition where the inversion is $-N$.

In most laser materials the laser transition is not homogeneously broadened and the assumption as it stands is invalid. However, the inhomogeneous line may be thought of as a "packet" of homogeneous lines, for each of which the assumption is valid and among which some appropriate coupling may be inserted to account for the (as yet unknown) broadening mechanisms. It may be hoped that a homogeneous analysis, if not accurate in a particular situation, may still serve as a useful starting point. Therefore, we shall proceed with our assumption, modifying it when necessary in a qualitative way, as no complete theory has as yet been worked out.

For the ruby R_1 laser transition (which we shall constantly consider as our theoretical and experimental example), N is essentially the total number of chromium ions when $\alpha_o(\nu)$ is measured at or below room temperature. For the pink ruby we employ, N is about 1.6×10^{19} times the crystal volume, and α_o(peak) is about 0.4 cm^{-1} at 300°K and

$10\ cm^{-1}$ at $77^{\circ}K$. For laser materials in which the lower laser level is not the ground state, α_o and N can be determined from fluorescence data.

We shall consider the common laser configuration in which a laser material rod of length ℓ cm is placed between flat, parallel, and partially reflecting end surfaces separated by a distance L cm. If the reflectivities of these surfaces are R_1 and R_2, then as light passes once back and forth between the end plates it is amplified (or attenuated) in intensity by $R_1R_2 \exp 2\alpha\ell$. We generally define a loss factor γ, which here would equal $-1/2 \ln R_1R_2$ but in general includes other (such as scattering) losses so that in a single pass of light between the end plates the average gain in intensity is $\exp(\alpha\ell - \gamma)$. Therefore, for normal laser oscillation, the fact that losses are nearly cancelled by gain means that at some frequency (usually the line center)

$$\alpha\ell \approx \gamma \ . \qquad (2)$$

The average output rate ϕ of photons is essentially determined by the rate at which pump photons are absorbed at some higher frequency. Ruby is quite efficient as a laser material in the sense that every pump photon absorbed is converted to an output photon (either spontaneous or induced) near the laser frequency. With this background, we shall now consider the non-steady-state operation of a laser which produces giant laser pulses.

As would be expected, if the losses γ were caused to vary with time, then the output would vary also. Giant pulses result from an especially simple variation of γ; they are formed by keeping the losses high during the pumping cycle and then suddenly switching them from their preswitch value γ_i to a lower loss value, which we shall henceforth refer to as γ. Before switching, the population excess has reached some value n_i and after switching tends toward a new equilibrium value n_f. If the pumping is strong enough and on long enough, then n_i is greater than n_f and the populations adjust between n_i and n_f through the induced emission of coherent laser light; this emission is the giant pulsing under consideration. The pump is assumed to be on throughout operation. It has a generally negligible effect during the relatively short span of a pulse and serves mainly to set the initial excitation n_i and the recovery rate after a pulse.

When a photon is emitted, the population inversion n decreases in number by 2. Therefore, the total output light energy U in a pulse is

$$U = \frac{1}{2} h\nu (n_i - n_f) \ , \qquad (3)$$

where h is Planck's constant and ν is the laser frequency in cps. For the ruby R_1 transition, the energy per photon $h\nu$ is 2.8×10^{-19} J. It is common to achieve an initial inversion of 25%, i.e., $n_i = 0.25\,N$. The final inversion n_f is at least as low as $N\gamma/a_o\ell$ and is often zero. Therefore, we might expect a typical pulse energy of order $1/2\, h/\nu\, n_i \approx 0.56$ J/cm^3 of ruby. In practice, we have obtained only a fraction of this energy because of nonoptimal output coupling and internal losses and because the periphery of the crystal is not very active; however, all of these obstacles to higher energy can probably be overcome, and the initial inversion also pushed much higher than 25%. The peak output power and other pulse characteristics will follow from more detailed analysis.

In order to discuss the time behavior of the populations n and output photon flux ϕ in a giant pulse, it is convenient to distinguish three domains of switching speed: (1) fast switching, where $\gamma(t)$ is switched quickly compared with the time it takes for n and ϕ to react; (2) intermediate switching, where the output flux has built up before the time when $\gamma(t)$ has reached its final value γ, but still continues past this time; and (3) slow switching, where $\gamma(t)$ is varying during the time that most of the output $\phi(t)$ is emitted. The fast switching case is the simplest to analyze, and we shall consider it first.

In Fig. 1 is plotted a typical time history of γ, n, and ϕ for fast switching. In order to estimate the delay, rise, and decay times of $\phi(t)$ indicated in Fig. 1, we shall assume that only one frequency (near the line center) of light is important (and hence omit ν in $a(\nu)$) because of laser action. This is generally not the case because inhomogeneous line broadening causes laser action at many adjacent frequencies. However, the analysis still gives useful estimates of the gross features of the giant pulses, and it is possible that a more exact solution can be constructed by superposing and coupling the single frequency packets.

If a_i is the gain built up before switching (related to n_2 by (1)), then after the instant of switching the light experiences an average gain $\exp[a_i\ell - \gamma]$ per pass. Therefore, if t_1 is the time for a single pass, we may write the initial buildup of the output ϕ as

$$\phi = \phi_o \exp t/\tau \ , \tag{4}$$

where

$$\tau = t_1/(a_i\ell - \gamma) \ . \tag{5}$$

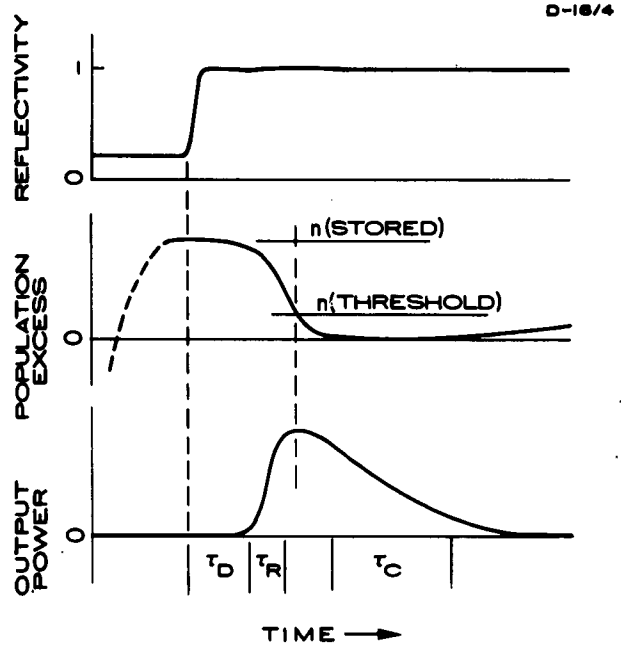

Fig. 1. Typical time sequence of effective reflectivity, population excess n, and output beam power for a giant pulse with fast switching.

At first, ϕ builds up essentially as in (4) until the emission begins to appreciably alter the initial gain a_i and also n_i. The time t_Δ required to reduce the initial gain a_i by a small amount Δa and hence reduce n_i by $\Delta n = N \Delta a/a_i$ is obtained approximately by calculating from (4) the time required such that

$$\int_o^{t_\Delta} \phi(s)\, ds = \Delta n/2 ;$$

this gives

$$t_\Delta = \tau \ell n\, (1 + \Delta n/2\phi_o \tau) \quad . \tag{6}$$

Suppose that before switching n had reached some (not necessarily equilibrium) value n_i. Then ϕ_o is some fraction ξ of the absorption rate of pump photons at equilibrium, which for ruby is $n_1 w$, where w is the probability per second for a laser atom to absorb a pump photon. For ruby, $n_1 = 1/2\,(N - n_i)$, since essentially all laser ions are either in state 1 or 2. Therefore, for ruby,

$$\phi_o \approx \frac{1}{2}\,(N - n_i)\, w \xi \quad , \tag{7}$$

and if we substitute f for the initial fractional inversion n_i/N, then (Refs. 1 and 3)

$$t_\Delta = \tau \ell n \left(1 + \frac{f}{1-f}\, \frac{\Delta a}{a_i w \tau \xi}\right). \tag{8}$$

This is a formula derived in Ref. 1 and used by Collins, et al. (Ref. 4), with ξ put equal to unity, to estimate the delay time τ_D of the pulse after fast switching (Fig. 1). It was estimated that the pulse appeared in the detector when $\Delta a/a_i \approx 0.1$, so $\tau_D \approx t_\Delta (\Delta a/a_i = 0.1)$. We shall find below that the result is useful and accurate to within about 20%. After the output pulse has started to form, it causes the gain to drop (quickly in a few τ) to where it equalizes the lower (after switching) losses ($a(t)\ell \approx \gamma$), and at this point ϕ reaches its maximum ϕ_m. That is, the rise time of the pulse τ_R is not much longer than τ, or

$$\tau_R \sim t_1/a_i \ell \quad , \tag{9}$$

especially when $a_i \ell \gg \gamma$.

After the maximum output is reached, the decay is determined by whether the initial gain was much greater than the losses. If $a_i \ell$ is much greater than γ, then there are enough photons left inside the laser cavity at the time of maximum output to erase the remaining population excess and drive it quickly to zero. In this case, the major portion of the decay proceeds with a characteristic time constant τ_c, which is the cavity time constant,

$$\tau_c \approx t_1/\gamma , \qquad (a_i \ell \gg \gamma) . \tag{10}$$

Therefore, the peak output flux ϕ_m in this case is roughly

$$\phi_m \approx \tfrac{1}{2} n_i \gamma / t_1 , \qquad (a_i \ell \gg \gamma) . \tag{11}$$

However, if $a_i \ell$ is not much different from γ, then both the rise time and decay time are of order τ and neither $a_i \ell$ nor γ dominates the other during any phase of the process. That is,

$$\tau_R \sim \tau_c \sim t_1/(a_i \ell - \gamma) , \qquad (a_i \ell \approx \gamma) . \tag{12}$$

Because the output pulse should be fairly symmetric about its peak in this case, the final inversion n_f is about the same amount below threshold n_o as n_i is above. This leads to an estimate of the pulse energy U in the fast, but slight, switching case:

$$U \approx \tfrac{1}{4} h\nu (n_i - n_o) , \qquad (n_i \approx n_o) , \tag{13}$$

which is less than the available energy $1/2\ h\nu\ n_i$. Therefore, the peak flux is of the order

$$\phi_m \approx \tfrac{1}{4} (n_i - n_o)^2 \gamma / n_o t_1 , \qquad (n_i \approx n_o) . \tag{14}$$

Because this latter case produces slower pulses which are easier to examine experimentally, it was chosen for the early experiments (Ref.3). Fast switching of γ from a value of about 0.4 to 0.3 with a pump rate just below that required to produce laser action normally at the higher value of γ produced the pulse shown in Fig. 2. The apparatus

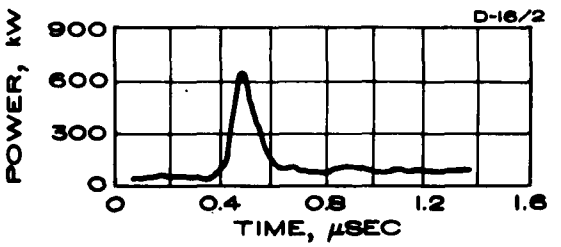

Fig. 2. Pulse power output versus time; moderate power but fast switching (Kerr cell without polarizer). The shutter opening time is at the onset of the small oscillations preceding the large pulse.

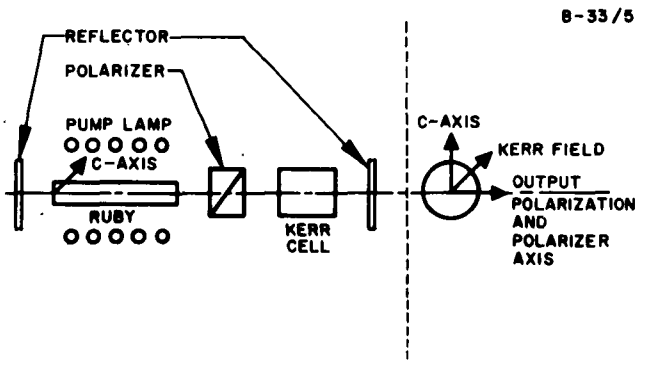

Fig. 3. Schematic of apparatus for extreme switching of regeneration.

was as shown in Fig. 3, but without the polarizer. The details of its operation are analyzed elsewhere (Ref. 3). The times τ_o, τ_R, and τ_c characterizing this pulse agree within 20% with the values predicted from (8) and (12). The pulse energy U delivered to the detector is about five times less than that given by (13) for reasons mentioned earlier in this section. All energy measurements reported here may involve experimental errors of 20%.

The fast switching experiments with the initial gain much larger than the losses are discussed in the following sections. Unfortunately, our measuring apparatus was not fast enough to measure τ_R and τ_c accurately, but τ_D was observed to be about three times faster than the previous case, and this is consistent with (8).

In the slow and intermediate switching cases, the above approximate treatment for ruby is made more inaccurate by the fact that relaxation processes in the laser line have more time to complicate matters than in the fast switching case. We shall suggest how the experimental results reported here may help guide a future theoretical treatment. The simplified approach we have outlined above is still useful in estimating the total energy and peak powers if the output pulse shape is not too irregular or at least has one main peak (which it often does). The main effect of stretching the period of switching is generally to liberate the energy $1/2\, h\nu(n_i - n_f)$ over a longer period of time which, as one approaches the slow switching case, occupies the whole switching period.

B. EXPERIMENTAL PROCEDURE

The apparatus used for the following experiments is shown in Fig. 3. The polarizer-Kerr-cell combination placed inside the laser cavity caused the regeneration to switch between very high and very low values at a controlled rate which depended on the discharge of the voltage on the Kerr cell. A 0.05% concentration, unclad pink ruby rod 2.84 cm long and 0.9 cm in diameter was employed. The reflecting end surfaces were multilayer-dielectric-coated optical flats with reflectivity of about 98%. The polarizer was a quartz Wollaston (optically contacted) prism. The nitrobenzene Kerr cell was discharged at three different rates, causing the effective transmission of the Kerr-cell polarizer combination to go from 0.1 to 0.9 in 0.005 (estimated), 0.11, and 0.5 μsec, respectively. These three rates are fairly representative of fast, intermediate, and slow switching rates. The estimated single pass time t_1 for light in this apparatus was 1.2 nsec.

The ruby was pumped by a G.E. FT506 helical flash lamp. The lamp was driven by a shaped pulse power supply. The lamp output came on in a few microseconds, stayed constant for 250 μsec, and then decreased to zero in 50 μsec. With the Kerr-cell voltage off, normal oscillation was observed at about 150 μsec after the lamp was fired,

remained roughly constant (with ~1-kW spontaneous pulsations) for 100 μsec, and then decreased to zero in 50 μsec, as was expected. The pump transition probability per second in the most favored part of the ruby therefore is estimated to be (assuming oscillation began when about half the ground state had been pumped) 3×10^3 per sec or about ten times threshold. This condition applies approximately in the experiments reported here unless otherwise noted. Normally, the Kerr shutter was opened about 250 μsec after the lamp was fired; the timing was not observed to be critical. The reflection coefficient of the end plates was so high (~0.98) that the total losses were undoubtedly set by internal losses and hence were difficult to estimate. However, we believe that the loss factor γ_ϵ (after switching) is typically in the neighborhood of 0.1 for the present experiments. For power measurement, the output from one end of the system was monitored with a 6217 photomultiplier, and a Tektronix 555 oscilloscope. Neutral density filters were used to attenuate the output beam. Power measurements from the oscilloscope trace are accurate to within ±20%, provided the pulse duration is longer than the response times of the oscilloscope and phototube. The measurements reported herein were made on the output from the other end of the system. Before describing the results of varying the switching time, two interesting effects at fast switching will be discussed below.

C. EXPERIMENTAL RESULTS

1. $\overline{E} \rightarrow 2\overline{A}$ Relaxation Time

The normal ruby laser R_1 transition is between the ground level (commonly labelled $^4A_2$) and the first excited level ($\overline{E}$) (Ref. 5). Another level ($2\overline{A}$) lies 29 cm^{-1} above the $\overline{E}$ level and is connected to the ground state by the R_2 transition whose peak absorption at room temperature is about 70% that of R_1 (Ref. 6). Because the Boltzmann factor at room temperature is near 0.9 for 29 cm^{-1}, the equilibrium gain at R_2 is about half that at R_1 under full inversion, and for any significant amount of inversion there is considerable gain at the R_2 frequency. Indeed, it has been demonstrated that if the losses at R_1 are made proportionately greater than the losses at R_2, normal laser oscillation occurs at R_2 (Ref. 7).

Certainly, just after fast switching to produce a giant pulse, the gain at the R_2 line exceeds the losses, and if nothing else disturbed the $2\overline{A}$ level population, a strong light pulse would be expected at the R_2 frequency. We have looked for emission in giant pulses at the R_2 line under a wide variety of conditions, but always without success. Evidently the populations of the $2\overline{A}$ level come into equilibrium so quickly with the $\overline{E}$ population that (just as in normal laser oscillation) the R_2 gain is "always" less than the R_1 gain and relatively little light can be formed at R_2 in any experiment where regeneration accentuates small differences in single pass gain. This fact allows us to place an upper limit on the $\overline{E} \rightarrow 2\overline{A}$ relaxation time as discussed below.

Previous experiments (Ref. 3) indicate a fractional inversion level at least 25% before switching. It is easy to estimate that at 25 % inversion for R_1, we have (in equilibrium) 12% inversion at the peak of R_2. This would correspond to $\alpha_i \ell = 0.3$ for the R_1 line and $\alpha_i \ell = 0.15$ for the R_2 line. (There is probably more inversion than this in some parts of the crystal.) From (8) we estimate that the delay time for a pulse at R_2 would be four times that of R_1, or between 0.2 and 0.3 μsec. This means that the relaxation time between the $\bar{E}$ and $2\bar{A}$ levels must be less than 0.1 to 0.2 μsec in order to prevent output at the R_2 frequency. Hence, we can place an upper limit of about 0.2 μsec on the $\bar{E} \rightarrow 2\bar{A}$ relaxation time in pink ruby at room temperature. To check this result further, we performed an experiment suggested by G. Birnbaum in which a fast (~ 30 nsec duration) giant pulse was fired into a second ruby and the subsequent fluorescence at the R_2 line monitored. There was no observable delay in the R_2 emission from the $2\bar{A}$ level after populating the $\bar{E}$ level with the pulse. The signal-to-noise ratio in this experiment was such that it placed an upper limit of 0.1 μsec on the $\bar{E} \rightarrow 2\bar{A}$ relaxation time.

To a good approximation, we may consider ruby to be a two-level system because of this fast relaxation. That is, for laser purposes, the $\bar{E}$ and $2\bar{A}$ levels are linked so closely that they act as one upper level (with a double-peaked line shape) with the same multiplicity (four-fold) as the ground level; thus taking (as we have done) the total level populations to be the sum of lower and upper laser levels is approximately valid.

2. Upper Level Lifetime Shortening

Normally, the lifetime of the upper laser level (in the absence of regeneration) is around 3 msec (Refs. 8 and 9). However, certain giant pulse characteristics show that the actual lifetime is a strong function of inversion, rapidly shortening as inversion increases, even in the absence of strong regeneration.

In early experiments (Ref. 3), where the losses and hence threshold inversion could be estimated, it was found that 25% inversion was typical under conditions similar to those of the present experiments. Because threshold for normal oscillations indicated a pump rate w about ten times the spontaneous emission rate a, we expected that peak inversion might approach 80%. This was because for a "two-level" system such as ruby,

$$n/N = (w - a)/(w + a) \quad . \tag{15}$$

The fact that n/N seemed closer to 25% than to 80% indicated (using (15) again) that the actual upper decay rate a' was about six times the spontaneous rate a.

To check this with the modified apparatus in Fig. 3, we measured the output pulse energy U when the Kerr cell was switched just after the termination of the pump pulse. We then measured the pulse energy again, but with the switching delayed another 50 μsec and found the output pulse energy would fall by about a factor of six in this 50 μsec. This meant that the fractional inversion had decreased from 25% to about 10% in 50 μsec, or that the upper level population would decrease from 5/8 N to 11/20 N. This is a fractional decrease of 12%, which indicates a decay rate of 2.5×10^3 sec^{-1}, or about eight times the spontaneous rate, thus confirming the nature of the earlier results.

The cause of this lifetime shortening has not yet been determined. Estimates of the self-induced decay from photons passing once across the crystal indicate that this effect is far too small to account for the observed shortening. The most likely explanation at this point is connected with the fact that only about one third of the cross-sectional area of the ruby is observed to emit light actively during a giant pulse. Quite possibly the active laser ions at the center lose their excitation to the less active ions at the periphery at a rate which increases with the gradient of excitation. That the center is more active probably results from (one or both of) the facts that (1) the ruby rod tends to focus the pump light into the center (Ref. 10), and (2) "whispering modes" or paths of high regeneration exist near the periphery because of total internal reflection (Ref. 11) and may hold the population excess there near zero. There is also the lesser possibility that a "whispering mode(s)" exists which extends into the center of the rod.

Experiments are being planned to verify that spatial transfer of energy takes place. It will be especially interesting to examine the mechanism and determine whether in this exchange of energy the center excitation tends to invert the periphery or only to heat it up.

3. Temporal Behavior of Giant Pulses with Various Switching Rates

A typical oscilloscope trace of output power versus time for fast switching (~ 0.005 μsec) is shown in Fig. 4. A single large pulse is observed. When the switching times were lengthened to 0.11 and 0.5 μsec, the output typically appeared as in Figs. 5 and 6, respectively. Such traces show an "after pulsing" which, from their magnitude, we can definitely associate with the giant pulse rather than with recovery to ordinary spontaneous pulsing. When coupled with the spectral results discussed in the next section, these results indicate that the R_1 line is inhomogeneously broadened. This, of course, was known from the fact that normal laser oscillation has a much broader spectrum than would

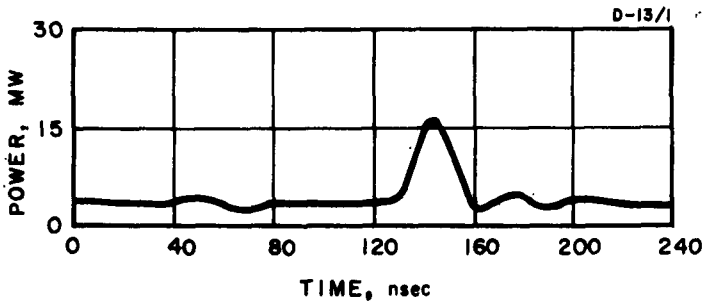

Fig. 4. Power output versus time for a typically fast (about 5 nsec) switching condition with apparatus shown in Fig. 3. Shutter opening time is at about 50 nsec. Small oscillations are electrical pickup.

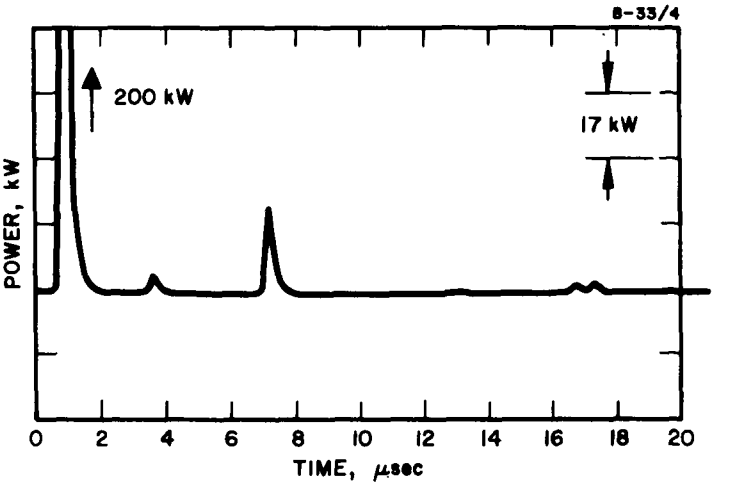

Fig. 5. Power output versus time for intermediate (0.11 μsec) switching time.

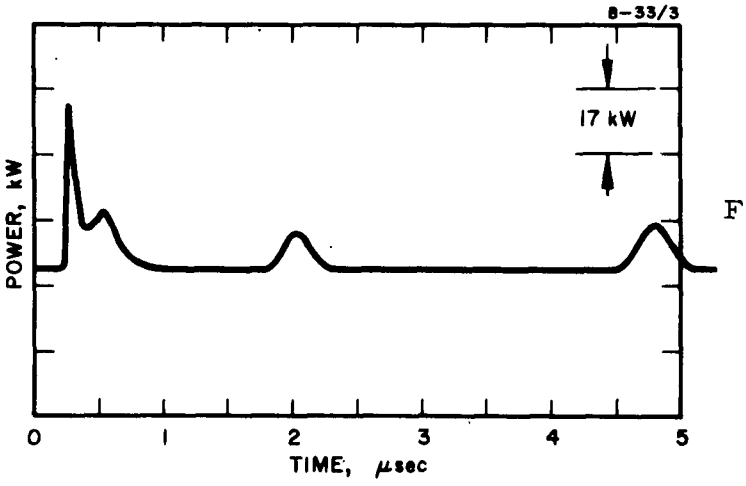

Fig. 6. Power output versus time for slow (0.5 μsec) switching time.

be the case for a homogeneous line. In Fig. 4 the pulse evidently was fast enough that the inversion was greatly reduced before transfer of energy between different wavelengths of the R_1 line (which we shall refer to as cross-relaxation) had time to play a strong role. (This cross-relaxation is doubtless related to the spatial transfer of energy discussed in Section II-C-2.) As the switching time is slowed and becomes comparable to the pulse buildup time (see Fig. 5) there is competition between cross-relaxation and light emission for the energy from the various "packets" that make up the line.

A tentative model for an "after pulse" is the following. As the losses become smaller and "meet" the gain during switching, the center of the line is "eaten out" with a burst of radiation accompanied by some transfer of energy from the wings. The losses halt at their final value, but because the switching process occurred relatively slowly, not enough photons remain in the cavity to drive the excitation much below the threshold set by the final loss value. Cross-relaxation then tries to reform the natural line shape from the considerably flattened and distorted line shape that exists at the end of the first light pulse. There is enough total population inversion remaining so that when cross-relaxation reforms the gain profile $\alpha(\nu)$ to its normal shape, the peak of the normal profile exceeds the losses and an "after pulse" is formed. The process of reformation of the normal profile can cause the gain to emerge over the losses for some time before the normal profile is actually re-established, so that a repeated after-pulsing can occur during the relaxation to the normal profile. Of course, several such processes can occur simultaneously in different parts of the line and of the crystal itself.

As the switching was slowed further, it was observed (see Fig. 6) that the "after pulsing" began sooner. This is consistent with the idea that the emission is not significantly reduced below the threshold value in the early pulse; hence the cross-relaxation recovery can cause the gain to overcome the losses even sooner because the gain has not as much to recover.

If a good theory of cross-relaxation existed, the recovery time and spacing of "after pulses" might be used to evaluate parameters. Unfortunately, the theory does not yet exist. It would appear, however, from Figs. 5 and 6 that these processes typically occur in times the order of microseconds.

4. Integrated and Time-Resolution Spectroscopy of Pulses at 6943 Å

It is to be expected that the fastest pulses would have the broadest spectrum, because each packet of the emitting line which has its gain greater than the losses tends to emit so quickly that little cross-relaxation takes place. As the switching time (and hence the time during which light is emitted) is lengthened, the wings of the line would tend to give up their

energy to the line center before having a chance to emit light and the spectrum would narrow. This tendency is illustrated in the spectra taken of giant pulses with three different switching times (and also of spontaneous pulses) shown in Fig. 7. Figure 7(d) is for 0.5 μsec switching time, but with about two thirds of the pump power for the other pulses, and it exhibits marked structure.

A second interesting feature of the spectra is the tendency to favor the long-wavelength side of the line. This tendency becomes stronger as the switching and pulse times decrease, which could be due to one of several causes: (1) a change in line shape under heavier pumping, perhaps due in part to the same processes which shorten the lifetime; (2) losses which increase toward higher frequencies; (3) asymmetric cross-relaxation; (4) shift with heating. The last possibility has been almost entirely eliminated on the basis of known temperature shifts. Symmetric cross-relaxation would tend to enhance the asymmetry of the spectrum that arose from any other cause. Experiments are being planned which would distinguish these various possibilities.

Since the R_1 line in ruby appears to be inhomogeneously broadened, there should be some characteristic relaxation time within the R_1 line. In order to make a reasonable estimate of this relaxation time, an STL image converter camera was used to look at the spectral output of the PRL. This camera, when operated in the streaking mode, is capable of time resolution of less than 10^{-9} sec.

Figure 7 has shown the time-integrated spectra of the giant pulse output under various switching conditions. The large width of the line for the fast switching case encompasses nearly the entire R_1 fluorescent line width, giving some evidence that relaxation processes occur at rates within the resolving times of fast switching pulse observation techniques. To analyze the spectrum, a Busch and Lomb dual grating 2-m spectrograph and a Fabry-Perot etalon were used. Figure 8 shows a typical Fabry-Perot spectrogram of the giant pulse; the etalon spacing is 1/2 mm, and the various photos are of selected regions on the face of the ruby with the comparison spectra of the cadmium red line through the same etalon as seen by the STL camera on a time exposure. The time duration for the streaking is 100 nsec. The tendency for the laser to "tune" to long wavelengths is clearly seen as a shift in the output wavelength, although the line is rather broad. The reason for this broadening as well as the shifting in time is not yet fully understood. A detailed series of photographs of this type was made for the various switching times, each showing that the time-integrated line width for each shutter switching time is composed of a broadening and a very fast shifting to the long wavelength side. A superposition of a normal laser action photograph on the streak of the pulsed reflector output for the slow switching case is shown in Fig. 9. The shutter timing was synchronized with the camera so that the normal

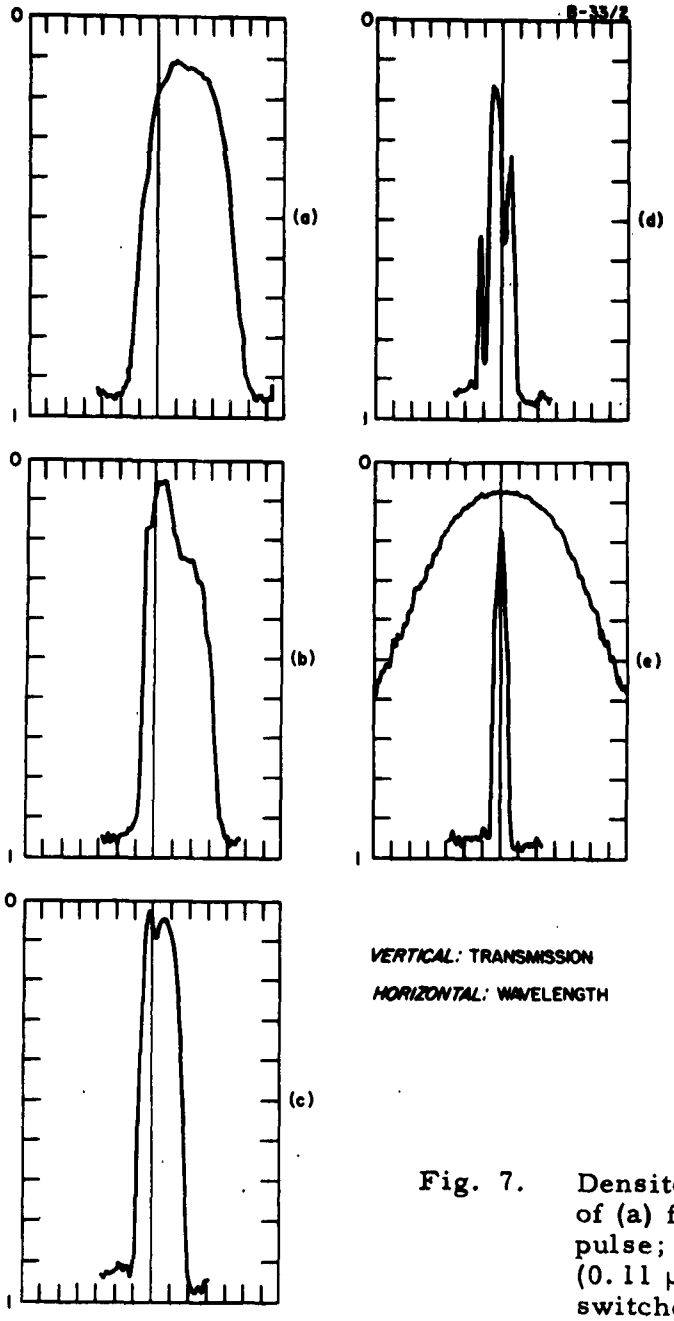

Fig. 7. Densitometer traces of the spectra of (a) fast switched (5 nsec) giant pulse; (b) intermediate switched (0.11 μsec) giant pulse; (c) slow switched (0.5 μsec) giant pulse; normal pumping (~ 10 times threshold); (d) slow switched (0.5 μsec) giant pulse under lighter (~5 x threshold) pumping; (e) spectrum of normal spontaneous pulsations superposed on normal R_1 fluorescence spectrum. All spectra taken with same beam attenuation. Eastman Kodak IIF spectral plates were used.

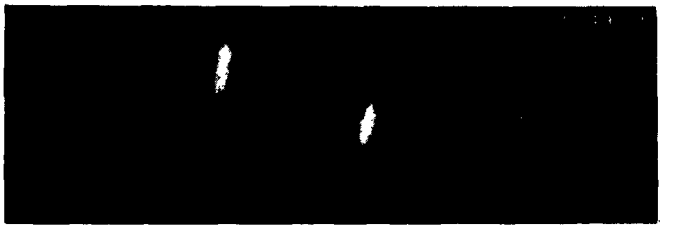

Fig. 8. Streak photographs of the PRL taken through the Fabry-Perot interferometer. The plate separation was 0.5 mm (10 cm^{-1} interorder separation $\cong$ 5 Å); the cadmium red line is shown for comparison. The streak photographs are from three different parts of the ruby crystal and show some slight variations between different areas of the crystal. The streak duration is 100 nsec.

Fig. 9. Normal laser action without streaking and streaked PRL output as seen through a 0.8-mm-separation Fabry-Perot interferometer (8.25 cm^{-1} interorder separation $\cong$ 4.12 Å). The streak duration is 200 nsec.

laser output appears directly above the giant pulse. From this picture, it can be seen that the pulsed reflector wavelength starts at the normal laser wavelength and then "tunes" toward longer wavelengths. Further work in this area has been delayed due to the temporary lack of the STL camera to continue the work.

5. Anomalous Spectra

Very recently Dr. E. Woodbury of the Hughes Aerospace Group, supported by other funding, has discovered spectral lines other than that at 6943 Å in the output of the PRL. The approximate wavelengths are reported to be 7660 Å, 8500 Å, and 9600 Å. We quickly verified this observation and proceeded on a careful investigation of these lines to determine their origin. Careful wavelength measurements showed that the series of lines were evenly spaced 1340 cm^{-1} apart on the long wavelength side of 6943 Å. The lines are relatively sharp and show the general collimation effects characteristic of the ruby laser in which they are generated. They only appear in the PRL mode of operation and then only when a nitrobenzene-type Kerr cell is used as a shutter, as can be seen in Figs. 10 and 11. Experiments with a KDP cell as a modulator have shown no trace of these other lines.

The presence of the longer wavelength lines definitely affects the power calibration of the output from the PRL, since the detectors that we have been using are actually more sensitive at these wavelengths due to lower absorption of optical attenuators used. A considerable effort is currently being put forth with Company funds to explain further this anomalous behavior in the output of the PRL. Exploitation of this effect may lead to a novel method of producing intense radiation at different wavelengths by using materials other than nitrobenzene in the PRL circuit.

6. Far Field Beam Patterns

Because it was difficult to determine relative intensities on the Polaroid film used to photograph far field beam patterns, we can only say that the beam divergence of the giant pulses under various conditions and of normal oscillations did not differ by more than a factor of two from 1 mrad.

Fast switching pulse beam patterns recorded with various amounts of optical attenuation and a normal pattern are compared in Fig. 12. Probably Figs. 12(c) and 12(d) give the closest comparison of normal and pulse beam divergence. Interesting, but comparatively low intensity, structure appears when the main beam is allowed to saturate the film as shown in Figs. 12(a) and 12(b). We suspect that this is caused by slightly misaligned dielectric interfaces within the PRL.

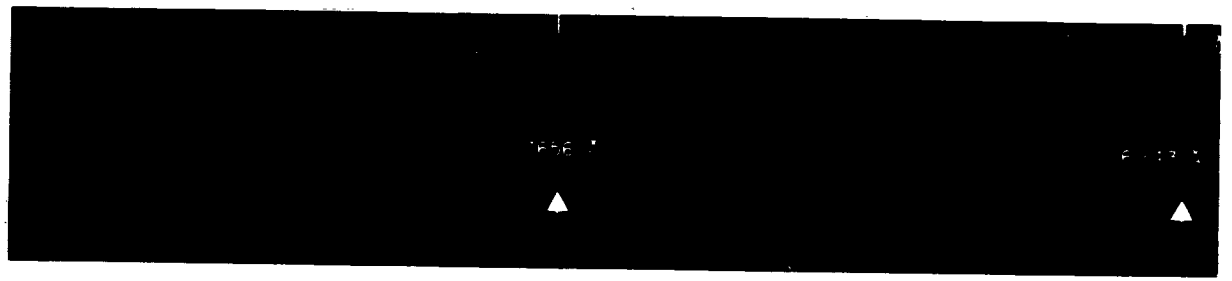

Fig. 10. The spectra of the PRL showing the satellite lines in nitrobenzene. Neon lines are shown for wavelength comparison. The wavelength span is from 6800 Å to 8000 Å.

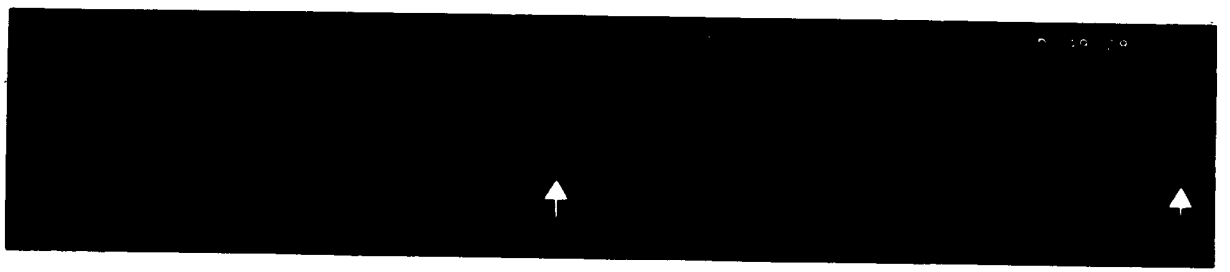

Fig. 11. The spectra of the PRL with a KDP modulator replacing the nitrobenzene Kerr cell. All other data are the same as those for Fig. 10.

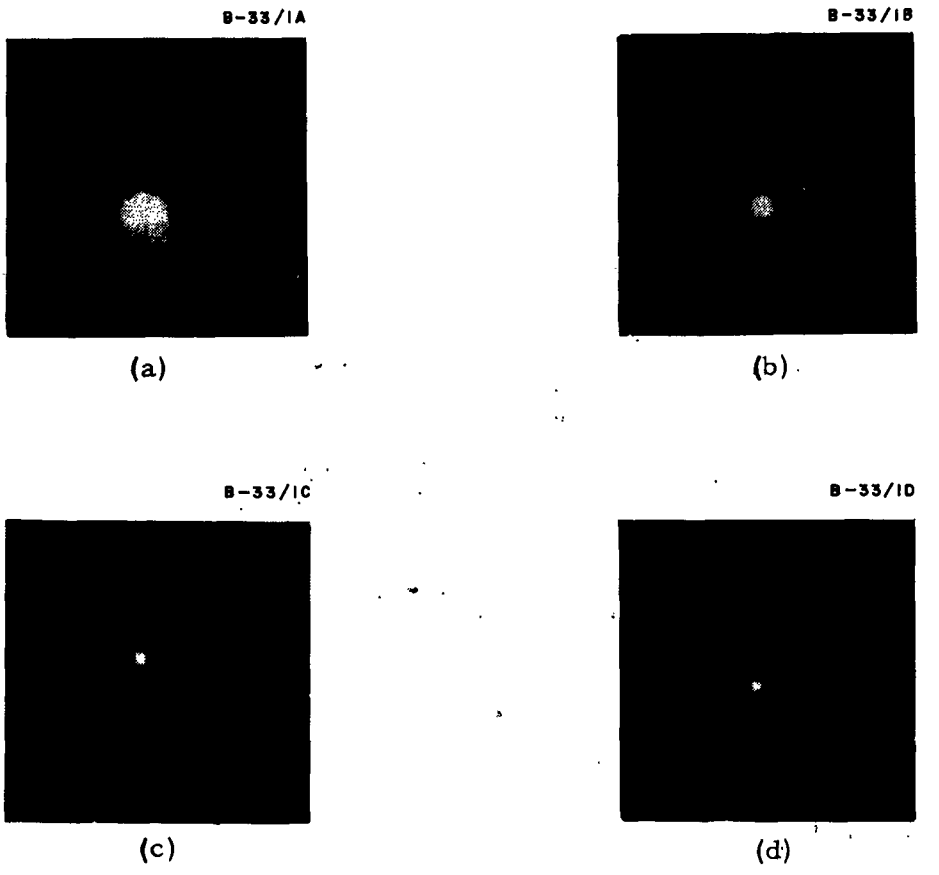

Fig. 12. Far field beam patterns of fast switching with beam attenuated by (a) 10, (b) 100, (c) 1000, (d) normal laser pattern, attenuated x 1000. (d) corresponds to 1 mrad at full width.

D. PROBLEM AREAS

All has not been easy in making the rather impressive steps forward to achieve high power pulses. The first problem that was encountered was the burning of the reflectors (see ISR No. 1). Silver reflectors, which gave no trouble at all for a conventional laser, immediately had holes burned in them when the giant pulse was produced. This burning of the reflector made reproducible operation impossible. The problem was solved by going to low-loss multilayer dielectric reflectors. However, dielectric reflectors themselves may not stand up under higher power operation. If they fail, a possible solution may be to use total internal reflection.

The next problem was to keep the detectors linear and fast enough to give accurate data. This is actually a continuing problem as we progress to operation at even higher power levels. The nonlinear optical side effects that occur with these power levels are totally new in physics, and very little is known about them. The general problem of nonlinear effects will be discussed below.

Conventional phototube detectors will give linear power measurements when operated below saturation, but the optical attenuators required may become nonlinear at high power levels. Thus different types of attenuators must be investigated for cross-checking purposes. To date, two types of neutral density attenuators have been used. The first is the neutral density gelatin filter, and the second is the metallic filter. Alternatively, the radiation can be diffusely reflected from a nonabsorbing surface. The power density in the filters can also be altered (reduced) by optically diverging the beam. Although all of the above mentioned arrangements have disadvantages, they do allow the use of fast detectors, and it is important to obtain agreement by at least two methods to show that unsuspected nonlinear effects are not present.

Several different types of calorimeters can be used for measuring total energy. At least one type of calorimeter should be constructed to check against the other types of detectors. The calorimeter has the advantage that the calibration can be effected from first principles and does not need attenuators. Another type of detector (which measures total energy in the beam) measures the light momentum (Ref. 12). A detector of this type is under construction at the Hughes Research Laboratories, but no tests have been made on it as yet. If the energy measuring devices are coupled to a fast uncalibrated but linear detector, the pulse waveform can be obtained, from which the peak power can be calculated.

As previously mentioned (ISR No. 3) when a high-quality low-loss polarizing prism, such as the calcite Glan-Thompson prism, was introduced

into the laser cavity, the giant pulses immediately caused significant damage to the cemented layer. The mechanism of this damage is not really understood, although it appears that it may be dielectric breakdown due to the high (optical frequency) electric fields present. It is also possible that the damage is merely caused by burning due to the absorption of energy. Other effects could cause the damage, but these are primarily nonlinear effects.

Several approaches to obtain a polarizing prism that will withstand the high powers present have been evaluated. Since the damage was in the cementing layer between the halves of the Glan-Thompson prism, the solution was to eliminate the cementing layer. There is an airspaced version of the Glan-Thompson prism called the "Glan prism." Unfortunately, this prism has a relatively higher internal reflection loss than the Glan-Thompson type. As a result of this loss, the pulsed-reflector-system performance was degraded.

A satisfactory replacement for the Glan-Thompson polarizing prism has been found. An examination of the damage reported in the Glan-Thompson prism (see ISR No. 3) showed that it was the cemented region between the two halves of the prism that had been burned. This same general burning has also been observed in conventional optical materials that are cemented together. The search for better cements has not progressed far enough yet to say that cements, as such, cannot be used. Some effort is still being made to find a suitable cement. The only successful results in the search for a low-loss polarizing material that will withstand the condition in this application have been obtained with optically contacted polarizing prisms. The type of prism that has been suitable is the Wollaston prism, a "split-image" type of prism rather than one which will absorb (or reflect) the undesired polarization of the light.

In the Wollaston prism the light is refracted differently for the two different polarizations. When the Wollaston prism is used in the PRL as a polarizing prism, it is properly oriented so that all of the light having the desired plane of polarization is refracted into only one direction, and the reflectors are then aligned in this direction. The Kerr cell will then operate in the same manner as with the Glan-Thompson prism. Laser action is suppressed by introducing an angular misalignment in the system when the plane of polarization is rotated by the Kerr cell. When the voltage is removed from the Kerr cell, the system will be in the proper alignment for high regeneration in the laser and "giant pulses" will be produced in the same manner as that reported in ISR's No. 1, 2, 3, and 4.

Optically contacted Wollaston prisms are more difficult to fabricate than cemented prisms, particularly when very low loss prisms are required. However, the results obtained so far indicate that the

Wollaston prism can be constructed so that the system performance is the same as that with the Glan-Thompson prism. Of course, there would be requirements on the angular deviation between the two beams of light in the Wollaston prism. Two Wollaston prisms have been tried, one with 42-min deviation and the other with 1.7° deviation. The 42-min deviation prism worked satisfactorily, although there were some rather weak secondary spots in the far field beam pattern which possibly resulted from the relatively low deviation in the prism. The 1.7° prism had more loss and, as a result, the system performance was degraded. However, the far field beam patterns were better than with the 42-min prism. It appears that the polarizing prism problem has been solved by a material that is capable of operation as long as the ruby itself will work.

The anomalous spectra mentioned above tend to limit the 6943 Å power output of the ruby PRL and may pose a severe limitation for systems applications. Operation of the PRL with a KDP shutter circumvents this difficulty.

III. GENERAL INVESTIGATION OF THE RUBY LASER

This phase of the program was concerned with the general investigation of the ruby laser. The spectroscopy of the ruby laser as previously reported (ISR's No. 2, 3, and 4) is summarized and reported in detail. A composite theoretical and experimental study of the oscillation threshold dependence on the various laser parameters is reviewed (ISR's No. 1, 2, 3, and 4), and additional information is given on the temperature dependence of oscillation threshold. The pumping requirement for room-temperature cw operation of ruby is determined in terms of a physically meaningful quantity, the product of energy density and pumping pulse length. Unsuccessful attempts at room-temperature cw operation are described. An extension of the threshold calculations to the dependence of energy output on the various laser parameters gives qualitative agreement with experiment and facilitates the optimization of a given laser configuration. Optimization of a pulsed ruby laser configuration to 16 J energy output is reported.

A. SPECTRAL ANALYSIS AND MODES OF A RUBY LASER

It is well known that the resonant cavity employed in laser oscillators is a very high order cavity, i.e., its dimensions are large compared with the wavelength of the radiation emitted. To obtain an order-of-magnitude estimate of the frequency separation between the various modes, we assume that the normal modes of an optical resonator are similar to those of a cylindrical microwave cavity. We then have for the frequencies of the normal modes

$$\bar{\nu} = \frac{1}{\sqrt{\epsilon}} \frac{p}{2l} \left[1 + \frac{1}{2} \frac{\beta_{mn}^2 d^2}{p^2 \pi^2} \right], \qquad (16)$$

where

$\sqrt{\epsilon}$ ≡ index of refraction of material inside the resonator

$\bar{\nu}$ ≡ frequency in wave numbers

l ≡ length of the resonator

β_{mn} ≡ transverse propagation constant

p ≡ axial mode index.

It should be noted that it is not necessary for all three mode indices to be large numbers. Thus, under ordinary circumstances, in an optical resonator the axial mode index p is very high (of the order of 10^5), while the other indices m and n are very much lower and sometimes may be the first few integers.

The frequency separation between the modes is

$$\Delta\nu = \frac{1}{2\sqrt{\epsilon}\,\ell}\,\Delta p + \frac{\ell}{4\sqrt{\epsilon}\,p\pi^2}\left(\beta_{mn}^2 - \beta_{mn}'^2\right), \quad (17)$$

from which it follows that for a 3-mm by 1-in. ruby, for example, the separation between two modes with $\Delta p = 1$ is approximately 0.11 cm^{-1}, while that between two adjacent modes with different β's is approximately 10^{-3} cm^{-1}. Thus, it becomes convenient to speak of longitudinal modes (distinguished by p indices) and transverse modes (distinguished by m, n indices) independently.

In principle, each mode has a relatively high Q, and therefore the corresponding line widths are very narrow. However, it is now well known that under ordinary circumstances the laser output consists of recurring pulses each of $\sim$ 1 μsec duration. This pulsating character is also observed in the only reported continuously operating ruby laser which works at liquid-nitrogen temperature (Ref. 13). Thus, aside from all other line-broadening effects, such as temperature shifts, the pulsations limit the minimum line width to approximately 1 Mc. It is worth mentioning, however, that in some cases smooth output is obtained from lasers at low temperature, as shown in Fig. 13. This suggests that spiking may be related to the lack of pump po r in both the room-temperature pulsed laser and the low-temperature c ntinuous laser.

1. Longitudinal Mode Studies

a. Room-Temperature Experiments

In room-temperature studies, the longitudinal mode structure of several ruby lasers was examined using a Fabry-Perot interferometer. The ruby samples used were 3-mm by 1-in. and 3-mm by 1-cm rods of 0.05% Cr^{3+} concentration. The c-axis was oriented along the cylinder axis within approximately 1°. Some of the most important results are shown in Figs. 14 through 16. It can be seen from Fig. 14 that three longitudinal modes appear in the case of the 1-in. ruby, even very close to threshold, where there is only one oscillation spike in the output. On the other hand, in the case of the 1-cm ruby, a single longitudinal mode appears, even for pumping power 10% above threshold. The reasons for the dependence of the number of longitudinal excited modes on the length of the cavity are not quite clear at present. Wagner and Birnbaum's (Ref. 14) analysis of quantum oscillators in a multimode cavity implies that for the case of a thermally broadened fluorescent line, very short cross-relaxation times within the line, and weakly coupled modes, only one longitudinal mode should be excited. If, on the other hand, we assume the cross-relaxation time to be relatively long (of the order of microseconds), we may argue as follows: Using (16), we find that the number of modes per unit λ per unit length is given by

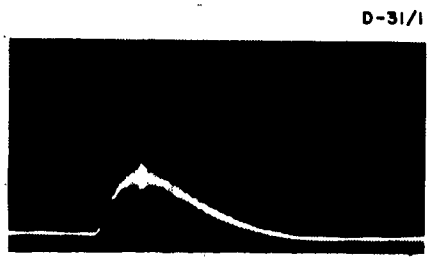

Fig. 13. Output of a ruby laser at low temperature. Note absence of highly pronounced spiking usually observed at room temperature. Sweep speed is 200 μsec/div.

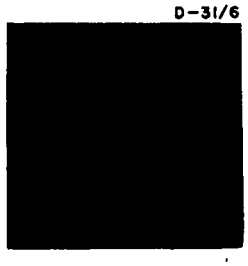

Fig. 14. Fabry-Perot analysis of the laser output at room temperature. Fabry-Perot order separation = 0.513 cm^{-1} (plate separation 0.975 cm). Sample: 3-mm by 1-in. silvered optical resonator (longitudinal mode separation = 0.111 cm^{-1}). Operation near threshold.

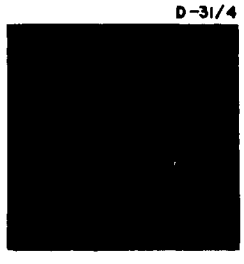

Fig. 15. Fabry-Perot analysis of the laser output at room temperature. Fabry-Perot order separation = 0.513 cm^{-1} (plate separation 0.975 cm). Sample: 3-mm by 1-cm silvered optical resonator (longitudinal mode separation = 0.281 cm^{-1}). Operation near threshold.

Fig. 16. Fabry-Perot analysis of the laser output at room temperature. Fabry-Perot order separation and sample same as in Fig. 15. Operation ~ 10% above threshold.

$$\frac{1}{\ell}\,\frac{dN}{d\lambda} = \frac{-2\sqrt{\epsilon}}{\lambda^2} \quad . \tag{18}$$

Therefore, at room temperature, the number of axial modes within the fluorescent line width (4Å) per centimeter of cavity length is

$$\frac{N}{\ell} = \frac{1}{\ell}\,\frac{dN}{d\lambda}\,\Delta\lambda = 28 \text{ modes}/4\text{Å}/\text{cm cavity length.} \tag{19}$$

Thus, in ruby, there are many cavity modes within the line width of the transition in which we wish to induce emission (Fig. 17). The Q of the individual modes is the same to a few parts in 10^4; hence there is no a priori preference by the ruby system to oscillate in a particular mode. It therefore seems reasonable to expect the ruby laser to act as a multimode oscillator.

Experimental results indicate that at higher input energies additional longitudinal modes are excited, possibly because the gain increases at the higher pumping levels and, in fact, may become large enough to sustain oscillation in the modes which are farther removed from the center transition frequency. However, this argument does not seem to account in full for the appearance of three longitudinal modes right at threshold in the case of the 1-in. ruby and of only one longitudinal mode 10% above threshold in the case of the 1-cm ruby.

Thus, neither analytical approach seems to give results in complete agreement with the experimental ones. There are, however, indications that the observed behavior is related to the inhomogeneous broadening of the fluorescent line (typically $\approx 0.1\ \text{cm}^{-1}$) and that the R_1 transition at room temperature is an unresolved doublet. The ground-state splitting of $0.38\ \text{cm}^{-1}$ (see Figs. 18 and 19) causes the gain function (negative absorption coefficient) to have two maxima separated by $0.38\ \text{cm}^{-1}$. Thus a mode separation $\Delta\overline{\nu} \gtrsim 0.4\ \text{cm}^{-1}$ should assure single mode operation at threshold for room-temperature ruby lasers. This implies crystals of length $\ell \lesssim 0.5$ cm, which is impractical from pumping considerations (see Section III-B).

b. Low-Temperature Experiments

Before discussing the low-temperature experiments, we should note that both the fluorescent transition frequency and the fluorescent line width in ruby depend significantly on temperature. The temperature dependence of the line width and the transition frequency in a particular ruby sample are shown in Fig. 18. There is a pronounced shift toward the violet with decreasing temperature. The splitting observable at 78° and 4.2° K is the ground-state splitting of $0.38\ \text{cm}^{-1}$ (11.4 Gc)

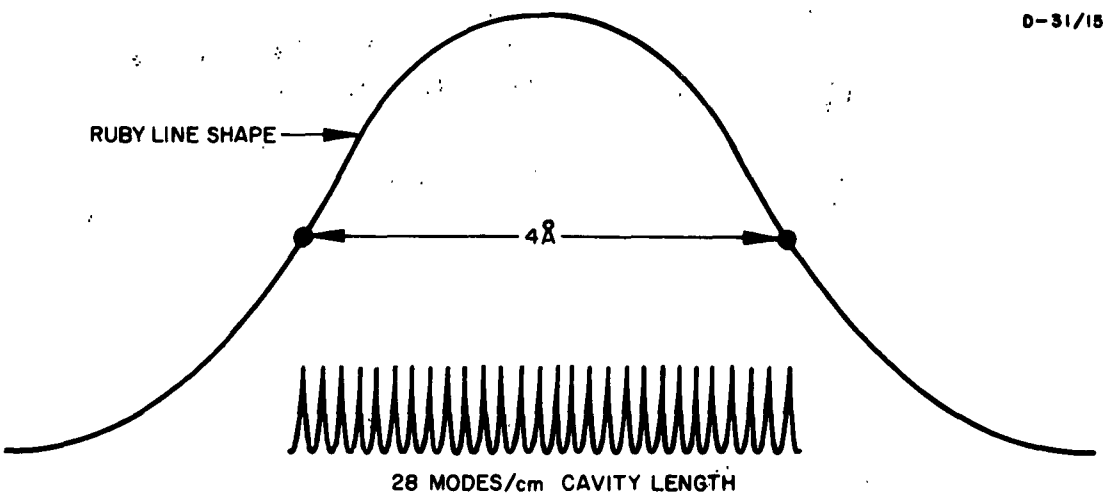

Fig. 17. Ruby line shape at 300°K and longitudinal cavity mode structure.

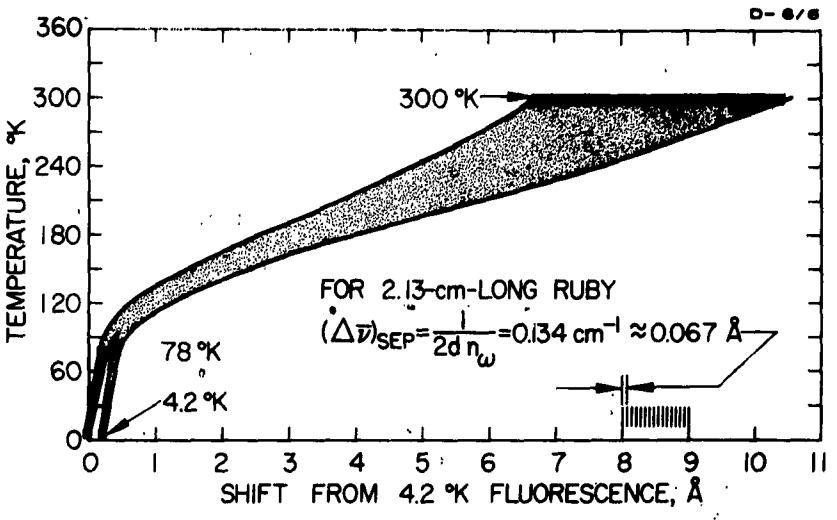

Fig. 18. Spectral shift and width of R_1 fluorescence versus temperature.

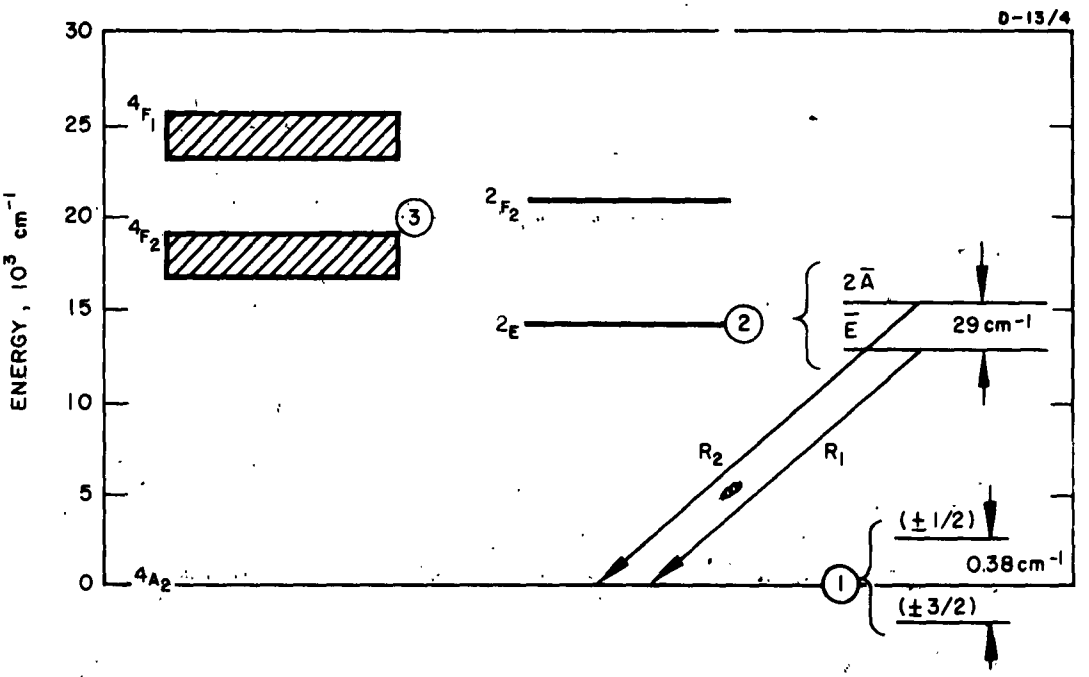

Fig. 19. Energy-level diagram for ruby showing the ground-state splitting.

into the $\pm 1/2$ and $\pm 3/2$ levels of the $^4A_2$ ground state (see Fig. 19). Measurement of the line widths at 4.2° and 300° K indicate that the transition line width changes by a factor of about 100 over this temperature range. Below 78° K, the number of cavity modes per centimeter length of cavity within the transition line width is less than two; therefore, the spectral character of the stimulated emission will be determined to a great extent by the transition itself.

It is extremely important in the ruby system that two transitions are involved in the R_1-line fluorescence. At temperatures below about 80° K, it becomes obvious that R_1 is a doublet, but the separation is masked by the line width at 300° K (see Fig. 18). The two transitions are identified as $\bar{E}\,(^2E) \rightarrow {}^4A_2\,(\pm 3/2)$ and $\bar{E}\,(^2E) \rightarrow {}^4A_2\,(\pm 1/2)$ Fig. 19). The transition probability for the $\rightarrow(\pm 3/2)$ transition is 3/2 that for the $\rightarrow(\pm 1/2)$ transition (Ref. 15). Because of the higher probability for the $\bar{E}\,(^2E) \rightarrow {}^4A_2\,(\pm 3/2)$ transition, in stimulated emission experiments we would expect the oscillation threshold for this transition to be less than that for the other.

Ruby can be considered as two three-level systems which are coupled through a ground-state relaxation mechanism. The relaxation time T_1 (time required for the ground levels to thermalize) is an extremely sensitive function of temperature, varying from about 10^{-8} sec at 300° K to about 10^{-1} sec at 4.2° K. This relaxation mechanism, if fast compared with the rate of populating (pumping into) the $\bar{E}\,(^2E)$ level, will in fact prevent the $\bar{E}\,(^2E) \rightarrow {}^4A_2\,(\pm 1/2)$ transition from being stimulated into emission in the presence of stimulated emission at the $\bar{E}\,(^2E) \rightarrow {}^4A_2\,(\pm 3/2)$ transition (if the induced emission rate is assumed to be infinitely fast). At 4.2° K we would expect both transitions to be seen in stimulated emission.

Most of the low-temperature experiments were performed with a 3/8- by 9/10-in. ruby cylinder of about 0.05% Cr^{3+} concentration. The optical axis of the crystal was oriented at 90° with respect to the cylinder axis. The cylinder was fabricated from a specially grown, 90° oriented Linde boule. The details of these experiments are described in Refs. 16 and 17. The following are some of the interesting results of this study: At approximately 130° K, the laser was found to oscillate in three modes when pumped near threshold (Fig. 20(c)). At approximately twice threshold pumping, an additional mode was excited and a continuous background was evident (Fig. 20(d)).

At 78° K (liquid-nitrogen temperature), the output consists of stimulated emission from the $\bar{E}\,(^2E) \rightarrow {}^4A_2\,(\pm 3/2)$ and the $\bar{E}\,(^2E) \rightarrow {}^4A_2\,(\pm 1/2)$ transitions. The output consists of two doublets, and the separations are as indicated in Figs. 20(e) and (f) and Fig. 21. A reasonable interpretation of these results is that each transition oscillates at its center frequency (Fig. 21,a and b); because of the finite line width, the transitions are also induced into oscillation in axial cavity modes (Fig. 21, c and d). The axial mode picture for this situation is as indicated

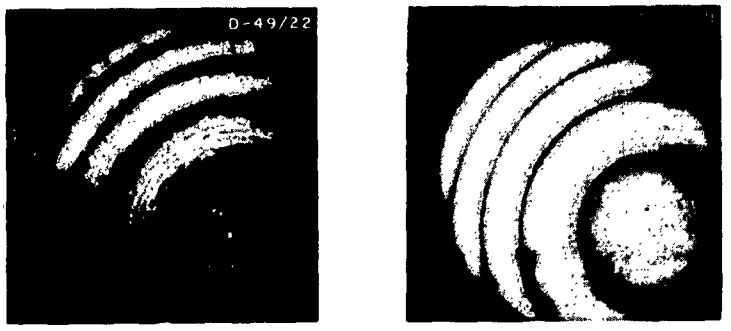

(a) Room temperature (300°K) stimulated emission at 1.05 times threshold pumping.

(b) Room temperature (300°K) stimulated emission at twice threshold pumping.

(c) 130°K stimulated emission at threshold pumping.

(d) 130°K stimulated emission at twice threshold pumping.

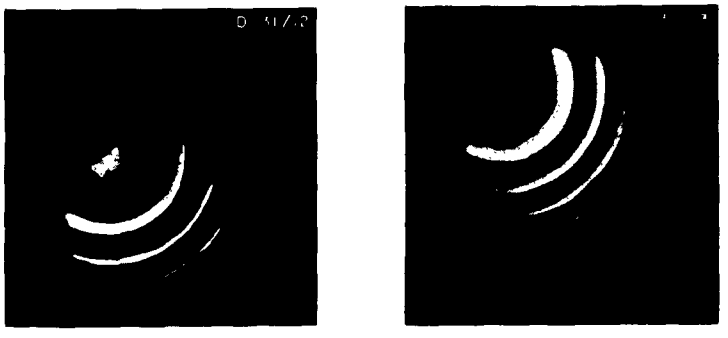

(e) 78°K stimulated emission; pumping level slightly above oscillation threshold for $\bar{E}(^2E) \rightarrow \pm 3/2(^4A_2)$ transition.

(f) 78°K stimulated emission; pumping level 1.1 times (e) at approximate oscillation threshold for $\bar{E}(^2E) \rightarrow \pm 1/2(^4A_2)$ transition in the presence of stimulated emission at $\bar{E}(^2E) \rightarrow \pm 3/2(^4A_2)$ transition.

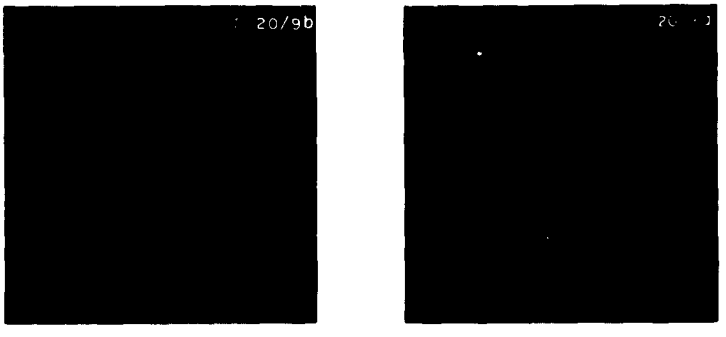

(g) 4.2°K stimulated emission; approximate oscillation threshold for $\bar{E}(^2E) \rightarrow \pm 3/2(^4A_2)$ transition. (Note threshold for $\rightarrow \pm 1/2 \approx 1.05$ x g.)

(h) 4.2°K stimulated emission; pumping level 1.2 times (a) showing both transitions in stimulated emission. The broadening is a result of thermal shift during the period of stimulated emission.

Fig. 20. Fabry-Perot spectrograms for a 2.13-cm-long ruby at different temperatures.

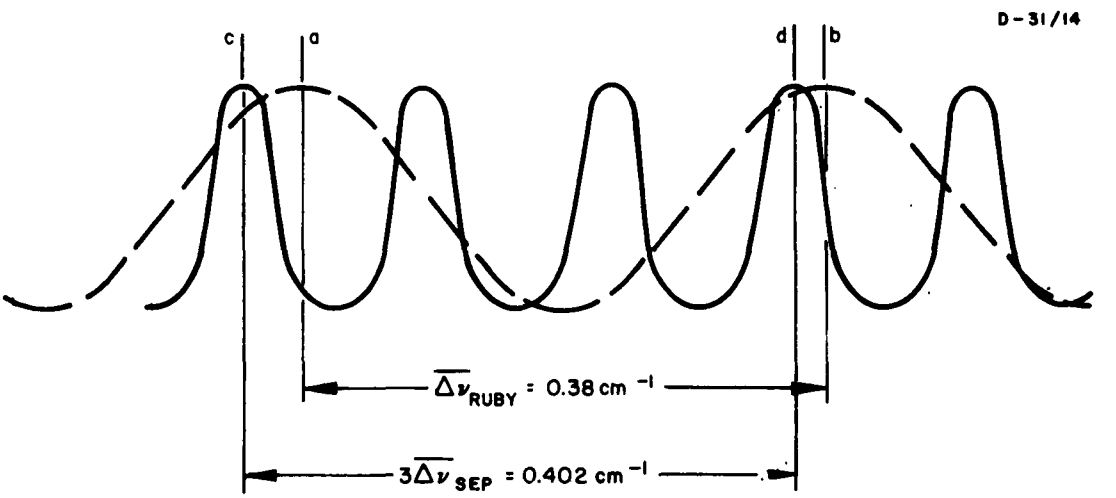

Fig. 21. Ruby line shape and cavity modes at 78°K.

in Fig. 21, the dashed lines showing the line shape and center frequencies (c, d) of the two transitions involved. The gain in the axial modes, although somewhat less than that at the center frequency of the transition, is still sufficient to overcome circuit losses and sustain oscillation. At the center of the transition, the off-axis mode Q is somewhat less; however, the higher gain here allows oscillation to be sustained.

The difference in oscillation threshold for the two transitions is shown most dramatically in Figs. 20(e) and (f). Exposure 20(e) was taken slightly above oscillation threshold for the $\overline{E}\,(^2E) \rightarrow {}^4A_2\,(\pm 3/2)$ transition; exposure 20(f) was taken at 1.2 times this energy input, slightly above oscillation threshold for the $\overline{E}\,(^2E) \rightarrow {}^4A_2\,(\pm 1/2)$ transition. The 20% difference in oscillation threshold for the two transitions is attributed to the T_1 relaxation between the $(\pm 3/2)$ and $(\pm 1/2)$ levels of the $^4A_2$ ground state. T_1, the relaxation time between the $(\pm 3/2)$, $(\pm 1/2)$ levels, is about 200 μsec at 78° K.

At 4.2° K, where the $(\pm 1/2)$ and $(\pm 3/2)$ levels of $^4A_2$ are essentially uncoupled, both transitions oscillate at their respective center frequencies with near equal oscillation thresholds (Figs. 20(g) and (h)).

2. Transverse Mode Studies

It was found that by operating a ruby laser sufficiently close to oscillation threshold (~1% above threshold) and using a high-quality crystal, it is possible to photograph symmetrical beam intensity variations across the partially transmitting face of the laser crystal (Ref. 18 and ISR No. 3). This sheds considerable light on the field distributions inside the optical resonator. It was observed that the patterns of intensity variation very closely resemble those observed in optical fibers (Ref. 19) and are reminiscent of the oscillation modes of a cylindrical microwave cavity. It is believed that these intensity variations are very closely related to the transverse modes of the optical resonator.

Experiments were performed using an elliptical pumping configuration with a xenon flash lamp similar to the EGG FX-1, but with its active length reduced to 2 in. Ruby samples having a 0.05% Cr^{3+} ion concentration and exhibiting an intrinsic (inhomogeneously broadened) line width of approximately 0.15 cm^{-1} were used. The samples and optical resonator configurations are summarized below. In all samples the c-axis was oriented along the cylinder axis within approximately 1°; the faces were flat and parallel within 10 μin.

Diameter, mm	Length	Type of Reflector	Reflector Transmission,	Remarks
3	1 in.	silver on ruby faces	0, 3.5	Two samples used
2	1 in.	silver on ruby faces	0, 3.5	
3	1 cm	silver on ruby faces	0, 3.5	
2	1.25 in.	silver on ruby faces	0, 8.5	Sapphire sheath 5-mm outside diameter
3	1 in.	detached silvered reflectors, 4.6 in. apart	5, 5	Ruby faces antireflection coated

Two approaches to the problem of determining the nature of the patterns have been used: (1) determination of the coherence properties of the emitted light, and (2) correlation of the patterns with the frequency spectrum of the laser output. Some of the experimental results are shown in Fig. 22. All the patterns shown in this figure were obtained using the 3-mm by 2.54-cm silvered sample; however, very similar patterns were obtained with the other samples and configurations tabulated above. In some cases we have attempted a tentative identification of the modes. This was done by comparing our patterns with those obtained in optical fibers by Snitzer and Osterberg (Ref. 19). It was found that the patterns could be altered by rotating the ruby around its own axis, thus changing the distribution of the pumping light intensity around the periphery of the rod. Simple polarization experiments indicated that patterns with only a two-fold symmetry axis are linearly polarized, whereas others are unpolarized. The pattern sizes were found to range between approximately 170 and 850 μ. Within the present accuracy of our measurements (10 to 15%), we found that the spot size is independent of the radius of the resonator, but is roughly proportional to the square root of the resonator length. This result is in qualitative agreement with the formula for "spot size" derived by Boyd and Gordon (Ref. 20) for the case of a confocal resonator. Such agreement is somewhat surprising since their analysis is not directly applicable to our case of a plane parallel resonator.

Careful measurements of the divergence of a laser beam radiated in a two-lobe pattern indicated that the angle of divergence between the two maxima is not constant close to the ruby (within approximately 20 cm in our case — see Fig. 23). In these experiments, we used a sapphire-clad ruby rod 3.23 cm long by 2 mm in diameter. The separation between

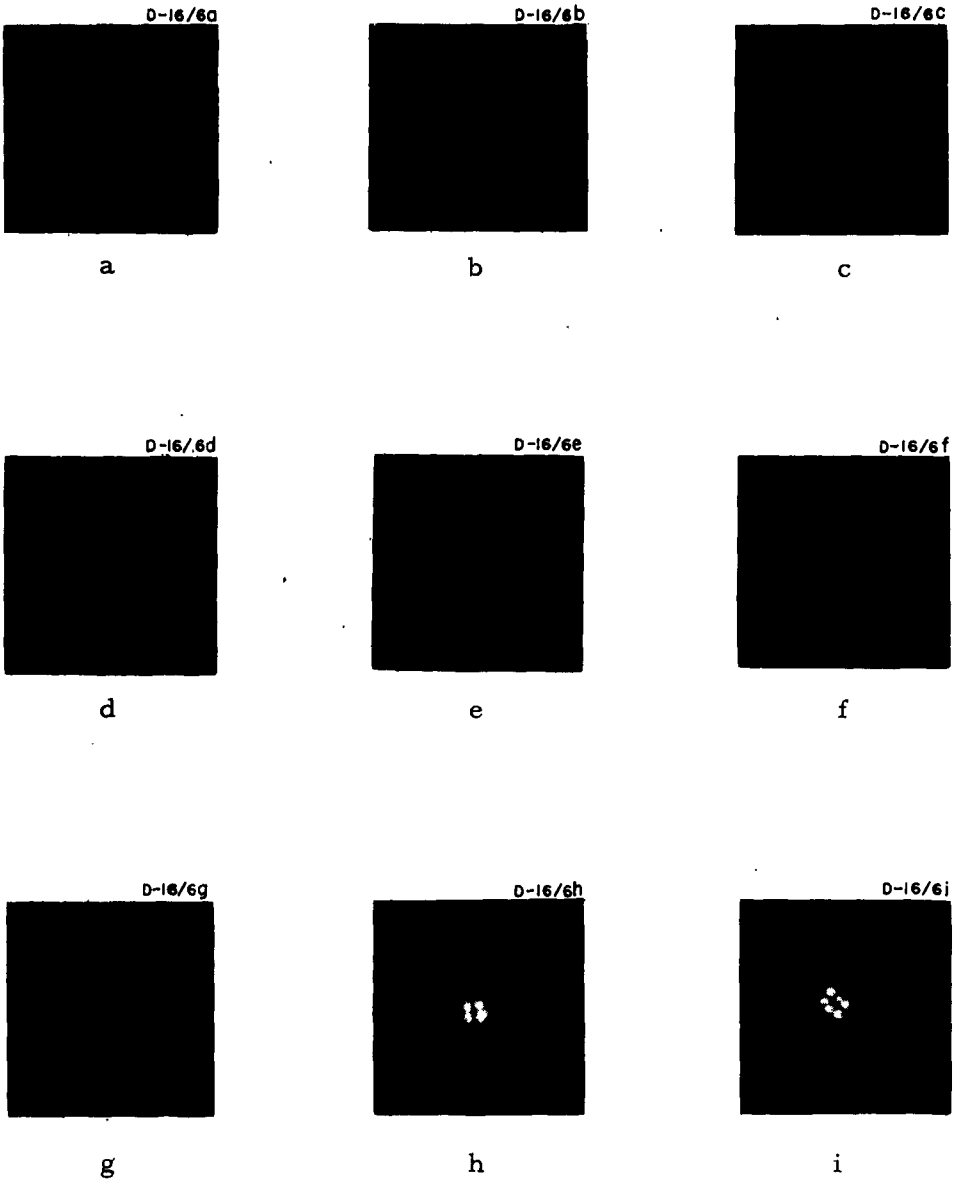

Fig. 22. Photographs of the end of a 3-mm by 2.54-cm ruby showing some of the typical transverse mode patterns. Modes are tentatively identified (Snitzer's notation) as follows: (a) HE_{11}; (b) mixture of TE_{01} or TM_{01} with HE_{21}; (c) mixture of EH_{11} or HE_{31} with HE_{12}; (d) mixture of TE_{02} or TM_{02} with HE_{22}; (e) → (i) not identified.

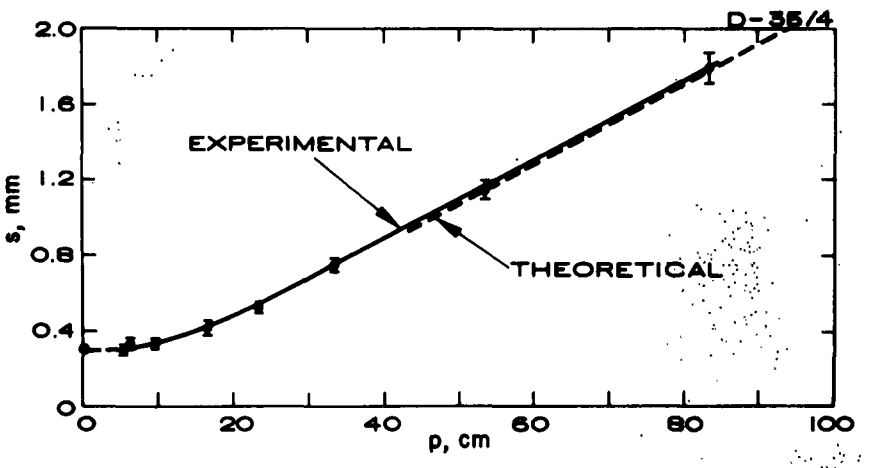

Fig. 23. Separation s between the two maxima of a two-lobe pattern as a function of distance p from the ruby face.

the maxima at the face of the ruby was approximately 300 μ. Within the accuracy of the measurements, the beams start out parallel to each other and then begin to diverge; in the far field they diverge at a constant angle of approximately 2.14 mrad.

Such behavior suggests that interference may be taking place between the beams radiated from the two parts of the pattern. To verify this hypothesis by computation, we assumed that the two-lobe pattern could be simulated by two apertures radiating constant amplitude plane waves 180° out of phase. We assumed the separation between the centers of the apertures to be 300 μ and the radius of each aperture to be 100 μ. We then performed the intermediate- and far-field Fraunhofer diffraction and interference calculation for this model. The predicted divergence of the pattern maxima was found to agree very well with that observed, as is shown in Fig. 23.

This agreement is a very strong indication that the two parts of the pattern are highly coherent and radiate 180° out of phase; these are characteristics of a simple transverse oscillation mode (Ref. 21). The intensity variation in the beam cross section 50 cm away from the ruby was also calculated and is shown in Fig. 24. The calculation predicts secondary intensity maxima which we have not been able to observe. However, it should be noted that a 15% error in the estimate of the aperture radius can change the magnitude of this maximum by a factor of approximately 2.5. Gradual intensity variations in the pattern may also significantly affect the secondary maxima. Thus, it is possible that the secondary maxima are nonexistent or unobservably small.

We also measured the divergence angle of a somewhat more complicated pattern (Fig. 25) and found it to be approximately 3.4 mrad. This may explain the commonly observed increase in the divergence angle with pump power (Refs. 17 and 22) since increased pump power implies excitation of more complicated patterns (Ref. 18).

Spectral analysis of the output of a laser has been performed using a Fabry-Perot interferometer and a traveling-wave phototube. Fabry-Perot analysis showed no correlation between the number of longitudinal modes excited and the emission patterns (Ref. 18).

The photomixing experiments were performed using an S-band traveling-wave tube with an oxide cathode. As in the beam divergence experiments, a sapphire-clad ruby rod 3.23 cm long by 2 mm in diameter (longitudinal mode separation $\sim 0.087\ \text{cm}^{-1} \approx 3$ Gc) was used. It was found that rf output was always present on the first laser oscillation spike, indicating that oscillation always starts in several adjacent longitudinal modes. Most of the experiments utilized the dc beats technique developed by McMurtry and Siegman (Refs. 2 and 23). However, in addition to analyzing the frequency content, we have simultaneously looked at the emission pattern, using both a still camera and an STL fast camera.

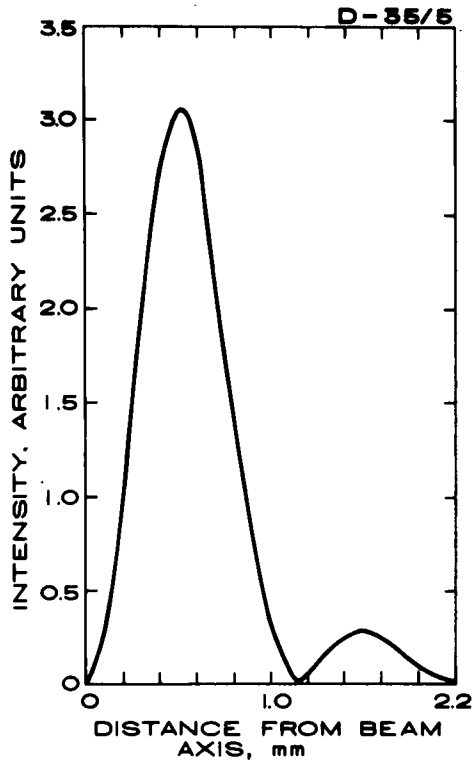

Fig. 24. Computed intermediate-field intensity distribution for a two-lobe pattern at 50 cm from ruby face.

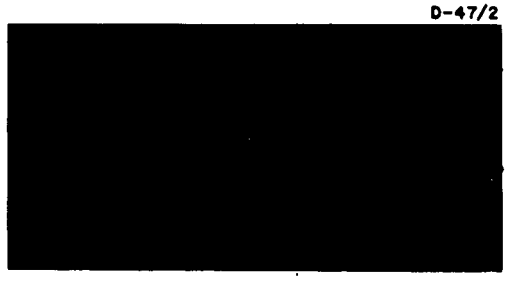

Fig. 25. Emission pattern showing greater far field divergence angle (approximately 3.4 mrad) between the principal maxima than that resulting from the two-lobe pattern.

A marked difference in behavior was found between operation near threshold and that a few percent above threshold. Figure 26 shows typical behavior near threshold. The pattern, two-lobe in this case, generally does not change throughout the output. Also, if the beat frequency changes at all, it changes only slightly; we have never observed changes exceeding ~2 Mc. (In Fig. 26 the change is ~ 1.5 Mc.) On the other hand, if the laser is driven ~ 10% or so above threshold, the pattern often changes from spike to spike (Fig. 27). Sometimes this is accompanied by fairly sudden and substantial frequency shifts; for example, in Fig. 27 the frequency shift is 5 to 6 Mc. More often, however, we observed little or no frequency change as the patterns shift, as shown in Fig. 28.

The following tentative model may be helpful in an attempt to understand these results. We assume that there are several transverse modes associated with each longitudinal mode index (Fig. 29). Near threshold we can assume that the laser oscillates in a certain set of modes (a). However, as pumping increases two kinds of mode hopping become possible: (1) from (a) to (b), which is accompanied by a change in pattern but not in beat frequency; and (2) from (a) to (c), which is accompanied by both a change in pattern and in beat frequency. However, most of the frequency shifts that we have observed were small (of the order of 2 Mc). Only in a few cases were the shifts 5 or 6 Mc. Additional data are therefore needed to verify the above model.

We have never been able to observe a pa tern change within a spike. However, since rather definite shifts in the beat frequency within a spike were sometimes observed, we assume that correspondingly fast changes in patterns are also possible.

B. OSCILLATION THRESHOLD CONSIDERATIONS

1. Effects of Cr^{3+} Concentration, Temperature, Sample Size, and Losses on Oscillation Threshold

a. Analysis

In the design of a ruby laser, one may control, among others, the following parameters related to the ruby sample: Cr^{3+} ion concentration, the sample diameter and its length, and the reflectivity of the cavity end plates. It is therefore of interest to study the effects of these parameters on the laser oscillation threshold. Briefly, the effects to be considered are the following: (1) As the Cr^{3+} ion concentration is lowered, the gain per passage through the ruby decreases and losses become more difficult to overcome, thus increasing the threshold. (2) As the operating temperature of the ruby is decreased, the transition cross section increases, resulting in increased gain and reduced threshold. (3) As the length of the ruby sample is increased, the gain increases, again decreasing the threshold. (4) The decrease in the reflectivity of the cavity end plates implies increased losses and

Fig. 26. Output characteristics near threshold. No change in pattern from spike to spike; frequency shifts $\leq$ 1.5 Mc.

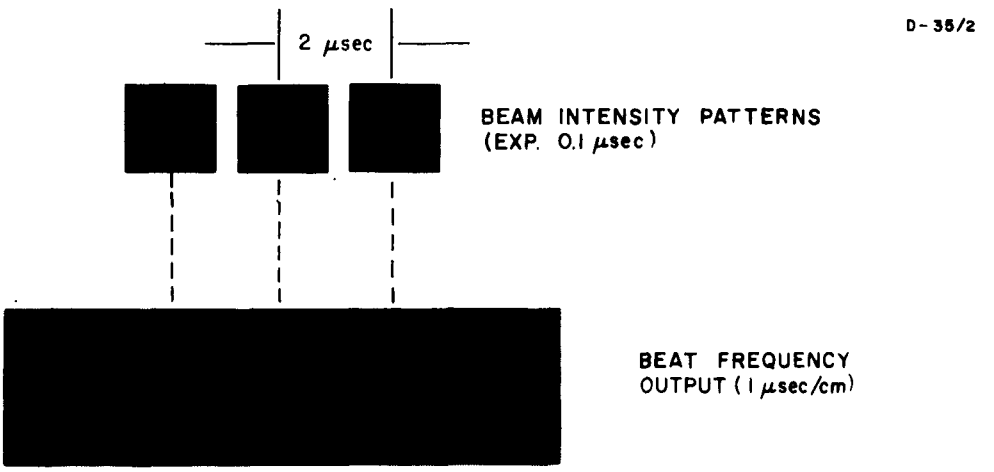

Fig. 27. Output characteristics approximately 10% above threshold. Patterns change from spike to spike; frequency shifts approximately 5 to 6 Mc.

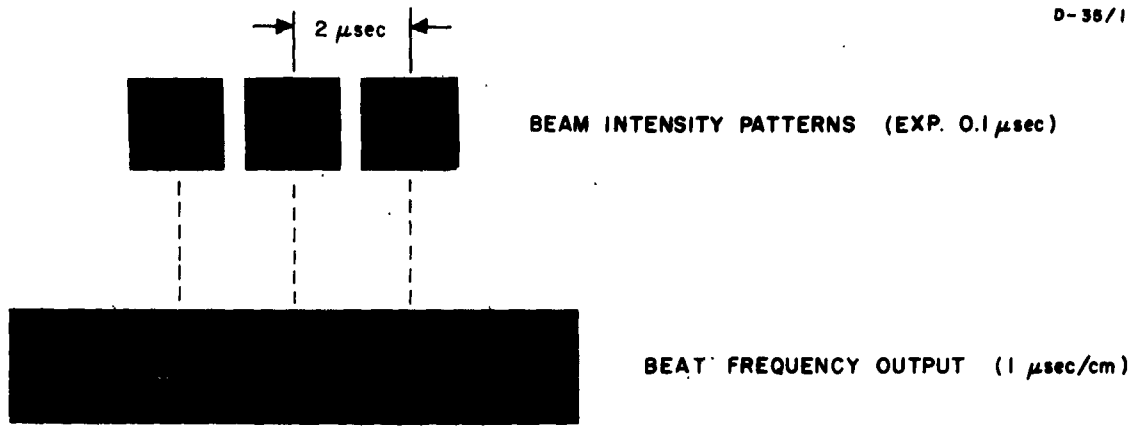

Fig. 28. Output characteristics approximately 10% above threshold. Patterns change from spike to spike; frequency shift < 2 Mc.

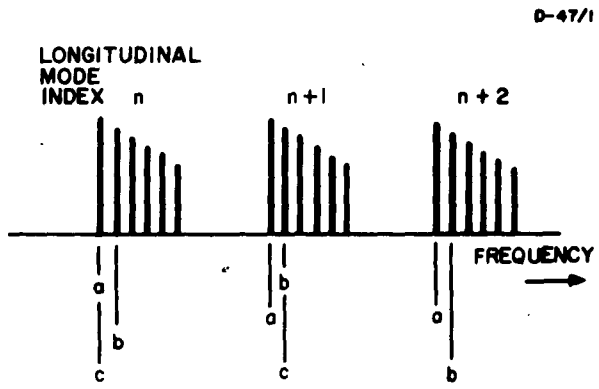

Fig. 29. Hypothetical mode spectrum of a ruby laser showing two kinds of mode hopping: (a) →(b) or (a) →(c).

therefore an increased threshold (here other sources of loss also must be considered). (5) As the diameter of the sample and/or the Cr^{3+} ion concentration is increased, the sample becomes optically thick for the pumping radiation and becomes more difficult to pump. (6) Since ruby has a relatively high dielectric constant (~ 1.76) the effects of refraction and reflection at the sample surface must be considered (Ref. 24). (7) As the Cr^{3+} ion concentration is increased, the character of the energy levels changes, affecting the oscillation threshold. We consider here only the first six effects, assuming that the last one is negligible at the Cr^{3+} concentration of interest (below 0.10%).

To deal with the first four effects, we recall the oscillation condition (Ref. 25) for a sample in a Fabry-Perot resonator:

$$\frac{N_2 - N_1}{N_o} = \frac{-\ln r}{\sigma_{12} \ell N_o} \quad , \tag{20}$$

where

N_o ≡ the total active ion density in the crystal

N_i ≡ population density in level i

r ≡ effective reflection coeffi ent of the cavity end plate, which should take i ıto account the combined effects of output coupling of the cavity, losses in the end plates, losses due to scattering in the crystal, diffraction losses, etc.

σ_{12} ≡ absorption cross section for the active laser transition

ℓ ≡ length of the sample and the resonator;

subscript 1 refers to the ground state, and subscript 2 refers to the R-line excited state.

Relating $\frac{N_2 - N_1}{N_o}$ to the induced pumping transition probability W and the fluorescent decay time τ of the metastable (R-line) state, we get the oscillation condition (see ISR No. 2):

$$\frac{-\ln r}{\sigma_{12} \ell N_o} = \frac{W - \frac{1}{\tau}}{W + \frac{1}{\tau}} - \frac{2W}{W + \frac{1}{\tau}} e^{-\left(W + \frac{1}{\tau}\right) t_o} \tag{21}$$

where t_o is the pump pulse duration. If $t_o \to 0$, i.e., very short pulse operation, threshold should be expressed in terms of Wt_o (proportional to energy),

$$Wt_o = \ln \frac{2\,GC}{CG - 1}, \tag{22}$$

where

$C \equiv$ wt % Cr^{3+} concentration = gm Cr_2O_3/gm Al_2O_3

$G \equiv \dfrac{\ell\,\sigma}{-\ln r}$

$\sigma \equiv \sigma_{12}$ expessed in terms of $cm^{-1}/\%\ Cr^{3+}$.

Effects 5 and 6 above are closely related. It appears that these effects will cause the maximum in pump energy density to appear somewhere inside the ruby rod rather than at its surface, as one might expect at first glance. Rigorous quantitative analysis of the above effects, however, is too complicated to be warranted. We therefore approximate them by assuming the following:

$$\frac{\text{maximum pump energy density in ruby}}{\text{pump energy density in optically thin sample with } \epsilon = 1} \approx \frac{e^{\frac{-\alpha_p d}{n}} + e^{\frac{-(n-1)}{n}\alpha_p d}}{2}, \tag{23}$$

where

$\alpha_p \equiv$ absorption coefficient at pump frequency

$d \equiv$ diameter of the sample

$n \equiv$ some number between 2 and ∞ to be chosen empirically.

In the case of ruby, expression (23) depends significantly on n only for Cr^{3+} concentrations above approximately 0.03%, and even then not very strongly for $n > 5$. This makes the choice of n not too critical. The effect of reflection at the surface of a ruby rod is assumed to be approximately the same for all samples and therefore may be omitted from present considerations.

Writing $\alpha_p = \sigma_p C$, where for ruby $\sigma_p \approx 60\ cm^{-1}/\%\ Cr^{3+}$, we obtain the final expression of threshold Wt_o as a function of Cr^{3+}

concentration, sample diameter, and the parameter G, which involves gain and loss per passage factors:

$$Wt_o = \frac{2}{e^{-\frac{1}{n}\sigma p\ Cd} + e^{-\frac{n-1}{n}\sigma p\ Cd}} \ln \frac{2CG}{CG-1} \quad (24)$$

Wt_o is plotted as a function of concentration C in Fig. 30 for several values of d and G and using n = 6 (a reasonable value, as rough estimates of reflection, refraction, and attenuation effects indicate).

b. Experiment

Oscillation thresholds have been measured for ruby samples of various Cr^{3+} concentrations (between 0.0066% and 0.091%) and various transmission coefficients (between 0.1% and 38%) of one of the Fabry-Perot cavity plates. At 25% transmission, threshold was measured as a function of temperature. All samples were 2 in. long and 1/4 in. in diameter. The losses at the silver reflecting plates were estimated to be approximately 2% at the nontransmitting end and between 2% at 0.1% transmission and 5% at 38% transmission at the partially transmitting end. The scattering losses were measured to be approximately 0.5%/cm of ruby. The results of these experiments are plotted in Fig. 31 and agree quite well with the theoretical curves shown in Fig. 30. Figure 32 shows the effect of temperature on oscillation threshold, and again there is excellent agreement with Fig. 30. In the next section, the ordinate of Fig. 30 is experimentally calibrated in terms of the actual energy density in the blue and green pumping bands at threshold.

2. Study of the Laser Oscillation Threshold Pumping Requirements

The program concerned with the detailed study of the general threshold requirements of ruby lasers had among its objectives the following: (1) The determination of laser pumping requirements for ruby in terms of the actual energy or photon density in the green and blue absorption bands for a given length pulse of pumping radiation. This determination to be made at the ruby position and inside the ruby. This is more generally meaningful than the usually given electrical input to the flash lamp. (2) Determination of the relationship between the pulse and cw threshold requirements. To achieve these objectives, it was necessary to study in detail the efficiency of the pumping configuration used in the measurements (in our case, an elliptical cavity); the effects on threshold of various ruby parameters such as Cr^{3+} concentration, sample size, and losses; and the efficiency and spectral characteristics of the pumping sources. These studies are discussed in Sections III-B-1 and IV-B-2 and ISR's No. 1, 2, 3, 4. In this section,

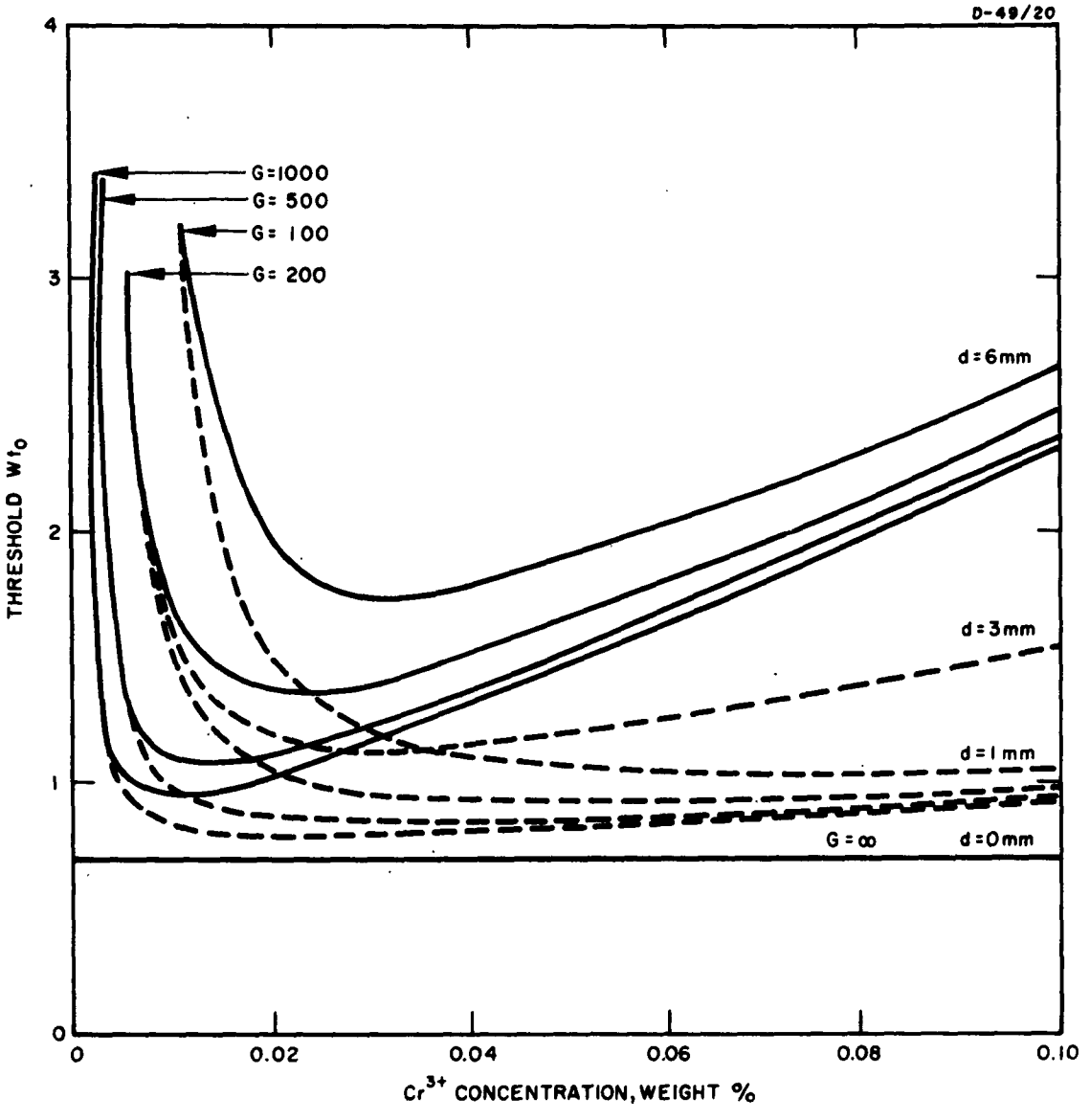

Fig. 30. Computed oscillation threshold as a function of Cr^{3+} ion concentration for various ruby rod diameters and gain parameters.

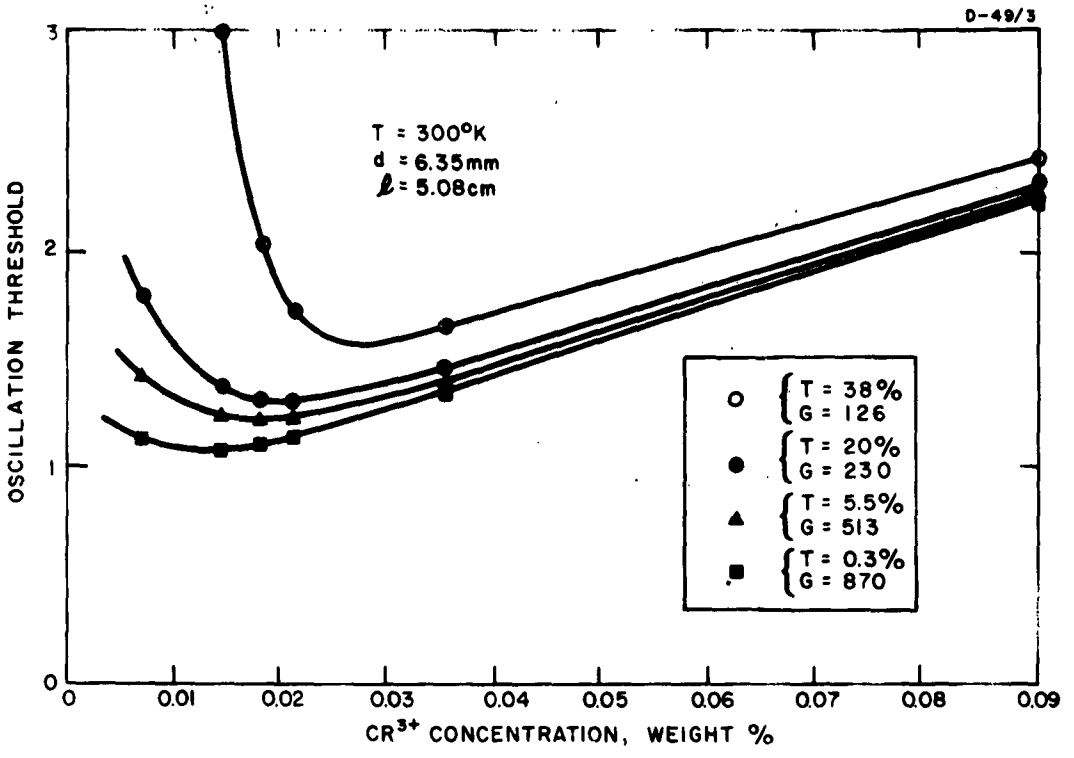

Fig. 31. Experimentally measured oscillation threshold as a function of concentration with reflectivity as the parameter

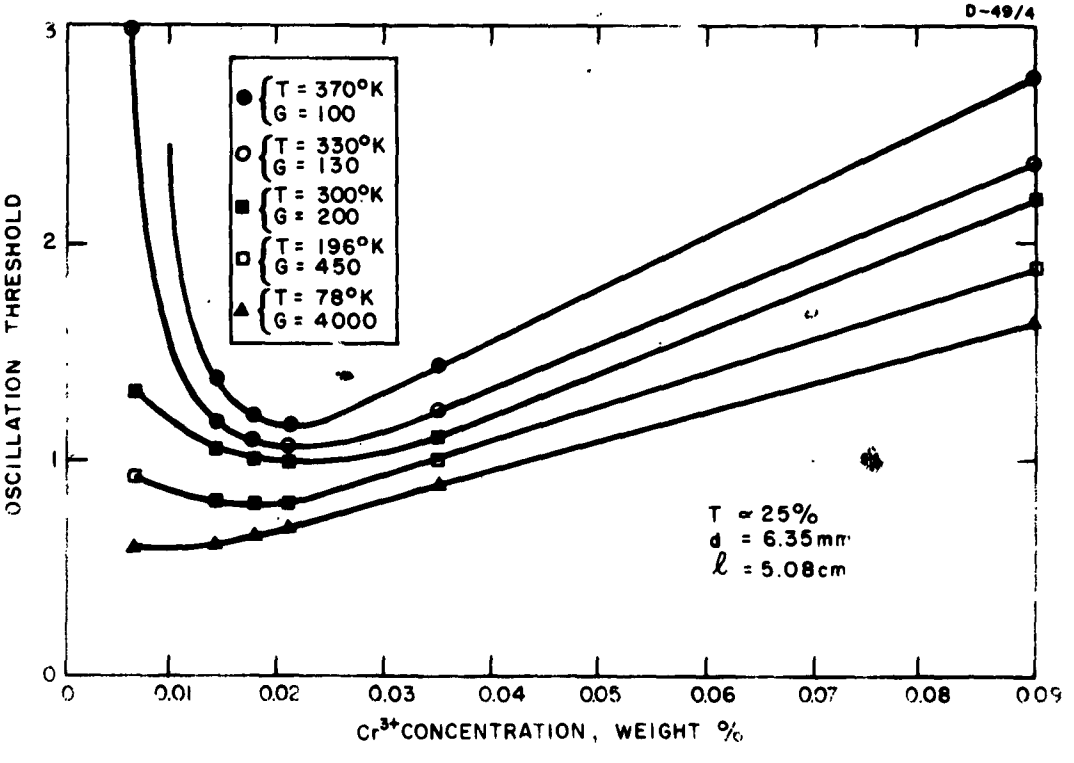

Fig. 32. Experimentally measured oscillation threshold as a function of concentration with temperature as the parameter

we are concerned with correlating the above information with threshold data obtained using an elliptical cylinder pumping configuration and an EGG FX-1 2-in. flash lamp and deducing the cw threshold requirements.

a. Pulsed Laser Pumping Requirements

Oscillation threshold measurements were made using ruby rods of various sizes, ranging from 0.5 mm in diameter by 1 cm long to 3mm in diameter by 1 in. long, all with 0.05% Cr^{3+} concentration. The 1-in. samples displayed relative thresholds in fair agreement with the theory given in Section III-B-1, while the 1-cm samples had thresholds higher than these predicted (see ISR No. 2). We believe this discrepancy is caused by optical resonator end-plate shadowing effects, which should be more pronounced for short ruby samples than for long ones. (Shadowing effects are described in some detail in the ISR No. 1.)

For the calculations in this section, we have used the data for a 3-mm by 1-in. ruby, which had a threshold of ~65 J at room temperature, when pumped with a 250-μsec-duration pulse. To convert this into erg-sec/cm^3 in the pumping bands at the ruby location, we use the following expressions:

$$(Ut_o)_{\text{green}} = \frac{Pt_o}{2\rho_s\, Lc}\ \eta_G\, R_{Al,\,G}\, \eta_c$$

$$(Ut_o)_{\text{blue}} = \frac{Pt_o}{2\rho_s\, Lc}\ \eta_B\, R_{Al,\,B}\, \eta_c \qquad (25)$$

where

U ≡ energy density at the ruby position in the cavity

P ≡ input power to the flash lamp during the pulse

t_o ≡ flash lamp pulse duration, or Pt_o ≡ energy input to the flash lamp

L ≡ flash lamp arc length

ρ_s ≡ flash lamp inside radius

c ≡ velocity of light

$\eta_{G,B}$ ≡ flash lamp pumping efficiency in the green and blue bands, respectively

$R_{Al,G,B}$ ≡ reflectivity of cavity walls Al in the green and blue, respectively

η_c ≡ cavity imaging efficiency.

The relevant numbers are as follows:

Pt_o = 65 J

L = 2 in.

ρ_s = 2 mm

η_G = 8.5% (ref. Sec. IV-B-2)

η_B = 9.3% (ref. Sec. IV-B-2)

$R_{Al,G}$ = 66% (see ISR No. 4)

$R_{Al,B}$ = 63% (see ISR No. 4)

L' = 1.82 L = 3.64 in. (see Sec. IV; A-1(b))

$$\eta_c = \frac{1}{\sqrt{16\left(\frac{a}{L'}\right)^2 + 1}} = 0.67 \text{ for } a = 1 \text{ in.} \qquad (26)$$

These numbers yield

$$(Ut_o)\,\text{green} = 3.98 \times 10^{-4} \text{ erg-sec/cm}^3$$

$$(Ut_o)\,\text{blue} = 4.16 \times 10^{-4} \text{ erg-sec/cm}^3 .$$

For the ruby in question, the Cr^{3+} concentration C = 0.05% and $G = \frac{\ell\,\sigma}{-\log r} = 540$. The reflectivities of the silver coating on the two ends of the ruby are 98% and 97%, respectively, and scattering losses are estimated to be 0.5%/cm for ruby (see ISR No. 2). These numbers for C and G enable us to locate a point on the graph in Fig. 30 and thus calibrate the ordinate of the graph in terms of erg-sec/cm^3 in the pumping bands at the ruby location. The calibration is as follows:

Wt_o = 1 in Fig. 30 corresponds to (Ut_o)green + (Ut_o)blue

$= 7.4 \times 10^{-4}$ erg-sec/cm^3 .

It may also be of interest to calculate the erg-sec/cm^3 inside the ruby at threshold. This is related to (Ut_o) in the following fashion:

$$(Ut_o)_R = (Ut_o)\,(1-R_R)\epsilon \left[\frac{e^{\frac{-a_p d}{n}} + e^{\frac{-(n-1)}{n} a_p d}}{2} \right], \qquad (27)$$

where

R_R ≡ reflection coefficient at the ruby surface

ϵ ≡ optical dielectric constant of ruby

a_p ≡ absorption coefficient at pump frequency

d ≡ diameter of the sample

n ≡ empirical constant chosen in the analysis in Section III-B-1.

Using $R_R = 0.32$ (see ISR No. 1), $\epsilon = 3.1$, and the above threshold data for 3-mm by 1-in. ruby, we calibrate the ordinate in Fig. 33 as shown.

b. CW Threshold Pumping Requirements

The threshold requirements of a pulsed laser may be related to those of a continuously operated one with the help of Fig. 34. This family of curves can be obtained rigorously by combining (21) and (24). However, for our purposes, it is sufficient to establish only the end points of the curves accurately. For $t_o/\tau << 1$, this has been done in Section III-B-1. For $t_o/\tau \to \infty$, combination of (21) and (24) yields

$$W = \frac{C + \frac{1}{G}}{C - \frac{1}{G}} \frac{2}{e^{-\frac{1}{n}\sigma_p Cd} + e^{-\frac{(n-1)}{n}\sigma_p Cd}} \frac{1}{\tau} \qquad (28)$$

The curves in Fig. 34 are plotted for $C = 0.05\%$ and $d = 3$ mm, except for the $G = \infty$ case, where the $d = 0$ curve is also included. The ordinate in Fig. 34 has been calibrated using the information presented in the preceding section.

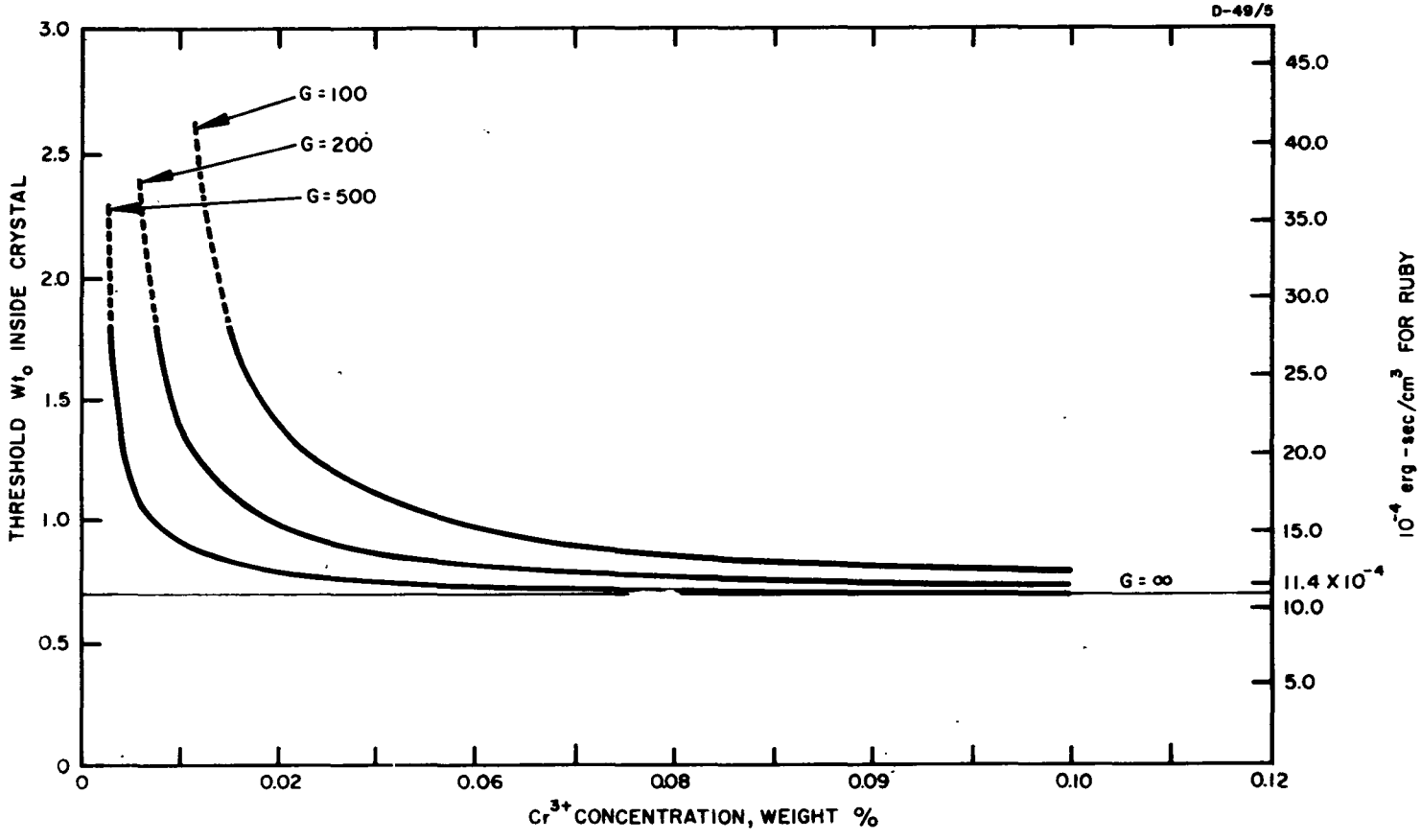

Fig. 33 Threshold inside crystal as a function of gain and concentration

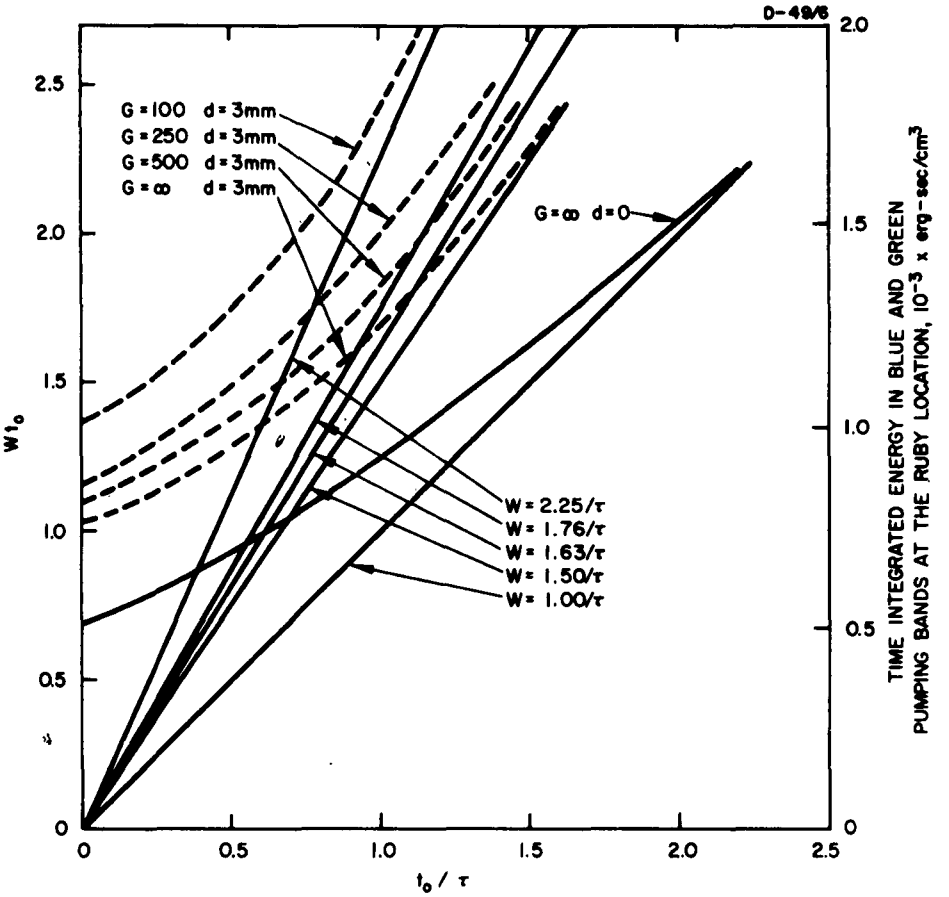

Fig. 34. Threshold conditions for various rubies as functions of pumping pulse length.

C. CW RUBY LASER STUDY

The purpose of the cw laser study was to determine the basic minimum pump power requirements for room-temperature cw operation using ruby and, if possible, achieve such operation. During the course of this study, three pumping geometries have been considered. (1) An elliptical cavity designed for use with the 2-kW Huggins-Bol Type-A mercury-arc lamp. The cavity is 1 in. long, has a 1/2-in. semimajor axis, and an eccentricity of 0.4. Cooling is accomplished by injecting a high velocity sheet-stream of water from a direction normal to the axis of the lamp. (2) A diffuse reflector cavity utilizing MgO and also designed for the 2-kW Huggins-Bol Type-A lamp. (3) A machined ellipsoidal housing for the 10-kW air-cooled mercury-arc lamp.

All three configurations are believed to be of approximately the same order of efficiency. Although a diffuse reflector cavity in pulsed operation gave a threshold lower than that in the elliptical cylinder by a factor of approximately 1.4 (see Section IV-A-3), it is not expected to be as effective for continuous pumping since the requirement for water cooling does not permit tight lamp and ruby packing inside the cavity. Similarly, in the ellipsoidal configuration, the brightness advantage of the 10-kW lamp is approximately cancelled by relatively low efficiency of the particular ellipsoidal housing used. The ellipsoid appears to be approximately 3.4 times less efficient than the elliptical cylinder because of shadowing by lamp electrodes, open back of the ellipsoid, and other factors. We should note that the ellipsoidal configuration has been briefly operated at 11 kW lamp input with a 3-mm by 1-cm ruby using multilayer dielectric reflectors without achieving laser action. However, the system may achieve oscillation threshold if the ruby is cooled to liquid-nitrogen temperature.

In view of the above, we use the elliptical cylinder to get an idea of the practicality of room-temperature cw operation using ruby. The following parameters describe the ruby sample and the elliptical cylinder cavity used:

$\ell \equiv$ ruby rod length = 2.5 cm

$d \equiv$ ruby rod diameter $\cong$ 0.2 cm

$C \equiv Cr^{3+}$ concentration = 0.05%

$G \approx$ 500 (silver coatings)

$L \equiv$ cavity length = 2.54 cm

$a \equiv$ semimajor axis of the ellipse = 1.77 cm

R_{Al} ≡ reflectivity of cavity walls ≈ 65%

η_c ≡ cavity imaging efficiency ≈ 68% .

From Fig. 34, we find that for a ruby sample having the above parameters, with d = 0.3 cm, the cw green and blue energy density required at the ruby location is 0.4 erg/cm^3. Using the analysis in Section III-B-2, we determine the corresponding requirement for d = 0.2 cm to be U = 0.35 erg/cm^3. The input power requirement for the Huggins-Bol Type-A lamp is therefore

$$P = U \frac{2\rho_{sA} L_A c}{(\eta_{G+B})_A R_{Al} \eta_c} = 1750 \text{ W} , \qquad (29)$$

where

ρ_{sA} ≡ Type-A lamp inside radius = 0.05 cm

L_A ≡ Type-A lamp active length = 2.54 cm

c ≡ velocity of light

$(\eta_{G+B})_A$ ≡ Type-A lamp conversion efficiency in green and blue ≈ 35%.

These figures would appear to indicate that cw operation would be marginal but possible. There are, however, several reasons why the prospect is not as optimistic as indicated here. First, there may be considerable heating in the ruby, leading to loss in quantum efficiency and broadening of the fluorescent line. Second, the cw elliptical cylinder is of smaller dimensions (one-half the size of the test flash lamp housing), and thus small protrusions, holes, etc., in the cavity have more effect. Also, in the cw cavity, the ruby sample length is equal to that of the cavity (rather than one-half the cavity length as in pulsed configuration), and thus the pump energy density distribution is nonuniform (see Section IV-A-1). Both these factors may lower the cavity efficiency to somewhat below the 67% used in the above calculations. Finally, the conversion efficiency of the cw lamp is really not as much better than the flash lamp as would be indicated by the ratio of 35 to 17.8% since the mercury lamp puts out relatively more blue light than does the flash lamp and a watt of blue pumping light is not as efficient as a watt of green. Unfortunately, our attempts to estimate the power required for cw operation by direct fluorescence-level measurements, and thus to verify the above results, have not met with success. The major difficulty stemmed from the fact that it has not been possible to operate the Huggins-Bol lamp at input powers above 1600 W, even under the conditions specified by the manufacturer.

Nelson and Boyle of BTL have recently demonstrated cw laser action in ruby at 78° K (Ref. 26). Their trumpet configuration (Fig. 35) assured maximum utilization of the pumping radiation by circulating it through the ruby. Operation at 78° K gave excellent thermal conductivity to avoid thermal gradients in the rod. To minimize heating effects and assure penetration of pump radiation, a 0.005% concentration ruby was used. Power outputs the order of 10 mW were reported.

The advantages which we believed our system offered would be room-temperature operation and power outputs at the watt level. We feel that if our system were modified to operate at 78° K, cw operation at the watt level would be achieved. The reasons for this optimism are the increases in thermal conductivity, quantum efficiency, and absorption cross section (gain) in ruby at 78° K.

D. OPTIMIZATION OF ENERGY OUTPUT IN THE PULSED RUBY LASER

1. Effect of the Various Parameters on Power Output

To enable us to determine approximately the dependence of power output on various device parameters, we consider a simplified three-level model of the ruby laser, where the three levels are designated 1, 2, 3, respectively. We define w_{ij} as the spontaneous transition probability from level i to level j, W as the induced transition probability between levels 1 and 3, W_{12} as the induced transition probability between levels 1 and 2.

Assuming w_{12}, w_{13}, and w_{23} to be negligible and $w_{32} >> W >> W_{31}$, we have the following approximate equations:

$$\frac{dN_1}{dt} = -WN_1 + \frac{N_2}{\tau} + W_{12} N_2 - W_{12} N_1$$

$$\frac{dN_2}{dt} = WN_1 - \frac{N_2}{\tau} - W_{12} N_2 + W_{12} N_1$$

$$N_1 + N_2 = N_o \; ; \; N_3 \simeq 0 \quad . \tag{30}$$

W_{12} is a complicated function of $(N_2 - N_1) - (N_2 - N_1)_{th}$, where $(N_2 - N_1)_{th}$ is value of $(N_2 - N_1)$ at oscillation threshold. Expanding this function in a power series and taking the first term, we have

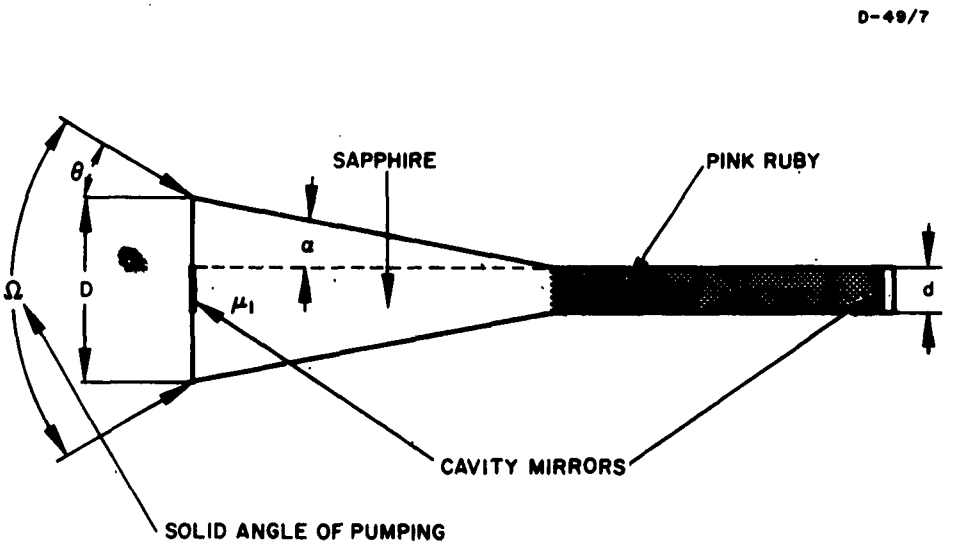

Fig. 35. BTL ruby sapphire trumpet configuration for 78°K cw ruby laser.

$$W_{12} = M\left[(N_2 - N_1) - (N_2 - N_1)_{th}\right] \quad \text{for } (N_2 - N_1) \geq (N_2 - N_1)_{th}$$

$$= 0 \qquad \text{for } (N_2 - N_1) < (N_2 - N_1)_{th}, \quad (31)$$

where M is a constant.

Assuming steady-state conditions, combining (30) and (31), and defining the fractional inversion

$$\frac{N_2 - N_1}{N_o} = f \ , \qquad \frac{(N_2 - N_1)_{th}}{N_o} = f_o \ ,$$

we obtain

$$0 = \frac{W - \frac{1}{\tau}}{N_o} - \left(\frac{W + \frac{1}{\tau}}{N_o} - 2M f_o\right) f - 2M f^2 \ . \qquad (32)$$

At threshold, we have

$$f = f_o = \frac{-\ln(r)}{\sigma \ell C} = \frac{1}{GC} \ . \qquad (33)$$

Substitution into (33) yields

$$W_o = \frac{1}{\tau} \frac{1 + f_o}{1 - f_o} \ . \qquad (34)$$

Defining $\Delta W = W - W_o$, $\Delta f = f - f_o$, and solving (32), we get

$$\Delta f = \frac{(\Delta W + 2MN_o f_o)(1 - f_o) + \frac{2}{\tau}}{4MN(1 - f_o)} + \frac{1}{4MN_o}$$

$$\sqrt{\frac{\left[(\Delta W + 2MN f_o)(1 - f_o) + \frac{2}{\tau}\right]^2 + 8MN\Delta W(1 - f_o)}{(1 - f_o)^2}} \ .$$

Now assuming M to be very large, which physically means that ΔN remains at its threshold value and any increase in pump power results in increased power output, we obtain

$$\Delta f \simeq \frac{\Delta W}{MN} \frac{1 - f_o}{2f_o} \quad .$$

Thus the induced transition probability W_{12} is given by

$$W_{12} = MN\Delta f$$

$$= \Delta W \left(\frac{1 - f_o}{2f_o} \right) \quad .$$

That is, the net induced transition probability is proportional to the amount by which oscillation threshold is exceeded, the constant of proportionality depending on the configuration parameters. Under the assumptions stated, $f = f_o$ when the system is oscillating; therefore, we can drop the subscript o.

We expect the power output of the laser to be given by the following expression:

$$P = \frac{\text{Power Out}}{h\nu \times \text{volume}} = \underbrace{(N_2 - N_1)}_{\text{population factor}} \times \underbrace{W_{12}}_{\substack{\text{net induced transition} \\ \text{probability for laser} \\ \text{transitions}}} \times \underbrace{(1 - r)}_{\substack{\text{coupled to} \\ \text{the outside}}} .$$

Now if W is measured in units of $1/\tau$, i.e.,

$$W = q\left(\frac{1}{\tau}\right) \quad ,$$

we then obtain the expression

$$P = \frac{N_o (1 - r)}{2\tau} \left[(q - 1) - (q + 1) f \right]$$

$$P \simeq \frac{N_o a_o \ell}{2\tau} f \left[(q - 1) - (q + 1) f \right] .$$

In order to maximize P with respect to the parameters, we require that

$$\frac{dP}{df} = 0 = \frac{N_o a_o \ell}{2} \left[(q - 1) - 2(q + 1) f \right] ;$$

therefore,

$$f_{max} = \frac{(q - 1)}{2(q + 1)}$$

and

$$P_{max} = \frac{N_o a_o \ell}{8\tau} \left[\frac{(q - 1)^2}{(q + 1)} \right] .$$

Also, we should note the maximum fractional inversion which the pumping power (specified by q) can maintain. This is the situation at

$$P = 0 = \frac{N_o a_o \ell}{2} f \left[(q - 1) - (q + 1) f \right] ;$$

therefore,

$$f(P = 0) = f_{min} = \left(\frac{q - 1}{q + 1} \right) .$$

Hence the normalized power output from the laser as a function of the fractional inversion will be given by Fig. 36. The results clearly indicate that for a given pumping parameter q, there is a combination of configuration parameters which maximizes the power output.

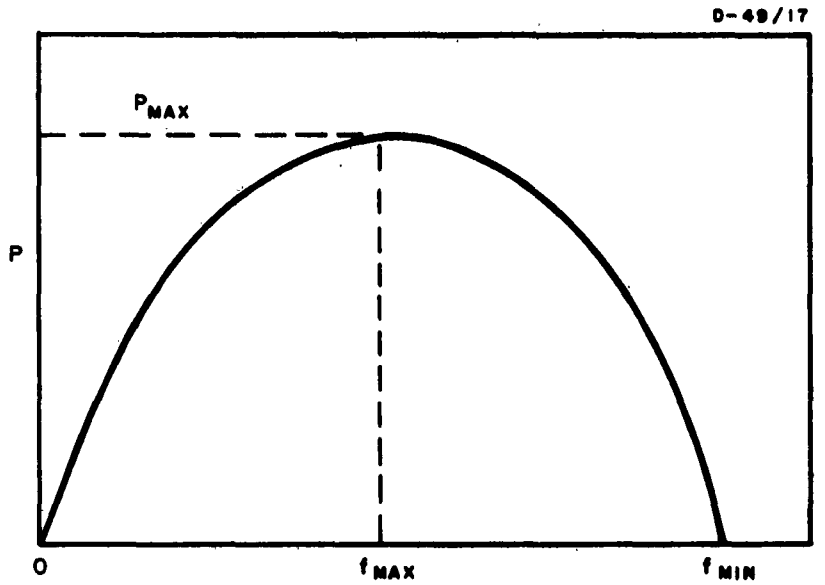

Fig. 36. Power output as a function of fractional inversion f.

It must be noted that these results are a consequence of the steady-state solution of the rate equations, i.e., they apply for cw operation. In extrapolating the results to the pulsed laser, we should not expect to find exact quantitative agreement with the cw analysis and experimental fact, but rather qualitative agreement. We can expect general agreement for time-integrated effects (i.e., energy output). This then is the basis for the comparison of these results with the following example:

Ruby 0.05% Cr^{3+} concentration ; $\ell = 1.5$ cm; $q = 2$.

A comparison of the experimental results (Fig. 37) with Fig. 36 indicates that the qualitative aspects of the theory are verified. Extrapolation to 78°K and 30-cm-long ruby crystals indicates that energy outputs in the 100-J region can be expected with currently available pumping sources.

2. High Energy Experiments

Initial tests of a power supply which can deliver 24,000 J, nominally at 10 kV, have been completed. The power supply consists of eight 60-μF, 10-kV condensers which are charged by means of a solid-state dc power supply. An ignitron is provided to suppress flash lamp gas ionization at 10 kV, if required, and a triggering circuit is used to ionize the flash lamp gas. Figure 38 shows the power supply with the access door closed. In Fig. 39 the access door is open, and the operator is changing the number of condensers in the condenser bank.

Another power supply of the pulse-shaped variety (which has been reported in ISR No. 3) has been constructed and is shown in Fig. 40. This unit can supply up to 8000 J into a matched flash lamp of 5Ω impedance at operating voltages up to 8 kV. It also utilizes an ignitron as a hold-off switch in series with the flash lamp. The effect of square-wave pumping may be observed in Fig. 41. It can be seen that laser action stops abruptly and that there is no exponential envelope as is usually observed. The crystal was a 9.5- in.-long ruby with silver on one end.

In order to produce high energy beams, the laser shown in Fig. 42 was constructed. A view of this unit without the outside cover cylinder is shown in Fig. 43. This laser, which will accommodate laser crystals up to 9 in. in length and 3/4 in. in diameter, operates at room temperature. A helical bifilar-wound flash lamp is used with a diffuse reflector surrounding it. At the present time, the unit has been tested at 10 kV with 11,000 J input. A photograph of the power output versus time is shown in Fig. 44 for a 3/8- by 7-in. ruby crystal with an opaque silver coating on one end and 8% dielectric reflection at the other end.

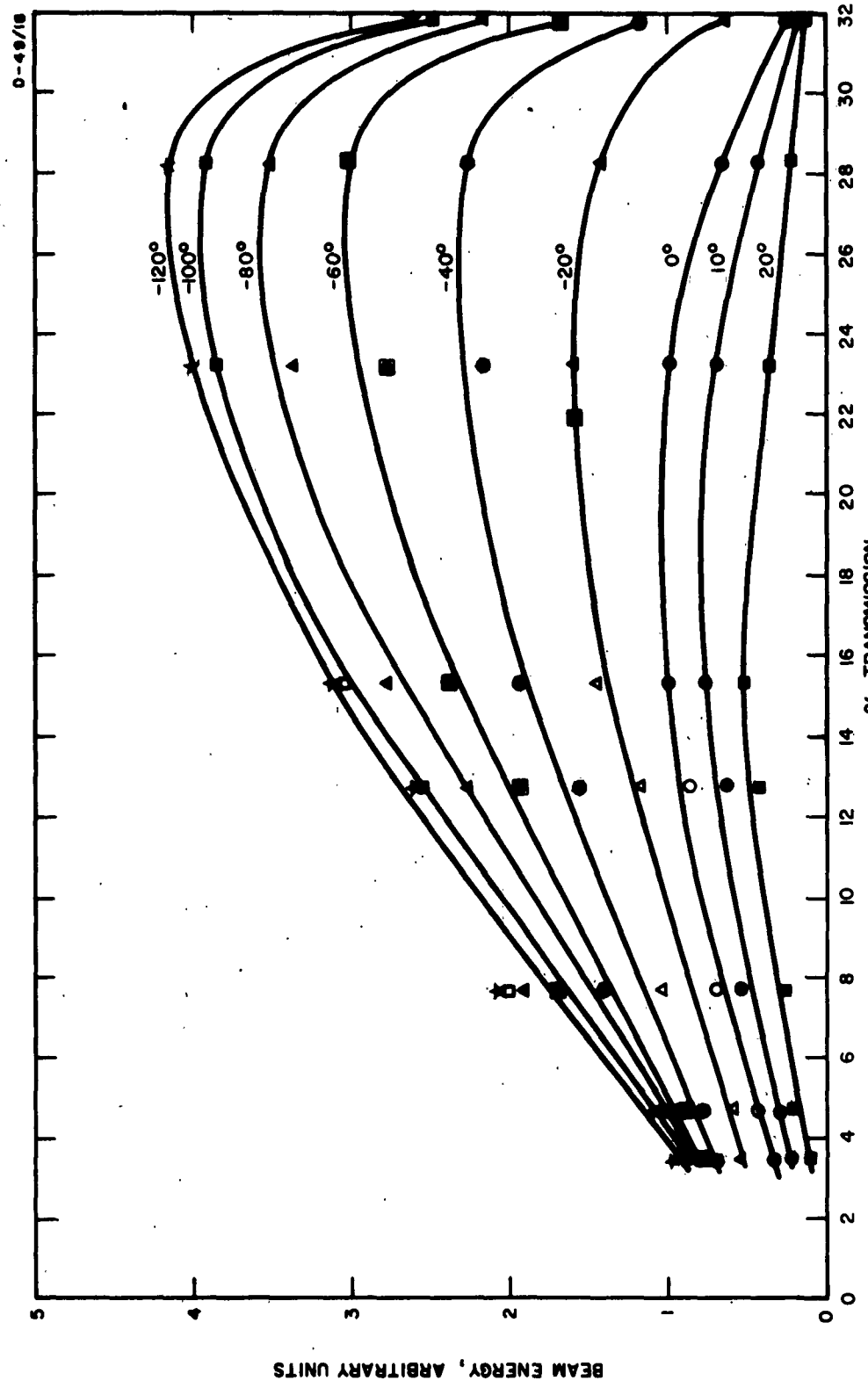

Fig. 37. Laser beam energy versus percent transmission with temperature as parameter (°C). The ruby was 1.5 cm long.

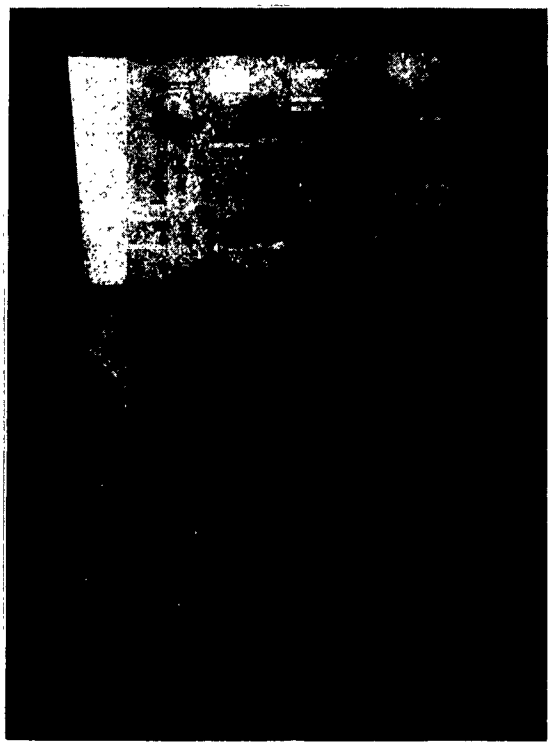

Fig. 38. 22,000-J laser power supply.

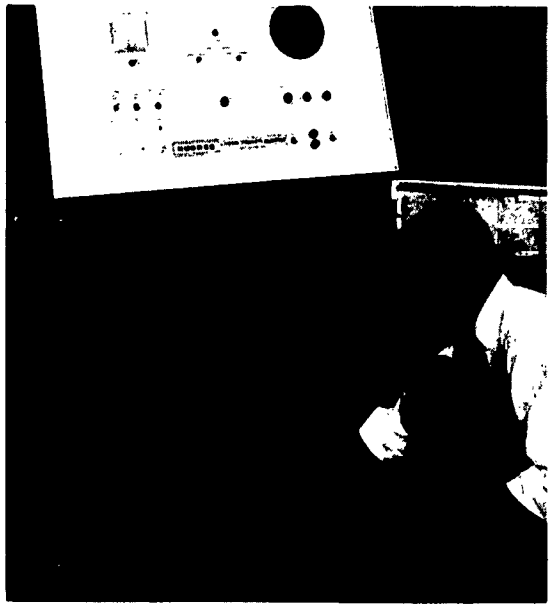

Fig. 39. 22,000-J laser power supply with operator switching storage condensers.

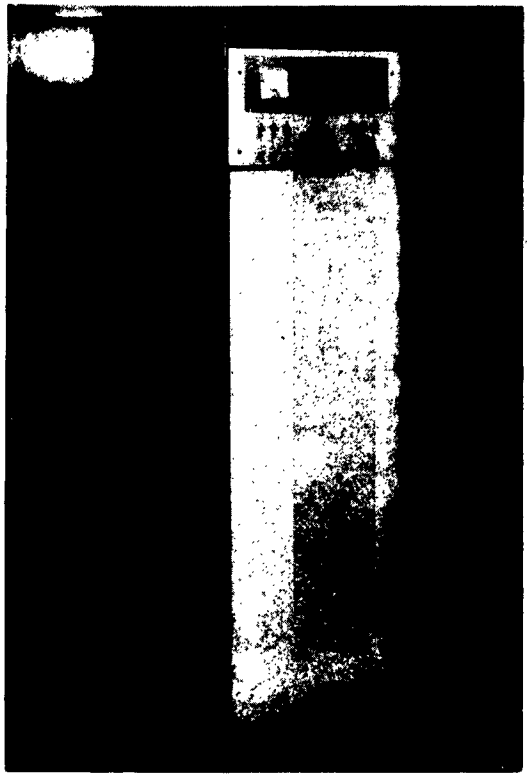

Fig. 40. 8000-J pulse-shaped laser power supply.

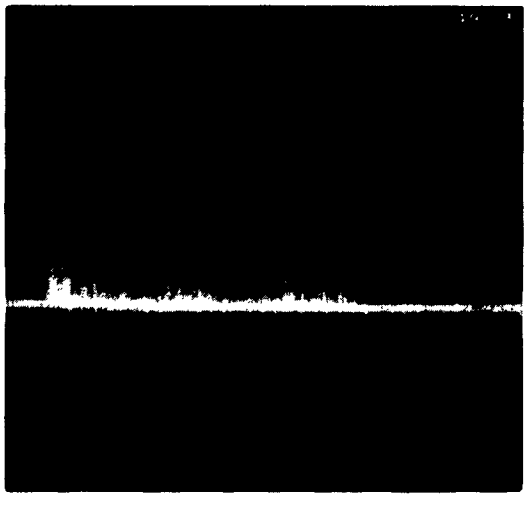

Fig. 41. Power output versus time for 9.5-in.-long ruby driven with shaped supply. Deflection sensitivities are 59 kW/div and 500 μsec/div.

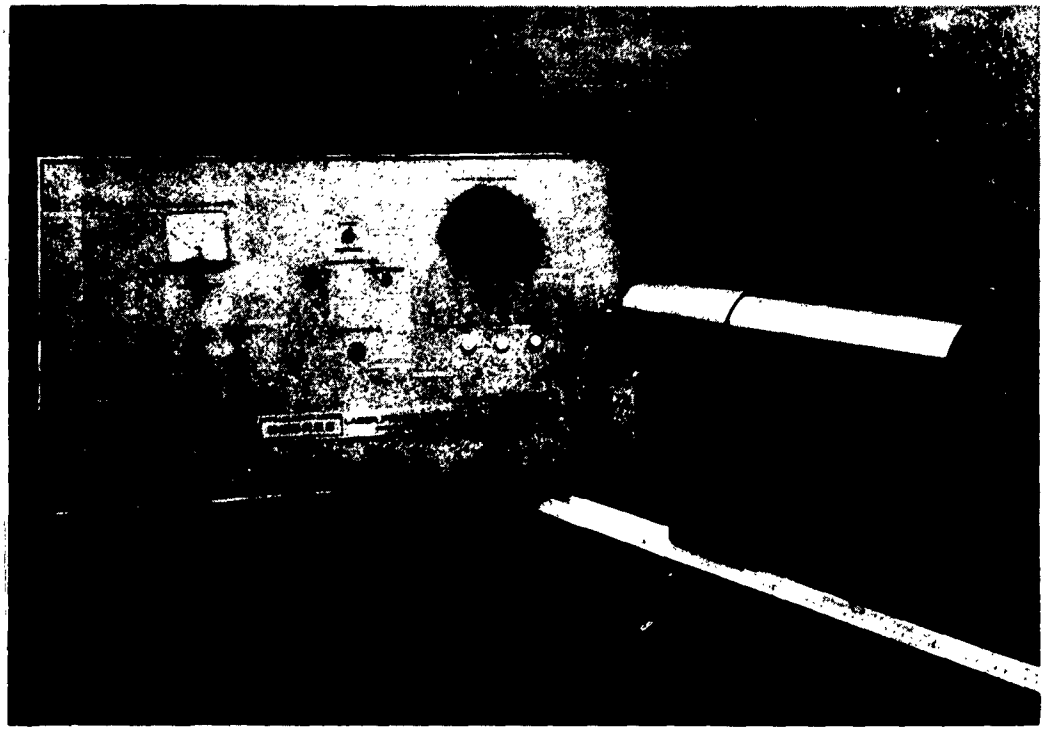

Fig. 42. Room-temperature high-energy laser assembly with power supply control panel.

Fig. 43. Laser assembly in Fig. 42 with outer housing removed.

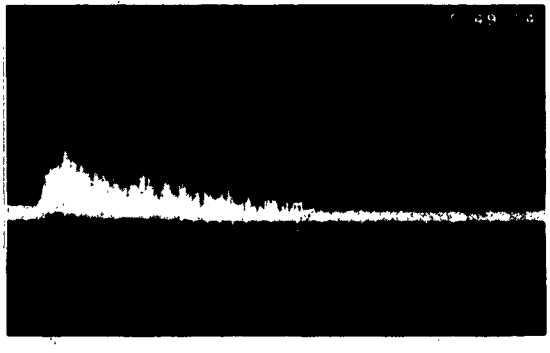

Fig. 44. Power output versus time for laser assembly in Figs. 42 and 43. Deflection sensitivities are 184 kW/div and 500 μsec/div.

Peak power output is approximately 590 kW. By electronically integrating the power output, one may determine the integrated or total beam energy, which is 16 J (at room temperature). With operation at 20,000 to 22,000 J, simple extrapolation indicates that 30 J will be obtained without cooling.

In order to increase the capability of this system further, a laser has been designed which will permit operation at liquid-nitrogen temperature. An exploded view of the laser is shown in Fig. 45. A dewar is provided which will permit storage of the liquid nitrogen which cools the laser crystal by thermal conduction. A ruby (shown on the right side of the picture) is attached and held in mechanical contact to the bottom of the nitrogen reservoir. The dewar jacket is slipped on the ruby and the system is evacuated. The package is then mounted on the axis of the helical flash lamp. To date, this system has only been checked at room temperature, verifying the results indicated above. Extrapolation of these results to operation at liquid-nitrogen temperature indicates that approximately 90 to 120 J should be obtained.

Fig. 45. Low-temperature laser disassembled to show component parts.

IV. PUMPING CONFIGURATIONS AND FLASH LAMPS FOR OPTICAL EXCITATION

This phase of the program was concerned generally with the investigation of laser pumping configurations and flash lamps and high intensity spark discharges for optical excitation. A summary of the analysis of the more practical configurations (i.e., elliptical cylinder and ellipsoid of revolution) from ISR No. 1 is presented and compared with experimental results. Experiments which determined the optimum gas and pressure for flash lamp excitation of ruby are included (also see ISR No. 1). Absolute spectral measurements of a xenon flash lamp which allow the determination of oscillation threshold requirements in terms of a physically meaningful quantity are included (see ISR No. 4). The thorough investigation of a high intensity spark discharge as a ruby laser pumping source is summarized in detail (ISR No. 1, 2, 3, 4).

The analytical calculations were supplemented by experimental measurements on the finite elliptical cylinder, permitting an evaluation of the effects of reflecting end plates, and on the diffuse reflector pumping configuration developed by M. L. Stitch under other funding.

It was found that from a practical point of view, the three most useful and efficient geometries (of those mentioned above) are the elliptical cylinder, the diffuse reflector, and the ellipsoid of revolution. The first two are most suitable for linear sources, whereas the last one is most useful for sources approximating a point source. All three of these geometries are being used in attempts to achieve cw operation (see Section III-D). The calculations and measurements relevant to these geometries are summarized below.

A. PUMPING CONFIGURATIONS

1. Elliptical Cylinder

a. Infinite Length Elliptical Cylinder

We consider the problem of a "line" source and a laser sample in the shape of a rod placed at the two foci of an elliptical cylinder with reflecting inside walls (see Fig. 46). We take the "line" source to be of length L and radius ρ_s and the total power radiated by it to be P_T. If we assume that each element dz' of the source radiates isotropically, the analysis yields

$$U = \frac{P_T a^2}{2\pi \rho_s c L} I_1 I_2 , \qquad (35)$$

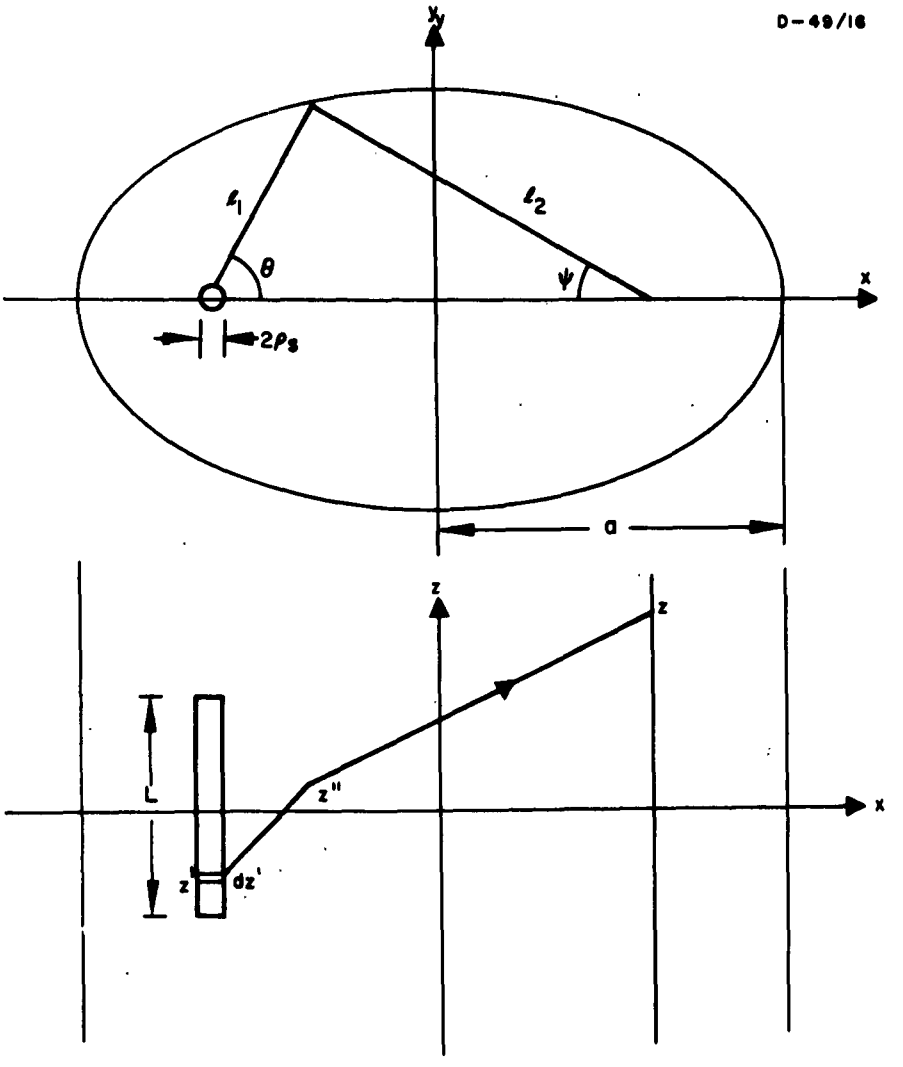

Fig. 46. A reflector in the form of an elliptical cylinder employing an artificial source.

where c is the speed of light and

$$I_1 = \int_{-L/2}^{L/2} \frac{dz'}{\left[4a^2 + (z - z')^2\right]^{3/2}}$$

$$= \frac{1}{4a^2} \left[\frac{z + L/2}{\sqrt{4a^2 + \left(z + \frac{L}{2}\right)^2}} - \frac{z - L/2}{\sqrt{4a^2 + \left(z - \frac{L}{2}\right)^2}} \right] \tag{36}$$

$$I_2 = \int_0^{2\pi} \frac{l_1}{l_2} \, d\theta = 2 \int_{-a}^{a} \frac{a}{a - ex} \sqrt{\frac{1 - e^2}{a^2 - x^2}} \, dx$$

$$= -2 \sin^{-1} \frac{ae - x}{a - ex} \Bigg|_{-a}^{a} = 2\left(\psi - \frac{\pi}{2}\right) \Bigg|_{0}^{\pi} = 2\pi \, . \tag{37}$$

Here e is the eccentricity of the ellipse; other symbols are defined in Fig. 46. Thus,

$$U = \frac{P_T}{4\rho_s c L} \left[\frac{z + L/2}{\sqrt{4a^2 + \left(z + \frac{L}{2}\right)^2}} - \frac{z - L/2}{\sqrt{4a^2 + \left(z - \frac{L}{2}\right)^2}} \right] . \tag{38}$$

At z = 0,

$$U = \frac{P_T}{2\rho_s L c} \frac{1}{\sqrt{16\left(\frac{a}{L}\right)^2 + 1}} \, . \tag{39}$$

The radius of the maximum energy density rod is given approximately (see Fig. 46) by

$$2\rho_r = 2\rho_s \frac{1 - e}{1 + e} \quad . \tag{40}$$

Actually, the cross section of the maximum energy density rod is slightly elongated along the x-axis.

b. Finite Length Elliptical Cylinder

In the above calculations, the effect of the reflecting end plates of an actual elliptical pumping cavity is neglected. However, these calculations are sufficient to enable one to determine the effect of the end plates experimentally and to compute the effective source length.

The cavity used in the experiments had the following parameters:

$$\frac{L}{a} = 2 , \quad e = 0.4 ,$$

where L is the axial length of the cavity. It was found that blocking off the reflecting end plates of the cavity increased the threshold by a factor of approximately 1.5. At threshold the energy density in a given ruby is the same under any circumstances. Therefore, using (39), we get

$$U_{th} \sim \frac{m}{\sqrt{16\left(\frac{a}{L_s}\right)^2 + 1}} = \frac{1}{\sqrt{16\left(\frac{a}{L'_s}\right)^2 + 1}} ,$$

where

U_{th} ≡ threshold energy density in the ruby

L_s ≡ actual length of the source

L'_s ≡ effective length of the source

m ≡ factor by which the presence of end plates reduces threshold.

Letting $L'_s = n L_s$, we get

$$n = \frac{1}{\sqrt{\frac{1}{m^2} + \frac{1}{16}\left(\frac{L_s}{a}\right)^2 \left(\frac{1}{m^2} - 1\right)}} .$$

Unfortunately, n depends on $(L_s/a$. For the cavity used in our experiments, $n = 1.82$.

To get an idea of the focusing properties of the elliptical cavity, we have measured the laser oscillation threshold as a function of the flash lamp position. For the PEK 1-mm bore lamp and a 3-mm-diameter ruby, the results are shown in Fig. 47. These results indicate that the positioning tolerances are quite narrow ($\pm \sim 0.2$ mm). Taking into account the fact that the PEK lamp has 2.5-mm quartz walls, which increases the apparent arc diameter to 1.5 to 2 mm, it appears the elliptical cylinder produces a fairly well-defined image of the source.

2. Ellipsoid of Revolution

Consider next an ellipsoid of revolution with the source and the sample at the two foci. We first determine the size of the maximum energy density volume. We restrict ourselves to determining the dimensions of the volume along the x-axis and normal to it. Thus, with reference to Fig. 48,

$$s_x = \frac{\alpha l_2}{\sin \beta} \tag{41}$$

$$\alpha = \frac{2\rho_s}{l_1} \tag{42}$$

$$\sin \beta = \frac{y}{\rho_2} .$$

Making use of the well-known properties of the ellipse, we obtain

$$s_x = 2\rho_s \frac{(a - ex)^2}{(a + ex)\sqrt{\left(1 - e^2\right)\left(a^2 - x^2\right)}} . \tag{43}$$

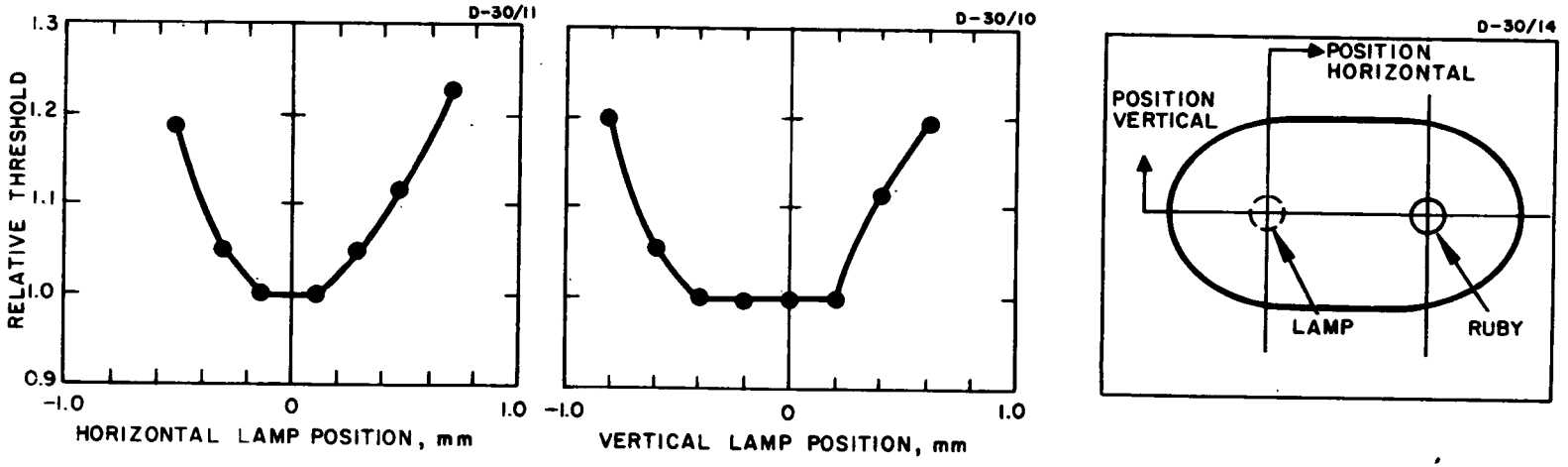

Fig. 47. Focusing properties of an elliptical cavity.

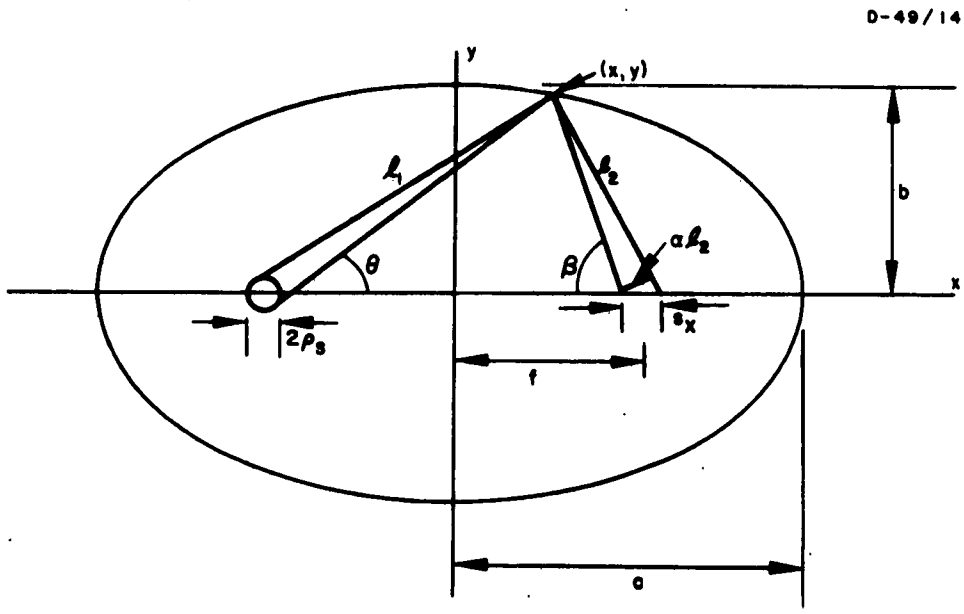

Fig. 48. Ellipsoidal reflector employing an artificial source.

This must be minimized with respect to x, with the result

$$s_{x\,\min} = h = 2\rho_s \frac{(1 - ek)^2}{(1 + ek)\sqrt{\left(1 - e^2\right)\left(1 - k^2\right)}}, \tag{44}$$

where

$$k = \frac{x}{a} = \frac{-\left(1 - e^2\right) + \sqrt{\left(1 - e^2\right)^2 + 36e^2}}{6e}. \tag{45}$$

The dimension of the maximum energy density volume in the y direction can be found by inspection and is given by (40). We now wish to examine (44) and (40) to determine whether e must be large or small to give as large a maximum energy density volume as possible. In the case of ρ_r, it is obvious from (40) that e must be as small as possible. Equation (44) must be examined in more detail. Because of its complicated nature, we consider the two extreme cases, $e \to 0$ and $e \to 1$, separately. For $e \to 0$, by expanding the square root in (45) to second order in e, we obtain

$$k \approx 3e. \tag{46}$$

Using (46), we obtain

$$h \approx 2\rho_s \frac{\left(1 - 3e^2\right)^2}{\left(1 + 3e^2\right)\left(1 - 5e^2\right)}. \tag{47}$$

For $e \to 1$, we may write

$$k = \frac{e^2 - 1 + \sqrt{36e^2\left[1 + \frac{\left(1 - e^2\right)^2}{36\rho^2}\right]}}{6e}$$

$$\approx 1 - \frac{1 - e^2}{6e} \quad . \tag{48}$$

This gives

$$h \approx 2\rho_s \frac{4}{3\sqrt{3}} (1 - e) . \tag{49}$$

Thus from (47) and (49) it appears that small e is to be preferred.

To determine the maximum energy density, we use methods exactly similar to those employed before, thus obtaining (again assuming an isotropic source)

$$U = \frac{P_T}{\pi \rho_s^2 c} , \tag{50}$$

i.e., the maximum energy density is equal to that in the source.

3. Diffuse Reflector Cavity

In the diffuse reflector pumping scheme, the laser material and a linear flash lamp are placed as close together as thermal and mechanical factors permit and are surrounded by a high reflectivity diffuse reflector, such as magnesium oxide. In this arrangement, the ruby has a large probability of capturing random radiation.

A cavity based on this principle has been built and compared with a 2-in.-long elliptical cylinder cavity with a 1-in. semimajor axis and an eccentricity of 0.4. A 2-in. EGG FX-1 flash lamp and 3-mm by 1-in. ruby were used. The MgO cavity gave a threshold lower by a factor of approximately 1.4, or ~40 J.

B. FLASH LAMP EVALUATION

1. Determination of Optimum Gas and Pressure

Two of the obvious parameters on which the efficiency of a given flash lamp geometry will depend are the type of gas and its pressure. An exhaustive study was made of the pumping efficiency of inert gases. The experimental method consisted of pumping a ruby with the flash discharge of the various gases in the same lamp geometry and measuring the fluorescent output (i.e., using the ruby as a spectral integrator). As a check on this, the oscillation threshold was also measured for the gases at optimum pressure (~ 150 mm Hg) and the separate results were found to be consistent. The results of these experiments (see Fig. 49) can be summarized by saying that xenon at approximately 150 mm Hg pressure is definitely the best gas to use in a pulsed source unit.

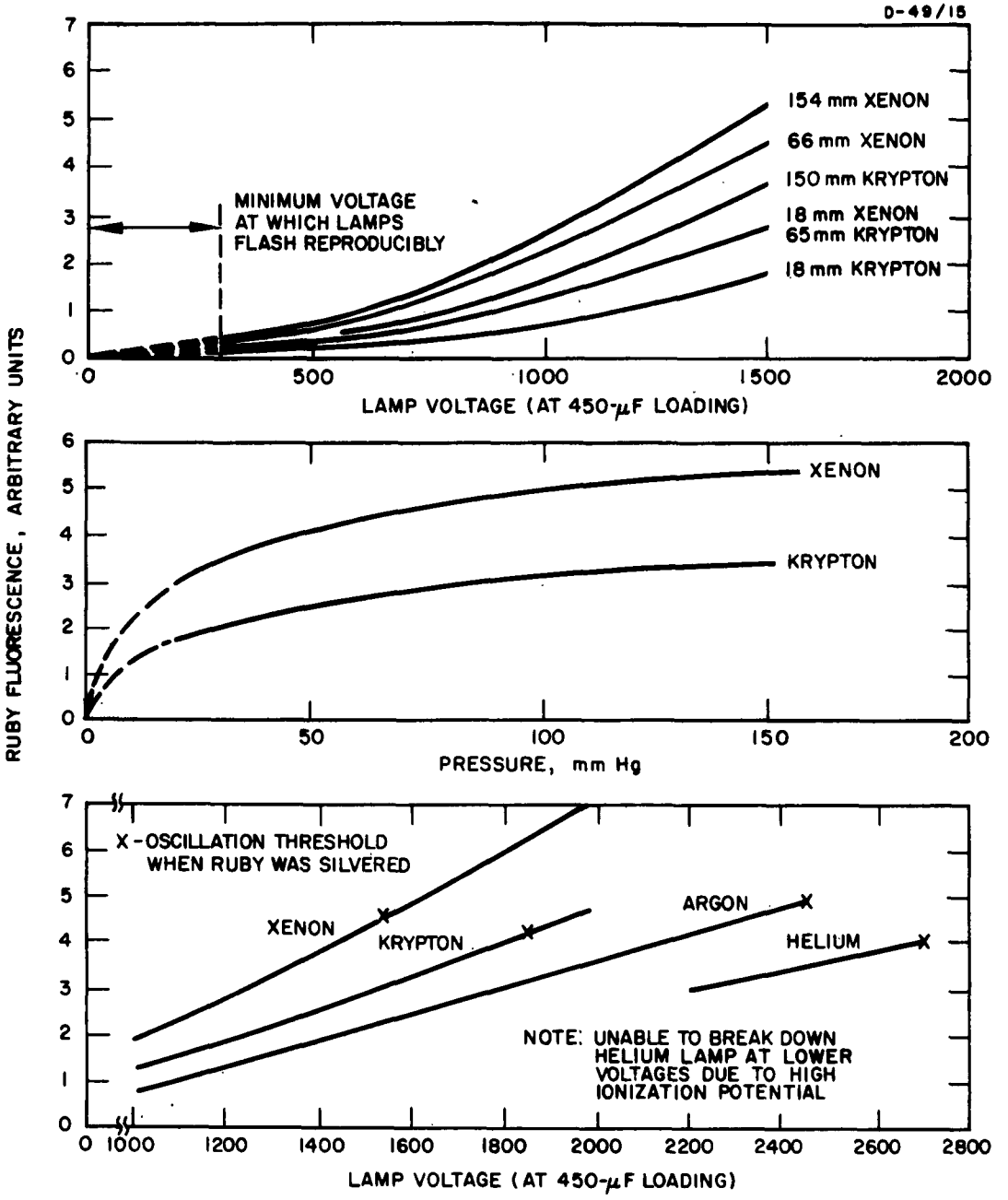

Fig. 49. (a) Pumping efficiency comparison of xenon-krypton in a Hughes coaxial flash lamp.

(b) Pumping efficiency of xenon-krypton versus pressure in a Hughes coaxial lamp.

(c) Pumping efficiency comparison of xenon-krypton-argon-helium in helical lamp (gases at optimum pressure, ~ 150 mm Hg).

2. Spectral Distribution of Xenon Flash Lamp

Spectral measurements of the EGG FX-1 2-in. flash lamp output were performed using a standard of spectral radiance obtained from the National Bureau of Standards, a Bausch and Lomb grating monochromators andan RCA 7265 photomultiplier. The details of the measurements were reported in ISR No. 4. As mentioned in that report, the results are subject to error due to inaccuracy of the standard-lamp input-current meter. This source of error has subsequently been eliminated by using a precision ammeter accurate to within 0.2% . The corrected results are shown in Fig. 50. However, for these new results it still is difficult to claim an accuracy of better than 10% (although it may be considerably better) because of the following difficulties: (1) It was found that the drift and fatigue effects in the photomultiplier are quite large, making it impossible to obtain reliably accurate measurements. (2) Wratten neutral density filters used in these experiments exhibit increasing absorption in the short wavelength region, making accurate measurements of actual attenuation very difficult. (3) The discharge in the flash lamp is very nonuniform during the first half of a 250-μsec pulse (see ISR No. 4).

Using Fig. 50, we may estimate the efficiency of the lamp by integrating the curve over wavelength and then over angles and the area of the lamp. The final result should be integrated over time using the monitor photodiode pulse shape. Assuming that each surface element of the lamp radiates according to Lambert's law, we get

$$E_{out} = 2\pi A \int_{\lambda, t} \frac{dP(\lambda, t)}{d\lambda} \, d\lambda dt \int_{o}^{\pi/2} \cos\theta \sin\theta \, d\theta \ .$$

Using the numbers given in Fig. 50, we obtain the electrical energy to visible light conversion efficiency:

$$\eta = 26.8\% .$$

In a similar way, we can compute the efficiency for conversion to light in green (5000 Å to 6000 Å) and blue (3500 Å to 4500 Å) bands:

$$\eta_B = 9.3\%$$

$$\eta_G = 8.5\% .$$

C. HIGH INTENSITY SPARK DISCHARGES

The purpose of this phase of the program was to determine the efficiency of microsecond-duration high-temperature sources as laser pumps and to maintain cognizance of related effort. The effort

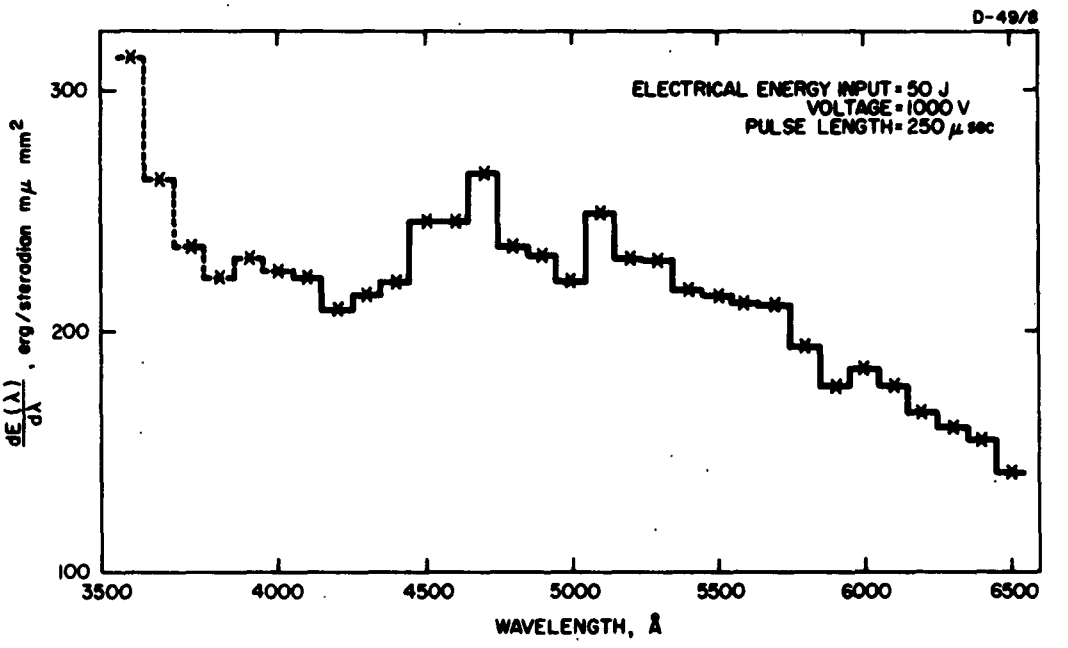

Fig. 50. EGG FX-1 flash lamp with 2-in. arc spectral distribution.

was devoted solely to ruby, and oscillation was not achieved. Peak pump temperatures in the range of $\sim$ 30,000°K for periods of $\sim$ 2 μsec were generated, as anticipated at the beginning of the project. Several pump configurations were used, including coaxial and elliptical cavities. The presence of the intense ultraviolet flux from the black-body pump, which peaks typically at 1000 Å, is believed to be the reason for not achieving oscillation. The effects likely to be produced are the ejection of electrons from the metastable or higher pumping states into higher levels and a possible reduction of transparency by transfer of charge from the ground states directly into the conduction band.

The technical work has been covered in detail in the ISR's. This report will give an over-all description of the work, with sufficient detail included to permit a meaningful description.

At the inception of the work, it was known that very high temperature black-body sources could be made with temperatures of 30,000°K or more, with a duration of a few microseconds. The possible value of these sources as ruby laser pumps was discussed. A military or field need existed for a way of generating a single coherent pulse of coherent radiation with an economical expenditure of primary electrical energy. It will be remembered that the randomly spaced numerous spikes of radiation were most difficult to utilize in an active ranging system because of the superposition of transmitted and back-scattered light upon the returning "echo." Thus, a simple way of generating a single coherent pulse would have been useful. Techniques of generating single or evenly spaced pulses have now been developed (Refs. 27 and 28), but these still require large primary energy expenditures. Measurements were made of radiance and energy emitted by a coaxial source of 0.4 μF expending 10 J electrical energy. This source configuration is schematically shown in Fig. 51, and the measurements indicated the generation of peak temperatures of $\sim$ 25,000°K. In later measurements at 20 J, the peak temperatures were in the neighborhood of 30,000°K. In Fig. 52 are shown the Planckian distributions for 5000°K (a typical temperature attained with a helical flash lamp configuration at ruby threshold), 25,000°K, and 30,000°K. Also shown are the three absorption bands of interest within ruby together with the cutoff wavelength of ruby represented by the difference between the Cr^{3+} ground state and the conduction band.

Table 1 gives the photon density within the three bands for the three temperatures of interest. In ISR No. 2, the data on fluorescent quantum efficiency versus wavelength indicated that the peak fluorescent quantum efficiencies were comparable for these three bands. Accordingly, a simple summation was used in predicting the pumping efficiency of the 30,000°K pump (this temperature was realized experimentally).

It was recognized that in these bands not only was peak pump flux important, but sufficient duration was also necessary. The effective photon density of 2×10^{23} photons $sec^{-1}cm^{-2}\Omega^{-1}$ for the 30,000°K case was 430 times that obtainable from a 5000°K black body.

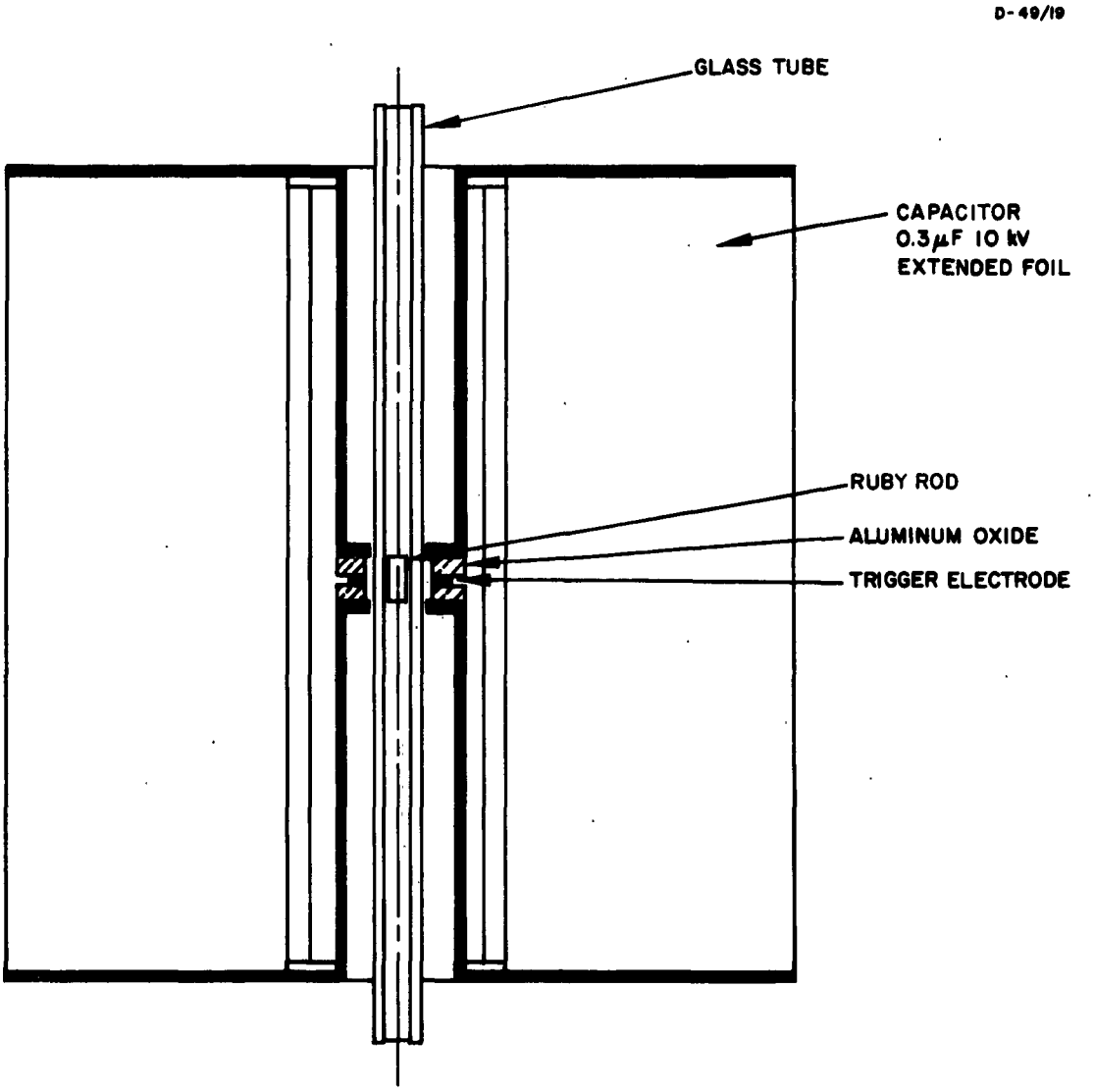

Fig. 51. Schematic of short-duration optical pump (discharge circuit shown in heavy black).

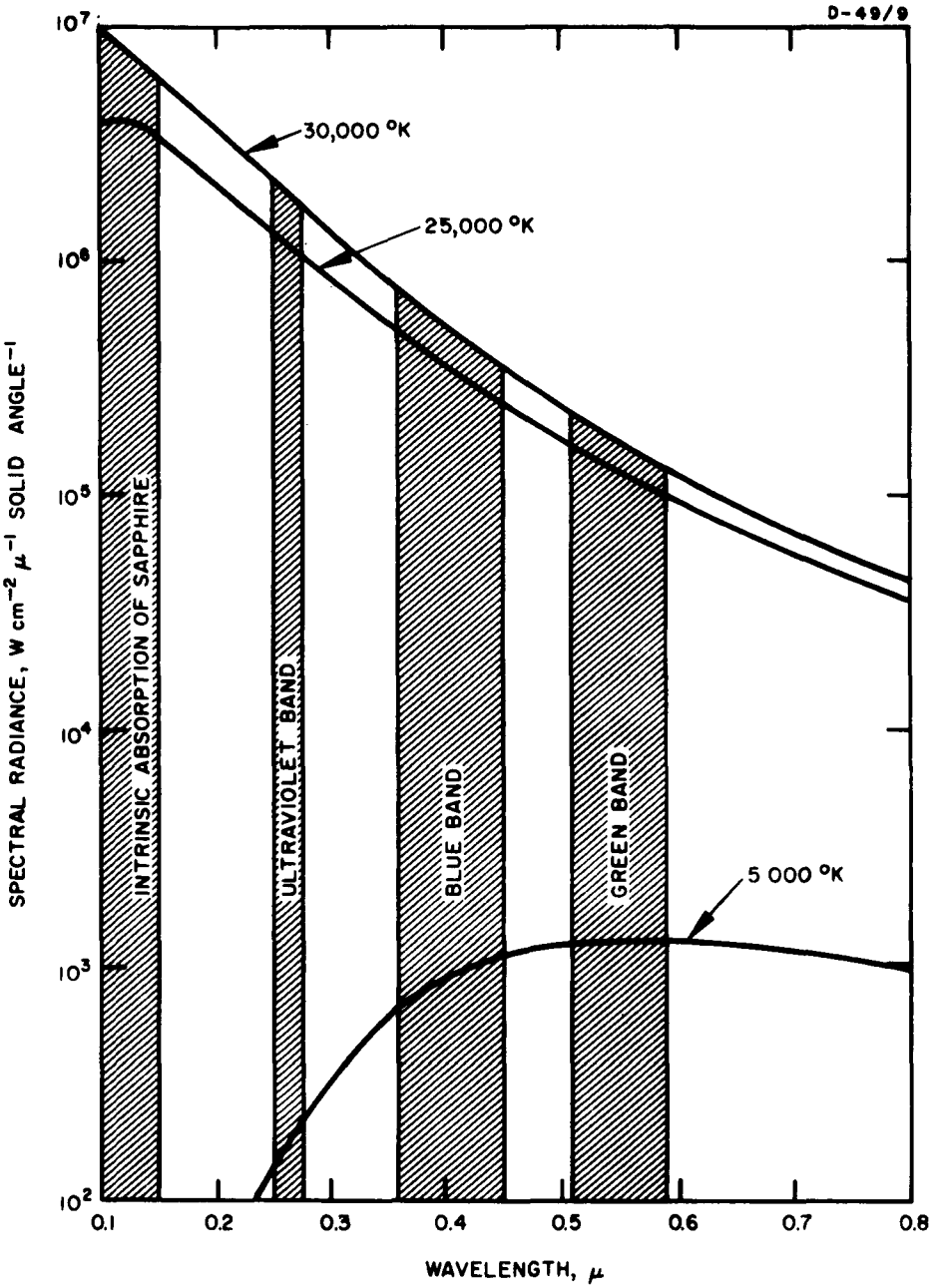

Fig. 52. Black-body radiance and ruby absorption bands

TABLE 1

Photon Density in Ruby Pumping Bands
Versus Black-Body Temperature

Temperature, ^{o}K	Radiant Photon Density for the Wavelength Intervals Shown, photons $sec^{-1}cm^{-2}$ solid $angle^{-1}$			
	2500-2750Å	3600-4500Å	5100-5500Å	Sum for these three bands
5000	7.0×10^{18}	1.7×10^{20}	2.9×10^{20}	4.7×10^{20}
25,000	4.0×10^{22}	6.5×10^{22}	2.9×10^{22}	1.3×10^{23}
30,000	7.3×10^{22}	8.9×10^{22}	3.8×10^{22}	2.0×10^{23}

Earlier in the project it was assumed that 100 μsec was a typical time at which oscillation would occur after the start of the pump pulse. Data taken later, however, showed that with the helical flash lamp set-up, oscillation set in at a little less than 400 μsec. Thus, the initial assumption was in error by a factor of four, and this made the assigned task more difficult by that factor. The duration of the microsecond pulse was variously found to be 1 to 2 μsec, with a pulse shape otherwise very similar to that of the millisecond helical pumps. Accordingly, pulse shape differences were considered to be only a small effect. The initial calculation assumed 1 μsec. Now, using what are known to be reasonable parameters for duration and radiance, the photon flux-duration products in the pumping bands may be calculated, as shown in Table 2.

TABLE 2

Comparison of Helical and Coaxial
Pumping Parameters

Source	Temperature, ^{o}K	Photon Flux, photons sec^{-1} $cm^{-2}\Omega^{-1}$	Duration, sec	Flux-Duration Product, photon $cm^{-2}\Omega^{-1}$
Helical	5000	4.7×10^{20}	400×10^{-6}	1.9×10^{17}
Coaxial	30,000	2×10^{23}	2×10^{-6}	4×10^{17}

An additional factor which was considered was that pumping with microsecond pulses avoided the loss of excited state population due to spontaneous emission during the pumping period. This factor is estimated to result in a 10% increase in efficiency over millisecond pumping.

The next point of concern was whether the high brightness was achieved over sufficient area to envelop the crystal. Measurements disclosed that the annular cavity (Fig. 53 shows detail of the cavity), bounded by a confining ceramic cylinder on the outside and a transparent tube (containing the ruby) in the inside, was not being filled at the time of peak brightness. In order to secure better filling of the volume with the radiating plasma, the inside diameter of the outer insulating cylinders was reduced; thus the volume in which the discharge occurred was reduced by about 50%. This did produce better filling, but both glass and quartz inner cylinders failed at energies above 10 J. A sapphire cylinder was then obtained, but this did not fire polish. Rather, "pocking" occurred in the surface, and these depressions filled with deposits of tungsten electrode material. At 20 J, the sapphire also broke, and further work on the coaxial design was discontinued.

Much effort was devoted to determining the effect on brightness of the atomic weight and pressure of the gas in the discharge gap. Measurements were made of brightness, intensity, and the efficiency of these sources as ruby pumps. Generally, it was observed that the brightness increased as the atomic number and pressure of the gas increased, provided the expansion of the heated plasma was not restricted by mechanical constraint. In a confining channel, however, the difference in brightness between different gases was largely eliminated. Fewer measurements were made of the intensity, which is the brightness-area product, but the differences between atomic weights were not great in either a confined or nonconfined channel. The parameter of most direct concern was the level of ruby fluorescence as the atomic weight and pressure of the gas were varied and as discharge channels of different configurations were used. Several configurations from which information under a variety of conditions was obtained are given below.

1. The coaxial source, as shown in Fig. 51, in which the discharge occurs at the center of the capacitor. This arrangement required pressurization of the full assembly and led eventually to breakdown of the capacitor during its immersion in the high atomic number gases.

2. An adaptation of the above source, in which the discharge gap is brought to one end plate and the gap alone is pressurized (Fig. 53).

3. A source identical to the latter, except for a smaller annular volume for the discharge.

4. An elliptical housing in which the ruby lies at one focal axis, and a linear discharge is at the other focal axis (Fig. 54). The housing was pressurized and the discharge driven by the 0.4-μF capacitor at up to 20 J. Electrical insulation necessitated that the end plates be epoxy rather than polished aluminum, which resulted in some loss of efficiency of the cavity.

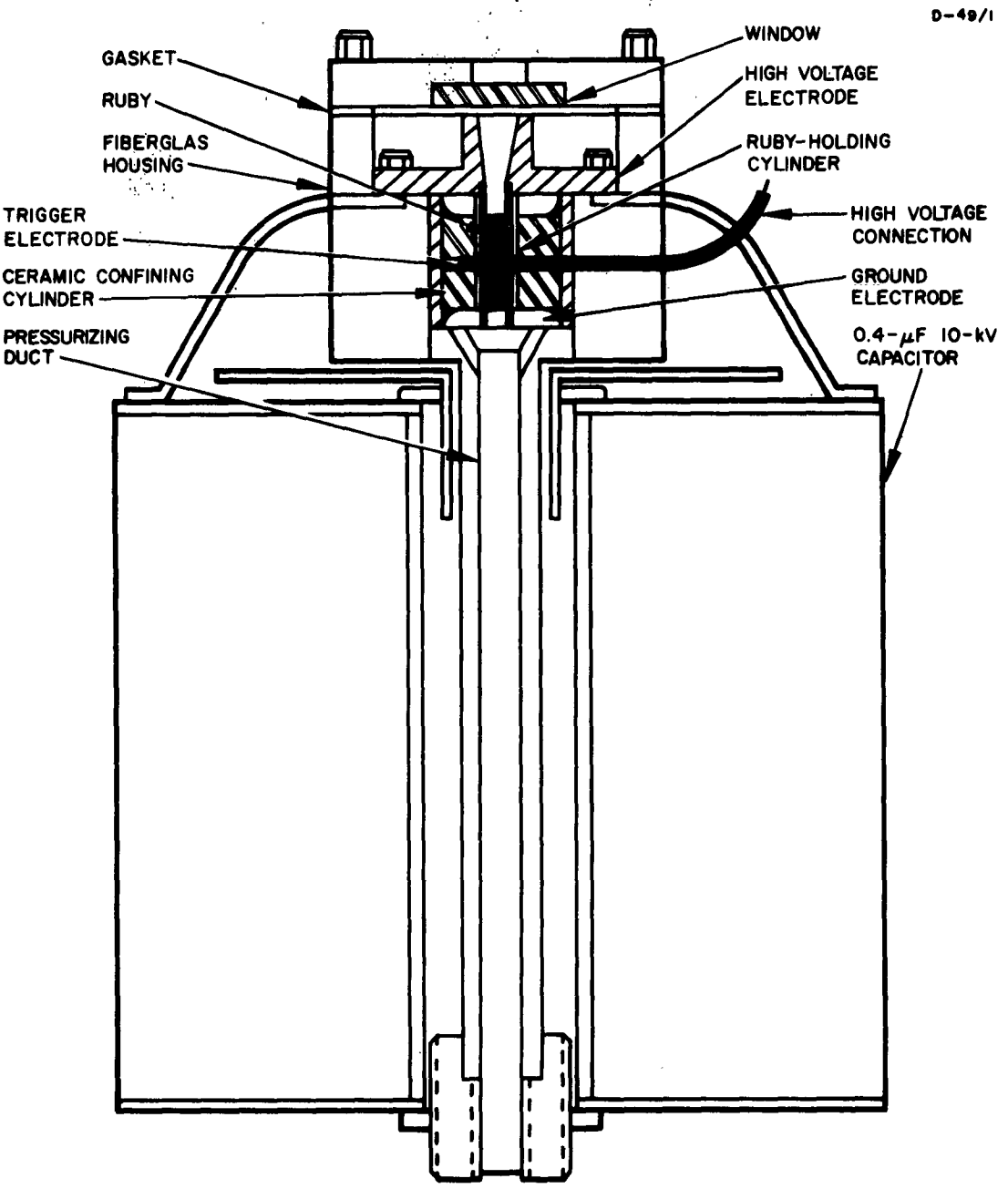

Fig. 53. Coaxial 0.4-μF source with pressurized Fiberglas housing.

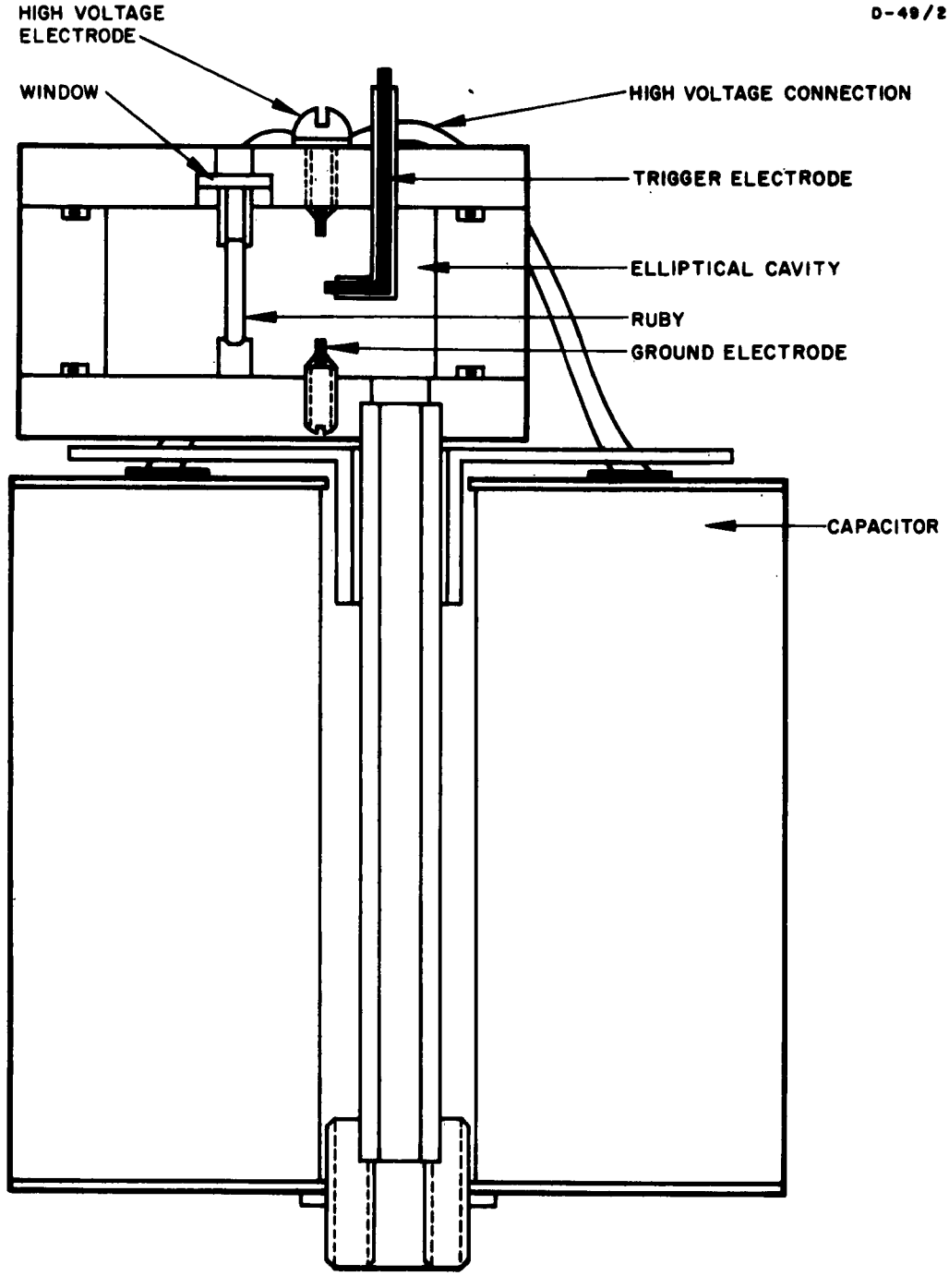

Fig. 54. Elliptical pressurized cavity

5. The elliptical cavity (item 4 above) was also driven with an 18-μF capacitor, permitting an energy expenditure of 450 J.

The effect of atomic number and gas pressure (hence energy) in producing ruby fluorescence for the coaxial assembly is shown in Fig. 55 and that for the elliptical cavity in Fig. 56. Also shown for reference in Fig. 56 are some data on ruby fluorescence with a helical flash lamp. All data are based upon a ruby 0.125 in. in diameter by 0.626 in. long. The ruby was resilvered between the taking of data for Figs. 55 and 56. Therefore, the ruby fluorescent emission is expressed in arbitrary units for Fig. 56, since absolute comparisons of the figures would not be valid.

The following conclusions may be drawn from Figs. 55 and 56:

1. In both sources, xenon is superior to the lower atomic number gases.

2. Doubling expended energy nearly doubles the ruby fluorescence.

3. The elliptical cavity was less efficient than the coaxial source.

4. The coaxial source with xenon was more efficient than a helical, high-energy flash lamp, although of insufficient energy to produce oscillation.

At the time the above data were collected, it appeared that threshold would not be obtained with the 0.4-μF source. The improvements in lowered threshold achieved with an elliptical cavity were not realized and possible reasons for nonoscillation were re-examined.

In the case of the coaxial cavity, we believed that failure to achieve uniform illumination at peak brightness due to a material limitation was precluding sufficient light flux into the crystal. Although this was probably a factor, it must be remembered that the crystal was thin — only 0.125 in. diameter. The most promising property of a pressurized elliptical cavity was that these problems were neatly side-stepped, and the design was approached with optimism.

The discharge column (Fig. 54) was made the same length as the ruby, thus producing efficient geometrical coupling. The walls of the cavity were well polished, and high reflectivity in the visible was measured. Some deposition of electrode materials occurred, but it was not excessive. Xenon was used in the cavity with discharge energies from 5 to 450 J. Again, oscillation was not attained, for reasons other than uniformity of illumination.

The most significant difference between the short duration pump and the more conventional pump is the difference in ultraviolet content

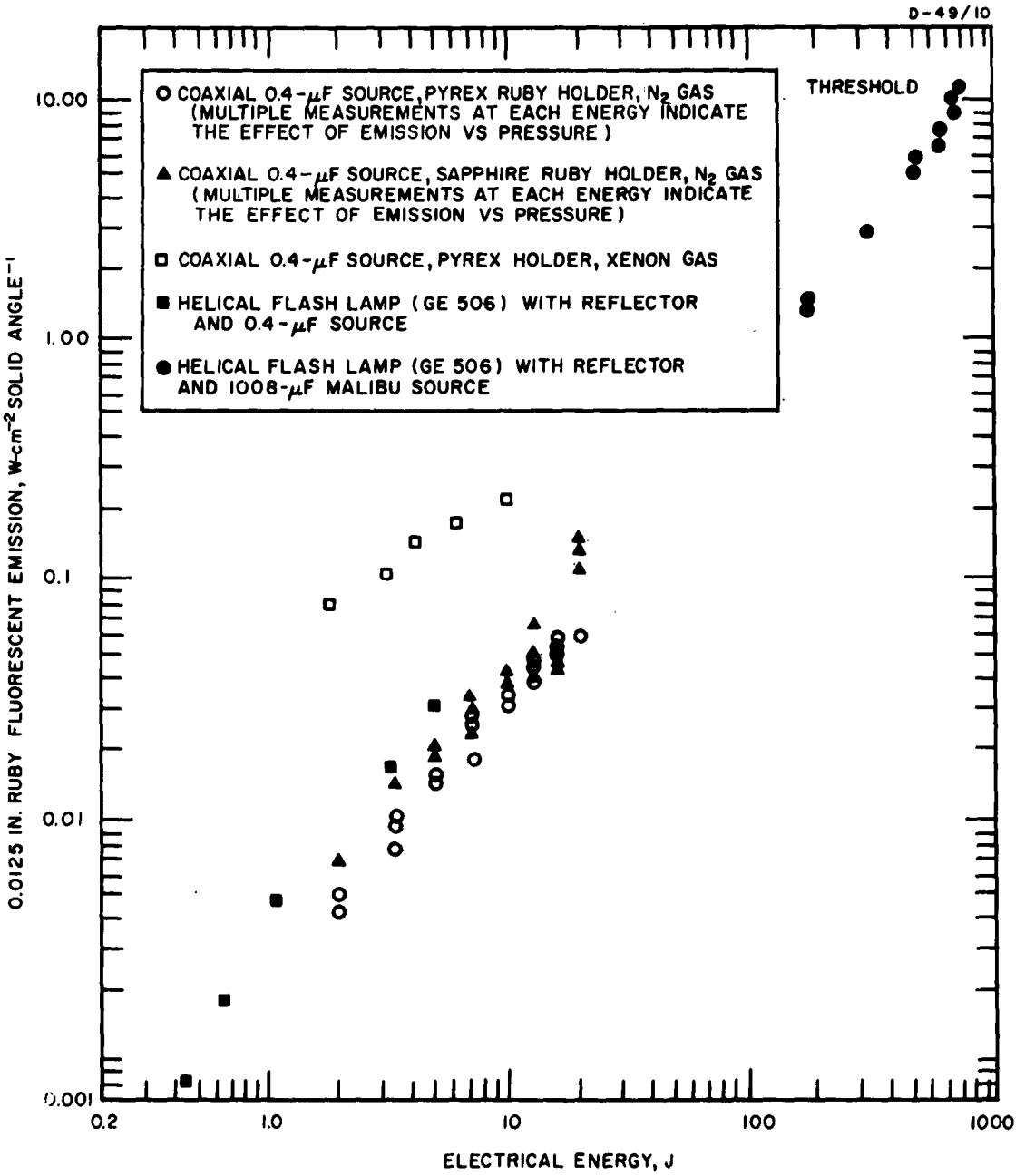

Fig. 55. Ruby fluorescence versus energy with source configuration and gas type as parameters.

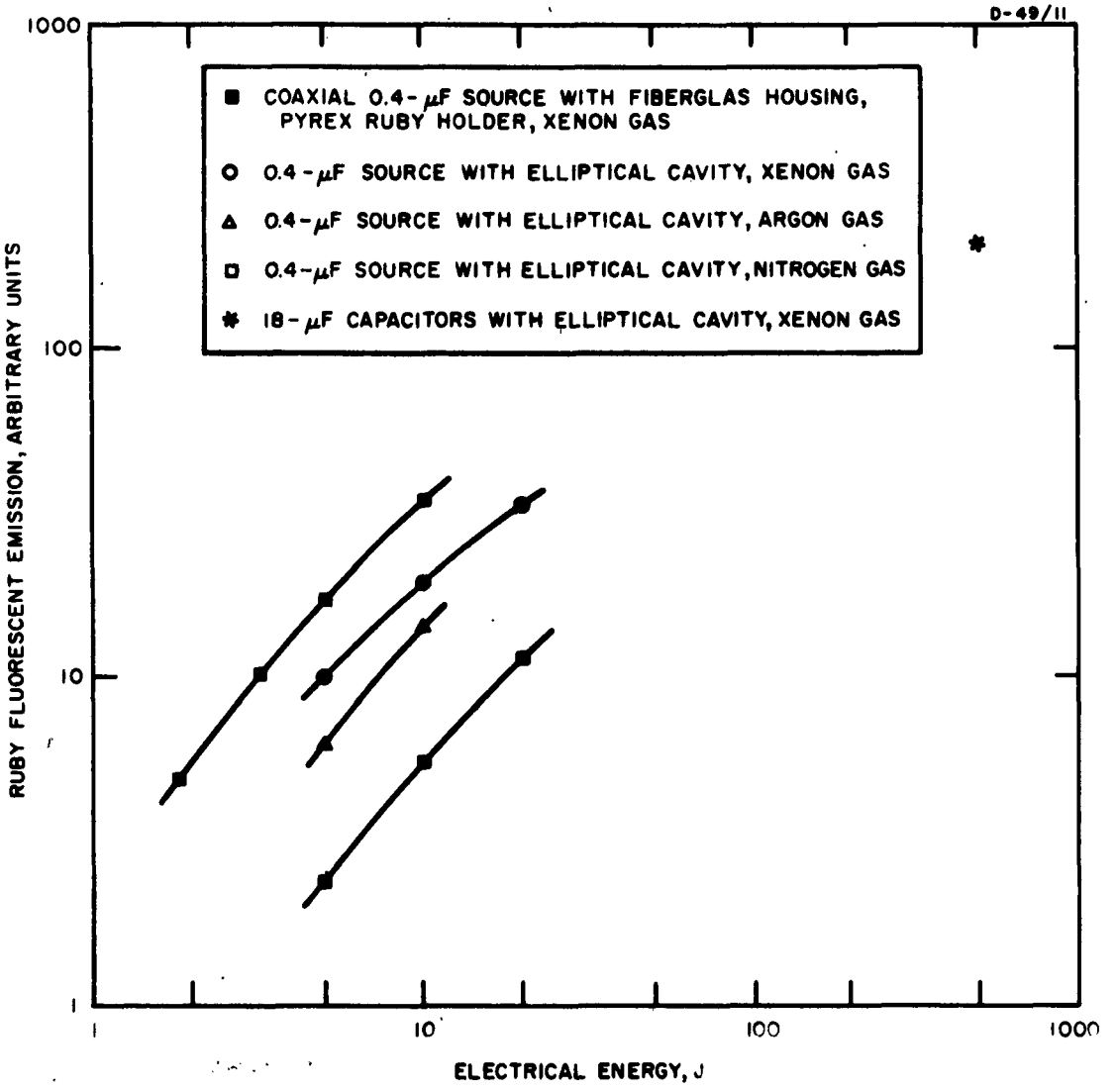

Fig. 56. Ruby fluorescence as a function of gas type and configuration

(see Fig. 52). Short ultraviolet radiation can produce transitions from the sapphire valence or chromium ground states to the sapphire conduction band. Figure 57 is included to illustrate the effects that the ultraviolet might have, but it must be recognized that diagrams such as this are really a simple view of the conditions existing in a crystal lattice (see Ref. 29).

The high energy discharge produces several effects which might inhibit laser action:

1. Metastable and higher states are emptied by excitation of electrons to the conduction band. It will be noted that wavelengths shorter than 2800 Å are sufficient and that the source peaks at about 1000 Å. Some of the earlier work (Ref. 30) on quantum efficiency in the near ultraviolet shows that decrease in fluorescence may occur in its presence. However, no data are available concerning fluorescence as the peak of the exciting pump moves to well beyond the absorption edge.

2. Presence of free carriers in the conduction band can affect the transparency of the crystal. Attempts to determine the magnitude of this effect were not successful. Only a small reduction of the transparency to both the pumping wavelengths and the oscillation wavelength would be needed to reduce the gain below threshold. The lifetime of the electrons in the conduction band of ruby was not know; hence a reliable calculation of the magnitude of this effect on transparency could not be made. With reasonable assumptions, however, the free-carrier concentration did not appear to be sufficient to justify nonoscillation.

3. Ion bombardment from the source was found to produce high surface conductivity lasting up to 100 μsec. In the coaxial design, in which the sapphire enclosing the ruby was bathed in the arc, this deposition of surface charge may have produced abnormally high surface reflectivity for the pump light. However, this mechanism could not have had an appreciable effect in the elliptical cavity configuration because the walls of the cavity and ruby were well removed from the arc and the time of ion bombardment would sufficiently lag the time of arrival of the light pulse.

In the course of work, an attempt was made to keep abreast of similar work in other companies. The following list covers such liaison:

1. At the University of California, Livermore, the use of the pinch effect as a ruby laser pump has been explored. Under certain experimental conditions, a constriction occurs in the high current conduction channel of a rare gas, and light is emitted at the time a minimum diameter column is obtained. Theoretical consideration was given, by Dr. Wangsness, to the value of a true 35,000°K black body compared with the pinch phenomenon as a ruby pump. He concluded

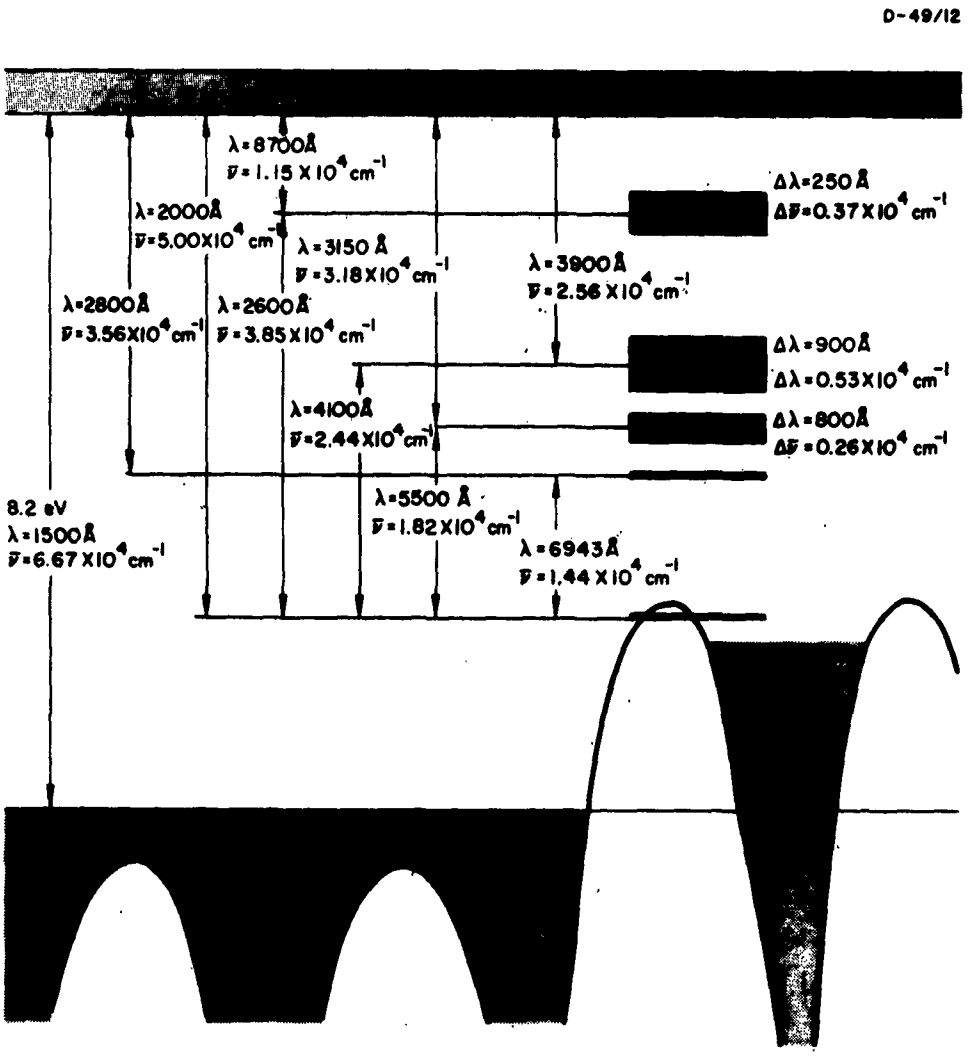

Fig. 57. Energy-level diagram of ruby.

that the black body should be better because the pinch occurs with a rarified gas, and although very high temperatures are achieved, the density of radiating particles is low. Recently, it was learned that ruby oscillation was not attained at Livermore and that the equipment ultimately failed. One wonders if, again, the presence of intense ultraviolet was deleterious, particularly when it is recognized that with the pinch even neutrons are produced (Ref. 31).

2. At Space Technology Laboratory, Canoga Park, research on high-temperature microsecond discharges has been conducted with several large capacitors and gaps in parallel and high pressure operation. Temperatures up to 60,000°K were claimed, and the reports were made available by Dr. F. Mastrup. His objective was battlefield illumination; his work was noteworthy, but offered little of value to our project (Ref. 32).

3. Motorola Research Laboratories, Riverside, have been experimenting with arc discharges in oil as laser pumps. This work is beset with problems of confinement, dispersing bubbles, and the optical properties of the oil. High brightness is achieved and the volume is small, but these do not alone constitute a good laser pump (Ref. 33).

4. Westinghouse and IBM have been experimenting with exploding wires as laser pumps. Westinghouse focused attention on low inductance discharge circuitry and achieved the discharge of 10,000 J in 8 μsec, with temperatures well in excess of 30,000°K. Oscillation was obtained at 12,000 J, but more energy did not significantly increase the output. IBM, using different circuit parameters to obtain a peak temperature of 3000°K, succeeded in getting oscillation at only 200 J. Again one is forced to conclude that the ultraviolet in the very hot pump accounts for this startling difference (Ref. 34).

V. CONSTRUCTION OF A PULSED REFLECTOR LASER FOR THE AIR FORCE

The requirements of the extended contract included the construction of a PRL for delivery to the contracting agency. This unit is presently in the assembly and testing phase, and we expect to deliver it as scheduled.

The various parts of the PRL are shown in Fig. 58. The optical apparatus is mounted on a special table some 90 cm long, which is designed to be mounted, in turn, on a Gaertner optical bench. The power supply is housed in its separate cabinet, and three cables (flash lamp, trigger, and Kerr cell) connect it with assemblies on the optical bench.

The optical apparatus is shown in Fig. 59. The cylindrical chamber at the left houses the 3-in. helical flash lamp and the 3- by 1/4-in., 90°, 0.05% concentration ruby. To the right of it is the holder for the 1° deviation optically contacted Wollaston prism, and to the right of that, the nitrobenzene Kerr cell. Holders for the 1-in. dielectric-coated mirrors (one low, ~80%, and one high, ~98%, reflectivity) are at each end. The power supply is shown in Fig. 60. At the top is the control unit, which includes the energy storage controls, trigger circuits, and delayed-pulse generator for the Kerr cell. Beneath it is the Kerr shutter apparatus, and at the bottom the capacitor bank for energy storage.

The instruction manual for this unit is still being prepared. A temporary set of instructions will be supplied.

M 2242

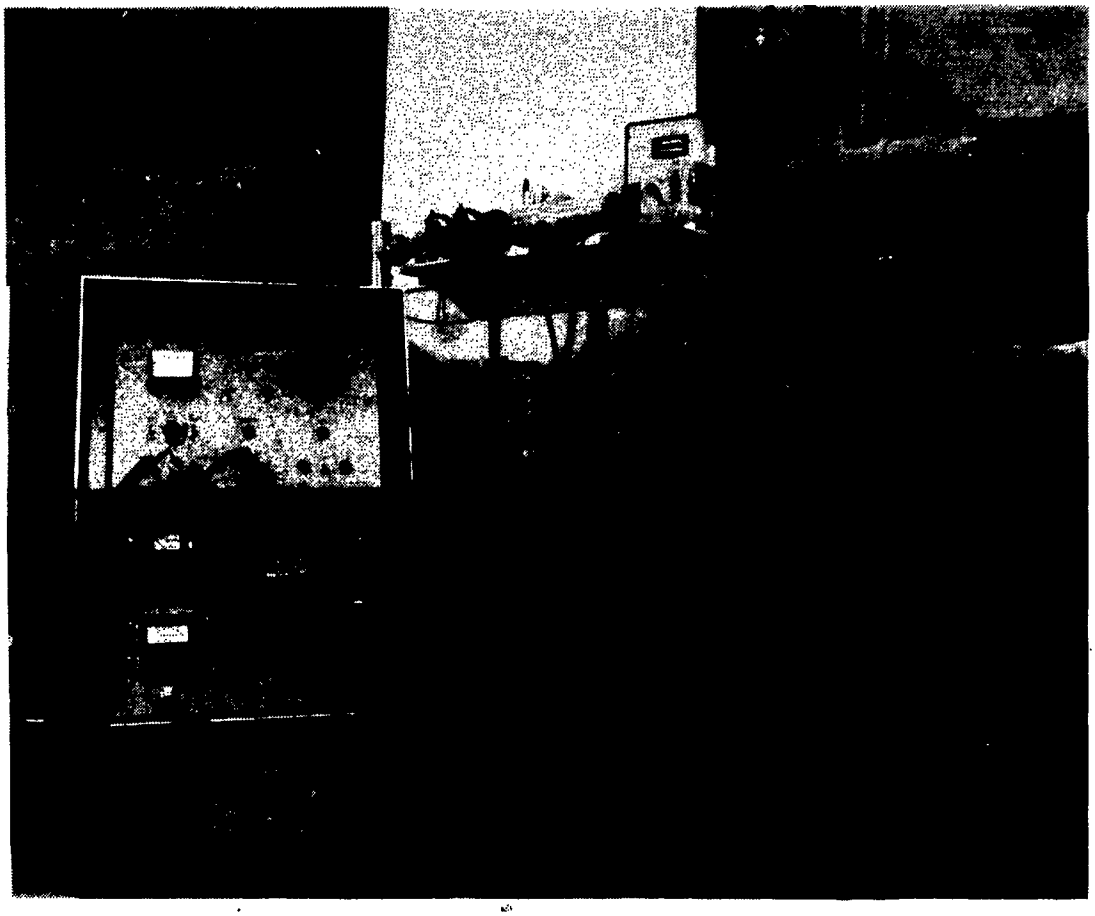

Fig. 58. Complete PRL assembly.

M 2243

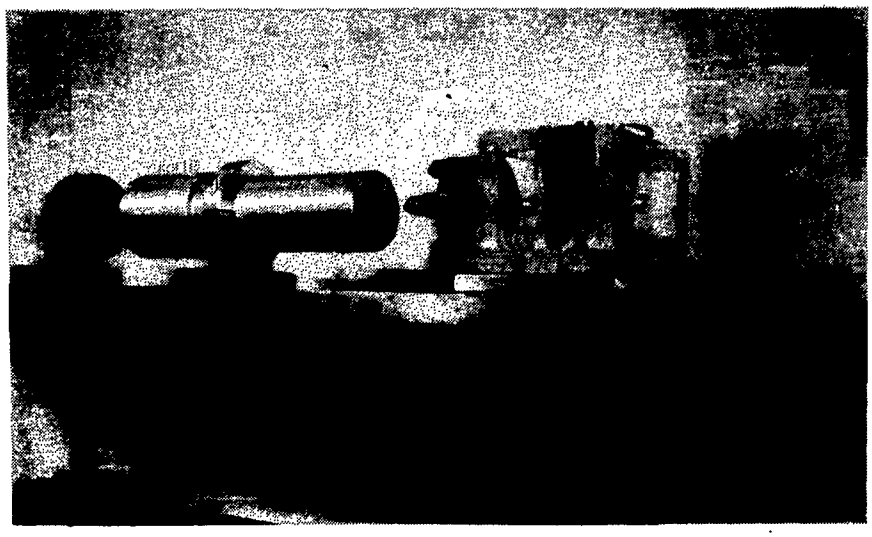

Fig. 59. PRL – optical apparatus.

M 2244

Fig. 60. PRL – power supply apparatus.

VI. LASER MATERIALS RESEARCH

A. INORGANIC CRYSTALS

The task of growing laser quality single crystals of refractory oxides by the flame fusion method was simplified considerably, since the knowledge gained from successfully utilizing this technique for the growth of large; homogeneous; inclusion- , strain- , and bubble-free single-crystal ruby aided significantly in anticipating the problems associated with the growth of new materials.

A technique for forming a solid solution of the material to be grown (substitutional feed) was developed which is far superior to the conventional mechanical mixture feed. The former represents the case where dopant ions are substituted for cations in the lattice of the finely divided starting powder. The latter is an intimate mixture of guest and host ion powder form.

Preparation of substitutional feeds (s-feeds) was accomplished by different methods: (1) direct hydrolysis, (2) slow hydrolysis through dialysis, and (3) thermal diffusion of a mechanical mix (m-feed). In all cases solid solution formation occurred at 1100°C (during calcination for methods (1) and (2)).

A comparison of the m-feeds and s-feeds relevant to growth of laser quality crystals is given below.

1. Undissolved guest species (specks) have been eliminated with s-feeds. These specks present sites of extreme changes in (1) dopant concentration and (2) elastic properties. With m-feeds, growth rate is severely limited by the solution rate of these specks. With s-feeds, this limitation is not encountered and growth may be programmed at higher rates approximating the value inherent for the axis employed.

2. Burn-out in the bulk melt phase is lower for s-feeds since the vapor pressure of the solute is lower. However, the parameter of significance in burn-out in the melting zone of trajection for the powder feed (molten) is dopant vapor pressure times total surface area. This product is greater for the s-feed and results in a larger over-all burn-out. Surface factor causes burn-out in the trajection zone to be more significant than that in the bulk melt. This was verified by the low burn-out in melted sections (bulk melt) of ruby rods.

An s-feed from a fine grade alumina gave a very large total burn-out. With the Verneuil method, zero burn-outs are the exception rather than the rule. Where solute volatility with respect to the host is considerable, the technology was directed toward a reproducible and

constant burn-out through a greater portion of the boule. This has been accomplished for the case of ruby, where an optimum standardized growth procedure was developed.

Substitutional feeds of α-alumina-doped Mn^{4+}, Eu^{3+}, Tb^{3+}, and Dy^{3+} were formed by the thermal diffusion process. Single crystals were grown and spectroscopically examined; however, only in the case of Mn^{4+}, where MgO was used as an additive for charge compensation, did the product exhibit a narrow-line fluorescence characteristic of the guest ion.

Of the many monocrystalline materials grown (e.g., La_2O_3, In_2O_3, Y_2O_3, $ZnTiO_3$, $BaTiO_3$, $CaTiO_3$, etc.) and doped with various rare earth and transition ions, the spinels seem most promising. The spinel family of compounds represents a mutually soluble group of hard crystals which can be grown into large boules by the Verneuil (flame fusion) technique. Because spinel is somewhat softer than sapphire, it is more easily worked for optical purposes. Of greater interest is the fact that the cations in the typical spinel A_2BO_4 can be distributed in the normal manner between tetrahedral and octahedral coordination sites in the so-called normal spinel $A_2^{VI}B^{IV}O_4$, in the inverse manner $(AB)^{VI}A^{IV}O_4$, or randomly with A and B ions statistically distributed over the sites.

Mutual experiments involving chromium-doped spinels, i.e., $MgAl_2O_4$ (inverse), $ZnAl_2O_4$ (regular), showed displacement of emission peak position. $MgAl_2O_4$ shows an emission peak at 6970 Å and $ZnAl_2O_4$ a peak at 7020 Å. Refinement of absorption bands has also been reported and explained by site occupation of cations and by temperature effects.

Laser testing of chromium-doped spinel is in progress. If laser action can be attained, the spinel family offers a new possibility to laser systems—a controlled systematic variation of output wavelength.

B. COLLOIDS

A method which indicates promise for observing cw laser operation in liquids is described as follows. A crystal that exhibits laser action in the solid state (ruby, for example) can be ground up to the point where the particle size is very small compared with the wavelength of laser light. The wavelength of light in the ruby laser is about 7000 Å; therefore, in this case, a particle size of 100 to 1000 Å is desired. The particles are dispersed in a liquid as a colloidal suspension.*

Such a system would show all the properties of a liquid, including being easily cooled, circulated, etc. In addition, the spectral properties

*C.R. Giuliano, Hughes Aircraft Company Invention Disclosure, 17 November 1961.

(line widths, lifetimes, etc.) would be those of ruby, which is known to show laser action. Collisions of these colloidal particles with the "solvent" molecules would have very little effect on the chromium ions inside. The effect of collisions with the solvent probably would be immeasurably small.

The reason for requiring the particles to be small compared with the wavelength is to reduce scattering reflections. The scattering due to such particles should be effectively no greater than that resulting from the molecules of the liquid itself.

Gamma alumina, which has an average particle size of only 300 Å, has been obtained and microcrystalline ruby has been prepared from this material by evaporating a water slurry containing chromic nitrate heptahydrate followed by calcination at 1000°C. Both diffusion of Cr^{3+} into the lattice and the transformation of gamma to alpha occur at appreciable rates at 1000°C. Although ruby powders have been prepared with the proper particle size, aggregation occurs in the dispersing medium (water). Absorbtion spectra of the remaining dilute dispersions show faint suggestions of the spectrum of ruby; however, since their intensity is low, positive identification cannot be made. Efforts are being made to achieve uniform dispersions.

C. GLASSES

The techniques for preparing optical quality glass of various formulations suitable for high powered laser operation have been developed. Glasses prepared by optimum standardized techniques show few, if any, of the usual defects of striae, bubbles, or undissolved materials under microscopic examination; they are strain free and transparent to visible and far ultraviolet light.

Lifetime measurements were made on homogeneously doped Nd^{3+} barium crown glass identical in composition to that reported by Snitzer (Ref. 32). The average mean lifetime for clad and unclad samples was 0.6 msec, which is in excellent agreement with the reported value. Several samples of the glass sectioned from rods in the ingot show a refractive index (N_D) of 1.5398 ±0.0001 (reported value is 1.54). However, testing of numerous specimens in a laser apparatus at energies many times greater than that required for ruby of equivalent size and reflectivity did not yield stimulated emission in the 1μ region. Lifetimes of Nd^{3+} in various glasses are given in Table 3.

TABLE 3.

Excited State Lifetime of Nd^{3+} in Various Glasses

% Nd_2O_3	Glass Composition	Mean Lifetime, msec
0.5	Corning 9741	0.05
0.3	H-Glass (Ref. 34)	0.34
5.0	H-Glass	0.23
1.0	Borax($Na_2B_4O_7$)	0.06
5.0	Borax	0.04
1.0	25 wt % BaO 1 wt % Sb_2O_3 74 wt % Borax	0.06

D. ORGANIC MATERIALS

The excitation and emission spectra of several europium chelates were examined in the pure state and in solvents of benzene, acetone, and E.P.A.* at room and liquid-nitrogen temperatures. The following compounds were inspected: europium-tris-dibenzoylmethide (EuDBM), europium-tris-benzoyl-acetonate (EuBAA), and europium-tri-(o-hydroxoacetophenone) (EuHAP). EuDBM and EuBAA are quite attractive owing to their high stabilities, extremely broad excitation bands, and narrow line fluorescence of europium at 6300 Å (see Fig. 61 and 62). It was observed that the width of the excitation band narrows and the fluorescent line broadens considerably in benzene and acetone at room temperature. However, 10^{-3} molar solutions of these materials in E.P.A. at liquid-nitrogen temperature give the much desired spectral shape of the pure compounds.

Chelates of Dy^{3+}, Tb^{3+}, Sm^{3+}, Nd^{3+} have been prepared and are being investigated. Excitation and fluorescence spectra and lifetimes are being determined in various solvents at several temperatures. Preliminary results give the following guides for the molecular design of such materials with improved laser properties:

1. The continuous absorbtion band is characteristic of the organic portion of the molecule and is shown to be independent of the rare earth used.

*2:5:5 mixture (by volume) of ethyl alcohol, diethyl ether, and isopentene.

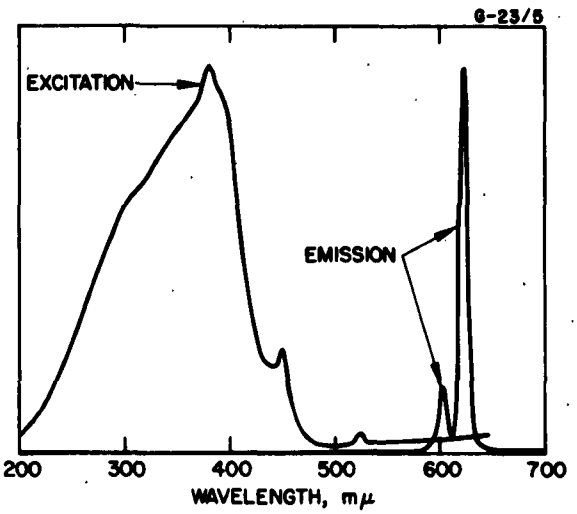

Fig. 61. Excitation and emission spectrum of europium-tris-dibenzoylmethide.

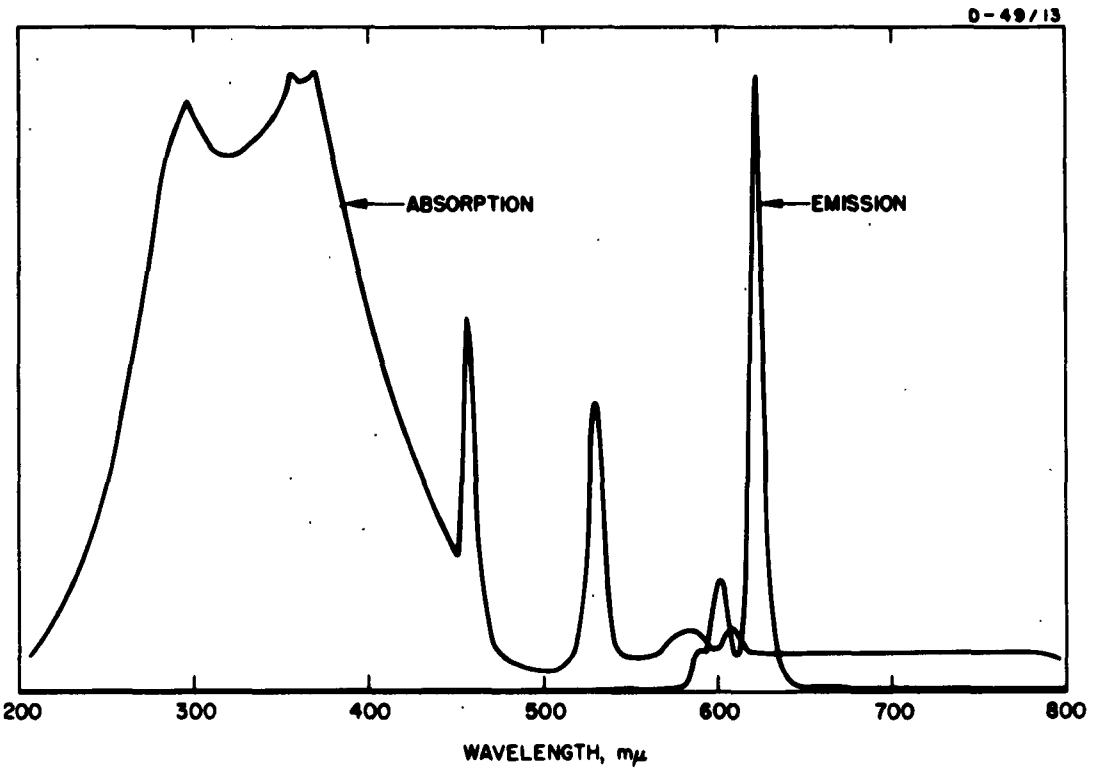

Fig. 62. Excitation and fluorescence spectrum of Eu(BAA).

2. The fluorescence efficiency increases dramatically when a nitro group replaces a hydrogen atom in the para position of the benzene ring.

3. The fluorescence efficiency increases with covalency.

4. The triplet state of the organic molecule must be above the fluorescent excited state of the ion to yield the sharp line emission of the rare earth.

A flash apparatus and power supply have been fabricated, and apparatus tests have been completed successfully. This apparatus permits evaluation of liquids as well as solids; in addition, it can be used for flash spectroscopy measurements.

VII. CONCLUSIONS

The embodiment of the proposal for a PRL by R. W. Hellwarth has led to a device which can generate giant pulses of optical radiation of some nanosecond duration in the multimegawatt region. Systematic elimination of problem areas has resulted in a practical device which can be operated indefinitely without degradation of performance. Such a device has been fabricated for delivery to the contracting agency. Operating efficiency of the PRL is limited by shortening of the metastable lifetime at high population inversions and by crystal inhomogeneities, which give poor optical quality to the crystal and introduce inhomogeneous broadening that impedes the transfer of energy within the metastable level. The lifetime shortening may be due to the focusing of the pump radiation at the center of the rod (Ref. 9) or to the existence of "whispering modes" (Ref. 11), i.e., paths of high regeneration, which exist near the periphery of the rod because of total internal reflection. The recently discovered satellite lines at 7660 Å, 8530 Å, and 9640 Å are also a source of inefficiency for generation of 6943 Å radiation. If the mechanism for producing these satellite lines can be determined, it may be used to generate radiation at different wavelengths.

The longitudinal mode characteristics of the ruby laser are well understood and are explained on the basis of the interaction of the optical Fabry-Perot resonator and the ruby system. The spectral character of stimulated emission at 300°K is determined by the length of the optical resonator. The spectral components in the laser spectrum are those which are generated in the axial cavity modes of wavelength $\lambda = \frac{2l\sqrt{\epsilon}}{p}$, where p is the mode number. At reduced temperatures, the emission is eventually determined by the center frequency of the laser transition. The spread in beam angle with increased beam energy is explained on the basis of the stimulation of a mode packet (a large number of closely spaced high transverse order modes). It is believed that this is due to the inhomogeneous broadening in ruby, which, in effect, limits the rate at which energy can diffuse within the excited level.

The symmetric radiation patterns in the near field at oscillation threshold have been studied and are believed to be evidence of single mode operation. A study of the frequency characteristics of these modes, using a traveling-wave phototube, has been incomplete in the sense that a definitive measurement of the frequency difference between such fundamental modes has not been made.

The analysis of the dependence of laser threshold on the various parameters (ruby length, concentration, temperature; cavity length and reflectivity; and pumping rate) is concluded to be accurate since it has been verified by experimental results. Extensions of this theory to the

prediction of energy output give good qualitative results, but as the extension is based on a cw analysis, agreement is not precise. The analysis does, however, facilitate the optimization of a given laser configuration. Such laser configurations have yielded a minimum oscillation threshold of 42 J electrical input energy at room temperature; a larger system has delivered 17 J of optical energy when operated at room temperature.

Several laser configurations have been analyzed and the results used to determine the most suitable for the design of cw laser systems. To date, the elliptical cylinder and ellipsoid of revolution systems have not resulted in cw laser action at room temperature. However, increased ruby efficiency at low temperatures should make possible cw ruby lasers with these configurations. Either of these systems would be adequate for pumping Nd in $CaWO_4$.

Xenon gas at 1/5 atmosphere pressure is the optimum gas and pressure for exciting the ruby system. Spectral analysis of a xenon lamp indicated on optical conversion efficiency of 26.8 %, of which 17.8% of the total is in the ruby absorption bands.

It appears not only from our work but from exploding wire data that the presence of intense ultraviolet flux in a ruby pump can suppress oscillation. This may result from the production of free carriers in the ruby conduction band, which alter the crystal transparency, and/or (more probably) from the emptying of the metastable state to higher levels.

The use of substitutional feeds (pre-preparation of powdered end product) in the Verneuil (flame fusion) process has resulted in the growth of crystals of improved optical quality.

VIII. RECOMMENDATIONS

In order to improve the peak power output or increase the energy output in the PRL, three separate approaches are recommended. The first involves scaling up of successful experiments or operating devices in parallel in order to obtain greater energy storage. The second approach consists of storing energy in another ruby crystal operating as an amplifier for the giant pulse generator. This, in addition to increasing the beam energy, could shorten the pulse length (Ref. 36), which would be advantageous for some applications. The third would be to improve the existing device to obtain greater efficiency. All three of these approaches are recommended. To scale up the existing devices would probably compound some of the problems already encountered. However, the amplifier approach may eliminate many of the problems encountered to date.

It is recommended that work be initiated on a laser power amplifier. Such a device appears to offer promise for at least two applications: (1) It now seems likely that maximum power output will probably require the use of an oscillator-amplifier combination. (2) Since single mode behavior will probably be achieved from ruby only at low power levels, it may be necessary to employ an oscillator-amplifier combination to obtain even moderate power in a single mode from a solid-state laser. Preliminary experiments, both at Hughes and elsewhere (Ref. 37), have demonstrated modest amplification through use of a pulsed ruby amplifier driven by a ruby laser oscillator. A more comprehensive study of the amplifier is warranted, both to achieve the objectives stated above and to provide further detailed information regarding the physics of the laser itself. The laser amplifier is a simpler device than the oscillator, since its operation is not complicated by the effects of regeneration; thus a detailed study of its properties should help to provide an improved understanding of the basic properties of lasers in general.

Other configurations for the PRL should be examined. To date, almost all laser configurations have been of the Fabry-Perot type, where a part of the energy is reflected directly back into the laser material. Other resonant structures are known, and some of them might offer advantages. For example, the fluorescent radiation can be recirculated through an external optical system and back in the opposite end of the crystal to provide the required feedback. This system can be easily adapted to the pulsed-modulation arrangement.

It is recommended that a study to determine the mechanism which is responsible for the satellite emission at 7660 Å, 8350 Å, and 9640 Å in the PRL be initiated. Exploitation of this effect may lead to

a novel method of producing intense radiation at different wavelengths by using materials other than nitrobenzene in the PRL circuit.

Various inefficiencies in the ruby laser, operated in both the normal and PRL modes, have been attributed to the inhomogeneous line broadening in ruby. It is possible that the intrinsic line width in the laser material is a cause of incomplete energy conversion. The separation between longitudinal modes can be narrower than the intrinsic line width which is due to inhomogeneous broadening. The homogeneous broadening (temperature-dependent part of the fluorescent line width) presents no particular problem, since the cross-relaxation within the line, when broadening is homogeneous, occurs in about 10^{-12} sec. This means that the very narrow laser mode lines will not "eat a hole" out of the homogeneously broadened line. The cross-relaxation time for inhomogeneous broadening is not known, but if it were long compared with the giant pulse duration, there would be an appreciable number of ions remaining in the excited state.

For the above reasons, it is recommended that the inhomogeneous broadening and cross-relaxation mechanisms in ruby be the subject of further investigation. A thorough knowledge of the kinetics of these mechanisms could well lead to improvement in the efficiency of the ruby laser.

As a result of the frequently mentioned inhomogeneous broadening, the ruby laser at reasonable power levels operates as a multimode oscillator. Continued investigation of the feasibility of single mode behavior, with further study of the spectral properties of small rubies showing symmetrical beam patterns, by means of the microwave phototube as a high-resolution spectrometer is recommended.

In the presence of inhomogeneous broadening, single mode oscillation at reasonable power levels may still be obtained by appropriate internal and/or external mode selection techniques. These approaches, coupled with the use of a power amplifier, are recommended for future support.

Further study of the cw ruby system at reduced temperatures is recommended. It is believed that conventional pumping configurations (with their several advantages over the trumpet configuration) can be made to provide cw operation. This has particular significance if this mode of pumping can be combined with the single mode operation in ruby discussed above.

Further work on very hot microsecond pulses of light as a ruby pump is not recommended. However, for shorter wavelength lasers (Ref. 38), where there exists a need for a pump supplying appreciable

intensity at shorter wavelengths, this technology can be applied. To this end, it is recommended that an investigation of the use of higher energy gap materials as host lattices be made.

Additional study of the mixed spinel (Al_2BO_4) crystal systems is recommended. If laser action can be obtained in this crystal system, it should be possible to vary the emission wavelength systematically.

APPENDIX

Since the Air Force Contract supported much of the research published by members of the Quantum Physics Department of the Hughes Research Laboratories, abstracts of the papers are included in the following section.

LASER AND LASER APPLICATIONS RESEARCH AT HUGHES AIRCRAFT COMPANY*,**

George F. Smith

Hughes Research Laboratories
Malibu, California

ABSTRACT

The laser research and development program, of which the first successful ruby laser experiment was a part, will be reviewed. This program includes fundamental laser research, research on modulation and detection techniques, studies of laser applications, and the development of practical laser systems.

Progress has been made in understanding and improving the ruby laser. Recent accomplishments include observations of zero-field ground-state splitting, fluorescent spectra and laser modes as a function of temperature, transverse mode patterns, and laser action at the R_2 line. Several gaseous lasers of the helium-neon type have been constructed and operated; other gaseous mixtures are being investigated. Two promising modulation techniques — regeneration and "hair-trigger" modulation — have been devised. Single pulses of 14-Mw peak power and 35-nsec duration have been obtained by means of the former method. Optical receivers have been studied; "microwave" phototubes have been designed and constructed.

Fundamental capabilities and limitations of laser communications and laser ranging systems have been examined. The narrow light beam available from the laser provides high transmission efficiency (angular resolution) but introduces aiming difficulties. The first laser ranging experiments utilized a pulsed ruby laser, a photomultiplier receiver, and modest optics. Daytime ranging to several kilometers was possible through the use of spectral filtering to discriminate against sunlight. More refined (COLIDAR) ranging systems are under development. Other applications of lasers will be discussed.

---

* This work was partially supported by Aeronautical Systems Division, Air Force Systems Command, under Contract AF 33(616)-8233.

** Presented at NATO-SADTC Symposium on Technical and Military Application of Laser Techniques, The Hague, Netherlands, April 3-5, 1962.

LASERS FOR COMMUNICATIONS AND OPTICAL RANGING*, **

George F. Smith

Hughes Research Laboratories
Malibu, California

ABSTRACT

The three key properties of the laser light source - brightness, focusability, and monochromaticity - enable it to transmit information efficiently to a distant point even in the presence of other undesired radiation "noise," because that noise can be rejected by a filter. To make full use of the 300,000 kMc of bandwidth available in the visible spectrum will require not only more and better lasers but also new means for modulation and detection. Regeneration modulation of a laser and superheterodyne detection with a microwave phototube are promising new techniques. Single pulses of 14-Mw peak power and 35-nsec duration have been obtained from a ruby laser by using regeneration modulation.

In a one-way communications link with constant-aperture diffraction-limited antennas, the fraction of transmitted power which is received is proportional to the square of the frequency. Signal fluctuation noise, however, increases linearly with frequency, so the S/N ratio improves only linearly with frequency. At optical frequencies, aiming problems are likely to limit the useful degree of beam collimation; thus, on the basis of bandwidth per transmitted watt, a laser space-communications link will be competitive with, but not drastically superior to, a futuristic microwave space link.

The high-power pulse performance of ruby lasers is promising for optical ranging. Although rudimentary ranging systems have operated only at several kilometers, it now appears feasible to range off the moon.

---

* This work was partially supported by Aeronautical Systems Division, Air Force Systems Command, under Contract AF 33(616)-8233.

** Presented at the Sixth Meeting of the AGARD Avionics Panel, Paris, France, July 9-11, 1962, and published in the Proceedings of that meeting.

PULSED-REFLECTOR MODE FOR PEAK-POWER ENHANCEMENT IN RUBY*,**

R. W. Hellwarth, F. J. McClung, and G. F. Smith

Hughes Research Laboratories
Malibu, California

ABSTRACT

Single output pulses of 14-Mw peak power and 35-nsec duration have been obtained from a ruby laser by suddenly changing the regeneration of the cavity. These pulses are several orders of magnitude more intense than the usual spontaneous pulsations which can be observed in the same apparatus without changing the regeneration. The regeneration is controlled by a Kerr cell shutter placed between the ruby and one of the reflectors. The physical principles of the system are outlined. The Kerr cell system is compared with others using different types of shutters. Some of the detailed mechanisms, potentialities, and limitations of the technique are discussed.

* This work was partially supported by Aeronautical Systems Division, Air Force Systems Command, under Contract AF 33(616)-8233.

** Presented at NATO-SADTC Symposium on Technical and Military Application of Laser Techniques, The Hague, Netherlands, April 3-5, 1962.

GIANT OPTICAL PULSATIONS FROM RUBY*, **

F. J. McClung and R. W. Hellwarth

Hughes Research Laboratories
Malibu, California

ABSTRACT

Giant pulses of optical maser radiation have been produced which are several orders of magnitude larger than the commonly observed spontaneous pulses. The pulses were produced by varying the effective reflectivity of the reflecting surfaces at the ends of the ruby rod through a Kerr-cell switching technique. The measured pulse characteristics are found to be in agreement with theoretical predictions.

---

* This work was supported in part by the Aeronautical Systems Division, Air Force System Command, under Contract AF 33(616)-8233.

** Published in J. Appl Phys. 33, 828-829 (March 1962).

CHARACTERISTICS OF GIANT OPTICAL PULSATIONS FROM RUBY*,**

F. J. McClung and R. W. Hellwarth

Hughes Research Laboratories
Malibu, California

ABSTRACT

A method of laser modulation is described which produces fast, intense, and controllable "giant" laser pulses. In experiments with ruby, pulses of peak power up to 15 MW and of duration less than 30 nsec have been studied. The principles of the technique are outlined and early experimental results reviewed. The temporal, spectral, and spatial structure of giant pulses under a variety of experimental conditions is reported. The pulse characteristics found to date yield information about the nature of various relaxation processes in ruby and point the way to further experiments to clarify many questions which are raised. The results (a) set an upper limit of 10^{-7} sec on the $\overline{E} \rightarrow 2\overline{A}$ relaxation time, (b) show a shortening of upper state relaxation time by about seven times under heavy pumping, (c) show relaxation of excitation taking place across the laser line in microseconds, (d) show progressive spectral broadening for shorter pulses to encompass most of the fluorescent line, (e) show increasing asymmetry of spectral output for faster, more intense pulses, and (f) show little broadening of beam divergence over normal, but with added structure.

---

* This work was supported in part by the Aeronautical Systems Division, Air Force Systems Command, under Contract AF 33(616)-8233.

** To be published in IRE Supplement on Quantum Electronics, January 1963, edited by Prof. J. R. Singer.

R_2 LINE OPTICAL MASER ACTION IN RUBY*

F. J. McClung, S. E. Schwarz, and F. J. Meyers

Hughes Research Laboratories
Malibu, California

ABSTRACT

Optical maser action at the R_2 line in ruby has been observed. Because of a fast thermal relaxation between the two ^2E levels, it is not usually possible to satisfy the maser conditions at R_2 when R_1 is masering. However, if the R_1 line can be suppressed from masering, even at high inversion, the R_2 line can be made to maser by the appropriate selection of operating conditions. This has been accomplished by using, for end reflectors, multi-layer dielectric interference filters which have high transmission at R_1 and low transmission at R_2. The selection of the operating conditions requires a correction to the absorption coefficients for the R_1 and R_2 lines based on the Boltzman distribution between the two excited states. When the Boltzman correction is made, the calculations show reasonable requirements on pumping threshold and reflectivities.

* Bull. Am. Phys. Soc. Winter Meeting at UCLA, December 27, 1961; Bull. Am. Phys. Soc. 6, 511 (1961). Also to be published in J. Appl. Phys.

LASERS AND THEIR APPLICATIONS*

I. J. D'Haenens and D. A. Buddenhagen

Hughes Research Laboratories
Malibu, California

ABSTRACT

The new coherent light sources, lasers, are a result of the extension of electronic techniques into the optical frequency region. Specifically, the laser is the result of a straightforward extension of the maser principle, hence the alternative title "optical maser." The optical maser was proposed by Schawlow and Townes in 1958. In June of 1960, laser action was first demonstrated in a single crystal of light pink ruby by T. H. Maiman of the Hughes Research Laboratories. In the year and a half following this significant technological breakthrough, a number of additional laser devices have been developed. Initial application of these lasers to useful systems has been demonstrated. The applications described or postulated below are only the beginning, and much work is needed before the full potential of the laser can be realized.

* Presented at the 6th SPIE Technical Symposium, August 7-11, 1961, Los Angeles, California, and published in the SPIE Newsletter.

STIMULATED AND FLUORESCENT OPTICAL EMISSION IN RUBY FROM 4.2 to 300°K: ZERO-FIELD SPLITTING AND MODE STRUCTURE*, **

I. J. D'Haenens and C. K. Asawa

Hughes Research Laboratories
Malibu, California

ABSTRACT

The spectral character of the stimulated emission from ruby has been investigated; we found that the zero-field splitting (0.38 cm^{-1}) of the $^4A_2$ ground level and the cavity optical length and its reflectivity determine the spectral character of this emission. At 300°K the system is induced into oscillation in a number of cavity modes separated by $\Delta\bar{\nu} = (2\ell\sqrt{\epsilon})^{-1}$, where ℓ is the length of the resonator and $\sqrt{\epsilon}$ is the index of refraction for the ordinary ray. At $T \cong 80°K$ the $\bar{E}(^2E) \rightarrow \pm 3/2$ $(^4A_2)$ and the $\bar{E}(^2E) \rightarrow \pm 1/2$ $(^4A_2)$ transitions were identified in the stimulated emission spectrum. Each can oscillate in an axial cavity mode (or modes) plus an off-axis mode at the center of the transition. At 4.2°K the system oscillates in off-axis modes, unless the length of the cavity ℓ is such that it has axial resonances coincident with the transition frequencies. An analysis of the temperature dependence of the oscillation threshold for the separate transitions is presented and is compared with the observed behavior.

---

* Bull. Am. Phys. Soc. Winter Meeting at UCLA December 27, 1961; Bull. Am. Phys. Soc. 6, 511 (1961). Published as Hughes Research Report No. 235 and submitted to J. of Appl. Phys.

** This work was supported in part by the Aeronautical Systems Division, Air Force Systems Command, under Contract AF 33(616)-8233.

MICROWAVE GENERATION IN RUBY DUE TO POPULATION INVERSION PRODUCED BY OPTICAL ABSORPTION*,**

D. P. Devor, I. J. D'Haenens, and C. K. Asawa

Hughes Research Laboratories
Malibu, California

ABSTRACT

Microwave amplification and generation by the stimulated emission of radiation (maser) were observed in ruby as a result of population inversion produced in the ground state of Cr^{3+} by the absorption of the coherent optical emission from a second ruby (optical maser). The maser crystal was oriented in a magnetic field of about 6700 Oe to obtain a transition between a ground $^4A_2$ Zeeman sublevel and an excited $\bar{E}(^2E)$ Zeeman sublevel which would match a spectral component of the output of the optical maser.

---

* This work was supported in part by the USASRDL, Department of the Army, under Contract DA36-039 SC-87221.

** Published in Phys. Rev. Letters 8, 432 (June 1962).

THEORY OF QUANTUM OSCILLATORS IN A MULTIMODE CAVITY*

W. G. Wagner and G. Birnbaum

Hughes Research Laboratories
Malibu, California

ABSTRACT

The spectrum of power radiated by a solid-state optical maser in steady-state operation is obtained by considering each atomic system to be a source of randomly fluctuating dipole moment which drives every mode of the cavity. The nonlinear behavior of the collection of atomic systems is treated in such a way that a detailed examination of the distribution of power in the various modes is possible. A number of examples are considered which show how critically dependent on the relative loss rates of the various modes are the characteristics of the output from a multimode oscillator. An interesting result of this calculation is the appearance in some cases of an abrupt transition as the pumping power is increased: above this point a large fraction of energy goes into the mode which is resonant with the atomic transition and which has the lowest loss rate. Another case is studied which does not have this feature, but which could be useful in analyzing the behavior of solid-state optical masers which have substantial scattering due to crystal imperfections.

* Published in J. Appl. Phys. 32, 1185-1194 (July 1961).

TRANSMISSION OF MONOCHROMATIC RADIATION IN A TWO-LEVEL MATERIAL*

W. G. Wagner, G. Birnbaum, and R. Bellman

Hughes Research Laboratories
Malibu, California

ABSTRACT

A theoretical study has been made of the transmission of a monochromatic, well-collimated beam of radiation normally incident on idealized material containing only two energy levels. The nonlinear partial differential equations governing the variation of population and photon density in space and time have been solved exactly for arbitrary initial conditions under the assumption that spontaneous emission and thermal relaxation from the excited state can be neglected. These conditions are satisfied in practice when the radiation is in the form of a pulse whose duration is short compared with the characteristic times of these relaxation processes. Two cases are considered in detail: (a) when all atoms are in the ground state and the material absorbs; and (b) when there is a population inversion and the material amplifies. In case (a), the radiation, with a characteristic velocity, "bores" its way through an optically dense substance emerging delayed in time and leaving the material in a perfectly transparent or saturated state. In case (b), an incoming pulse is amplified and sharpened - to a degree determined by the gain of the medium. In addition to these cases, the dependence of the apparent spontaneous emission lifetime on the size and population distribution of the material is mentioned.

* Published in the Opt. Soc. Am. Program of the 1962 Fall Meeting, p. 19.

TIME-RESOLUTION SPECTROSCOPY OF THE PULSED REFLECTOR RUBY LASER*,**

F. J. McClung, R. W. Hellwarth, and D. Weiner

Hughes Research Laboratories
Malibu, California

ABSTRACT

Stimulated laser emission occurs very quickly when under high pumping, and the laser loss is switched rapidly from a value higher than, to a value lower than, the gain. Streak photographs of the spectral output vs. time, from a ruby laser, under various switching conditions have been taken with the S. T. L. image-converter camera. The spectra were analyzed with both a Fabry-Perot interferometer and a 2-m grating spectrograph. We have observed that, as the stimulated emission occurs more and more rapidly, each spectral region of the emitting R_1 line tends to emit more and more independently of the others, causing a spectrally broad emission by jumping or tuning to different wavelengths. As the switching time is slowed, relaxation processes in ruby compete more and more with induced emission, and the spectrum collapses toward the relatively narrow central line of normal laser oscillation. Asymmetry of the "fast" spectrum about the line center is observed, and as induced emission is slowed a wealth of structure in time and frequency appears. From these results, we give a tentative picture of various relaxation processes in ruby.

* Supported in part by the Aeronautical Systems Division, U. S. Air Force Systems Command, under Contract AF 33(616)-8233.

** Published in the Opt. Soc. Am. Program of the 1962 Fall Meeting, p. 19.

OBSERVATIONS RELATING TO THE TRANSVERSE AND LONGITUDINAL MODES OF A RUBY LASER*,**

V. Evtuhov and J. K. Neeland

Hughes Research Laboratories
Malibu, California

ABSTRACT

Observations of the light intensity variations across the partially transmitting face of a laser crystal operated near threshold are reported. The intensity variation patterns are suggestive of the modes of a cylindrical microwave cavity and are believed to be closely related to the transverse modes of the optical resonator. Preliminary polarization studies indicated that patterns with only a twofold symmetry axis are linearly polarized, whereas others are unpolarized. The pattern sizes range between approximately 170 and 850 μ. The divergence of the emerging beam (several milliradians) decreased with increasing resonator length. Fabry-Perot analysis showed only one excited longitudinal mode for a 1-cm long resonator, but the number increased with the resonator length.

* This work was supported in part by the Aeronautical Systems Division, Air Force Systems Command, under Contract AF 33(616)-8233.

** Published in Appl. Optics 1, 517 (1962).

MODES OF A RUBY LASER*

V. Evtuhov, J. K. Neeland, and W. B. Bridges

Hughes Research Laboratories
Malibu, California

ABSTRACT

Although it has been argued that simple modes such as those of the gas lasers will be unobservable in ruby lasers due to crystal imperfections, a rather high degree of orderly behavior in ruby lasers has been reported. Moreover, by operating a ruby laser very close to threshold and using high quality crystals, it has been possible to observe emission patterns at the end of the ruby which are believed to be very closely related to the modes of the optical resonator. It was found that each ruby crystal could be made to oscillate in a number of different patterns simply by changing the pump energy distribution on the periphery of the ruby. Two approaches to the problem of determining the nature of the patterns have been used: (1) determination of the coherence properties of the emitted light, and (2) correlation of the patterns with the frequency spectrum of the laser output.

* To be presented at Northeastern Research and Engineering Meeting, Boston, Mass., November 5, 6, 7, 1962, and to be published in NEREM 1962 Record.

MEASUREMENTS AND INTERPRETATION OF LASER BEAM DIVERGENCE*

V. Evtuhov and J. K. Neeland

Hughes Research Laboratories
Malibu, California

ABSTRACT

Careful measurements of the divergence of the beam radiated by a laser operating in a 2-lobe pattern indicated a behavior which could be explained on the basis of diffraction and interference of light emitted by a completely coherent source. This strongly supports the mode interpretation of the laser emission patterns.

* To be submitted for publication in Appl. Phys. Letters.

REFERENCES

1. R. W. Hellwarth, "Control of Fluorescent Pulsations," in Advances in Quantum Electronics (Columbia University Press, New York, 1961), p 334.

2. B. J. McMurtry and A. E. Siegman, "Photomixing experiments with a ruby optical maser and a traveling wave microwave phototube," Appl. Optics 1, 51 (1962).

3. F. J. McClung and R. W. Hellwarth, "Giant optical pulsations from ruby," Bull. Am. Phys. Soc. 6, 414 (November 24, 1961). Also J. Appl. Phys. 33, 828 (1962).

4. R. J. Collins, D. F. Nelson, A. L. Schawlow, W. L. Bond, C. G. B. Garrett, and W. Kaiser, "Coherence, narrowing, directionality, and relaxation oscillations in the light emission from ruby," Phys. Rev. Letters 5, 303 (1960).

5. S. Sugano and Y. Tanabe, "Absorption spectra of Cr^{3+} in Al_2O_3. Part A. Theoretical studies of the absorption bands and lines," J. Phys. Soc. Japan 13, 880 (1958).

6. S. Sugano and I. Tsujikawa, "Absorption spectra of Cr^{3+} in Al_2O_3. Part B. Experimental studies of the Zeeman effect and other properties of the line spectra," J. Phys. Soc. Japan 13, 899 (1958).

7. F. J. McClung, S. Schwarz, and F. Meyers, "R_2-line optical maser action in ruby," J. Appl Phys. 33, 3139 (1962).

8. F. Varsanyi, D. L. Wood, and A. L. Schawlow, "Self-absorption and trapping of sharp-line resonance radiation in ruby," Phys. Rev. Letters 3, 544 (1959).

9. T. H. Maiman, R. H. Hoskins, I. J. D'Haenens, C. K. Asawa, and V. Evtuhov, "Stimulated optical emission in fluorescent solids. II. Spectroscopy and stimulated emission in ruby," Phys. Rev. 123, 1151 (1961).

10. G. E. Devlin, J. McKenna, A. D. May, and A. L. Schawlow, "Composite rod optical maser," Appl. Optics 1, 11 (1962).

11. C. G. B. Garrett, W. Kaiser, and W. L. Bond, "Stimulated emission into optical whispering modes of spheres," Phys. Rev. 124, 1807 (1961).

12. J. J. Cook, W. L. Flowers, and C. B. Arnold, "Measurement of laser output by light pressure," Proc. IRE 50, 1693 (1962).

13. D. F. Nelson and W. S. Boyle, "A continuously operating ruby optical maser," Appl. Optics 1, 181 (1962).

14. W. G. Wagner and G. Birnbaum, "Theory of quantum oscillators in a multimode cavity," J. Appl. Phys. 32, 1185 (1961).

15. F. Varsanyi, et al., loc. cit.

16. Interim Scientific Report No. 2, Contract AF 33(616)-8233, Hughes Research Laboratories, Malibu, California.

17. I. J. D'Haenens and C. K. Asawa, "Stimulated and Fluorescent Optical Emission in Ruby from 4.2 to 300°K: Zero-Field Splitting and Mode Structure," Hughes Research Laboratories Research Report No. 235, March 1962. Accepted for publication in J. Appl. Phys. 33, 1962.

18. V. Evtuhov and J. K. Neeland, "Observations relating to the transverse and longitudinal modes of a ruby laser," Appl. Optics 1, 517 (1962).

19. E. Snitzer and H. Osterberg, "Observed dielectric waveguide modes in the visible spectrum," J. Opt. Soc. Am. 51, 499 (1961).

20. G. D. Boyd and J. P. Gordon, "Confocal multimode resonator for millimeter through optical wavelength masers," Bell System Tech. J. 40, 489 (1961).

21. A. G. Fox and Tingye Li, "Resonant modes in a maser interferometer," Bell System Tech. J. 40, 453 (1961).

22. T. H. Maiman, et al., loc. cit.

23. B. J. McMurtry and A. E. Siegman, "Multimoding and frequency-pulling experiments on a ruby optical maser," Opt. Soc. Am. Program of the 1962 Spring Meeting, p. 10.

24. G. E. Devlin, et al., loc. cit.

25. T. H. Maiman, et al., loc. cit.

26. D. F. Nelson and W. F. Boyle, loc. cit.

27. R. W. Hellwarth, loc. cit.

28. M. L. Stitch, E. J. Woodbury, and J. H. Morse, "Repetitive hair-trigger mode of optical maser operation," Proc. IRE 49, 1571 (1961).

29. J. N. Shive, The Properties, Physics, and Design of Semiconductor Devices (D. Van Nostrand Company, New York, 1959), pp. 261-284.

30. T. H. Maiman, "Optical and microwave-optical experiments in ruby," Phys. Rev. Letters 4, 564 (1960).

31. O. A. Anderson, W. R. Baker, S. A. Colgate, John Ise, Jr., and R. V. Pyle, "Neutron production in linear deuterium pinches," Phys. Rev. 110, 1375 (1958).

32. F. Mastrup, Final Report (No. 6, 25 April, 1961) Contract No. DA 44-009-ENG-4412, "Studies on Microsecond Flash Arc Light Sources" Research Labs, Systems Technology Laboratories, Inc.

33. M. H. Horman, Interim Engineering Report (No. 2, March-May, 1961), Contract No. AF-33(616)-7680 Task No. 50723, Motorola Inc. Systems Research Labs, Riverside, California.

34. C. H. Church, R. D. Haun, T. A. Osial, and E. Z. Somers, Paper No. FD-19, "Optical Pumping of Lasers Using Exploding Wires," Optical Society of America Program, (Spring Meeting, Washington D. C., 1962).

35. E. Snitzer, "Optical maser action of Nd^{+3} in a barium crown glass," Phys. Rev. Letters 7, 444 (1961).

36. W. Wagner and G. Birnbaum, "Transmission of monochromatic radiation in a two-level material," Opt. Soc. Am. Program of the 1962 Fall meeting, p. 19.

37. J. E. Geusic and H. E. D. Scovil, "A unidirectional traveling-wave optical maser," Bell System Tech. J. 41, 1371 (1962).

38. H. W. Gandy and R. J. Ginther, "Stimulated emission of ultraviolet radiation from gadolinium-activated glass," Appl. Phys. Letters 1, 25 (1962).